Engineering the Tumor Microenvironment using Microfluidics: Effects of Cell-cell Interactions and Endothelial Barrier Function on Tumor Cell Intravasation

By

Ioannis K. Zervantonakis

Dipl. Ing. Mechanical Engineering (2005), Technical University of Munich
M. Sc. Mechanical Engineering (2006), National Technical University of Athens

Submitted to the Department of Mechanical Engineering in partial fulfillment of the requirements of the degree of

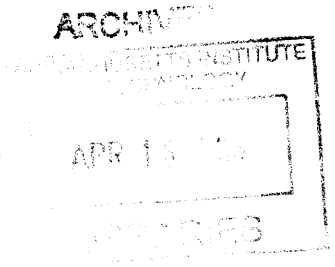

Doctor of Philosophy in Mechanical Engineering

at the

MASSACHUSETTS INSTITUTE OF TECHNOLOGY

February 2013

Author .....
Department of Mechanical Engineering
January 11th 2013

Certified by.....
Roger D. Kamm,
Professor of Biological and Mechanical Engineering
Thesis Supervisor

Accepted by .....
David E. Hardt
Professor of Mechanical Engineering
Graduate Officer

Engineering the Tumor Microenvironment using Microfluidics: Effects of cell-cell interactions and endothelial barrier function on tumor cell intravasation

By

Ioannis K. Zervantonakis

Submitted to the Department of Mechanical Engineering on January 11th 2013 in partial fulfillment of the requirements for the degree of Doctor of Philosophy in Mechanical Engineering

ABSTRACT

90% of cancer related deaths are due to metastatic disease and there is a need for a better understanding of cell-microenvironment interactions to identify new therapeutic targets. A key step during cancer metastasis is cancer cell intravasation (entry of cancer cells into the blood vessels) that results in tumor cell dissemination into distant organs. During this process, tumor cells navigate a complex microenvironment and interact with multiple cell types. This thesis is aimed to develop a microfluidic-based intravasation assay that allows for direct observation of tumor cell motility combined with quantitation of the endothelial barrier function. Compared with traditional *in vitro* assays, microfluidic assays enable "user-defined" design of the cellular and acellular microenvironment with spatio-temporal control and live high-resolution imaging.

Formation of confluent endothelial layers in the device was confirmed with immunofluorescence staining for endothelial cell-cell junctions and we compared our diffusive permeability values with published *in vivo* and *in vitro* data. We employ this microfluidic assay to investigate the role of endothelial barrier function during tumor cell intravasation to address a critical question in cancer research: does tumor cell intravasation require a leaky endothelium? To induce vessel leakiness we perturb the barrier using biochemical factors, endothelial cells with low expression of basement membrane proteins and signaling with macrophages. Under all these conditions, tumor cell intravasation rates increased and we confirmed these results for multiple tumor cell types. Characterization of macrophage secreted factors and M1/M2 polarization status, identified that blocking macrophage-secreted TNF-α restored endothelial permeability and reduced tumor cell intravasation. In agreement with these results, we also found that the number and dynamics of tumor-endothelial interactions were dependent on endothelial barrier function. A novel feature of the developed assay is the ability to image in real-time the process of tumor cell intravasation, while also enabling accurate control and quantitation of the functional characteristics of the endothelial barrier. Our results not only demonstrate the important role of cell-cell paracrine signaling and biochemical factors in regulating tumor cell intravasation, but also have important implications for strategies aimed to disrupt or normalize vasculature *in vivo.*

Keywords: 3D Microfluidics, Endothelial permeability, Cancer cell Intravasation, Macrophages

Thesis committee:
Thesis Supervisor: Roger D. Kamm, Professor of Biological and Mechanical Engineering, MIT
Professor Joan S. Brugge, Department of Cell Biology, Harvard Medical School
Professor C. Forbes Dewey Jr., Department of Mechanical and Biological Engineering, MIT
Professor Douglas A. Lauffenburger, Department of Biological Engineering, MIT

Acknowledgements

I am very fortunate and privileged to have had the opportunity to work with Professor Roger Kamm, who has been an excellent mentor and advisor. Roger is a role model for me, and is an example of a bioengineer truly committed to educating the next generation, while at the same time he is known worldwide for the quality and breadth of his work.

Also, I would like to thank the members of my thesis committee, Professors Joan Brugge, Forbes Dewey and Douglas Lauffenburger. They have provided continuous support and very insightful comments, and have helped me shape my doctoral research. Many stimulating discussions and interactions with Professors Frank Gertler, John Condeelis and Dr. Joe Charest have also been extremely important for my thesis research.

I owe a very special thank you to my mentors in the Kamm lab, Professor Seok Chung and Professor Ryo Sudo, who were always available to answer my questions and kindly sharing any material I may have needed. Working with them has been a crucial part of my "introduction" into the exciting worlds of microfluidics and cellular engineering. Also, I feel very privileged to have been part of the Mechanobiology Laboratory and to have had the opportunity to interact with friends, colleagues and collaborators including: Dr. Joy Rimchala, Dr. Levi Wood, Dr. Waleed Farahat, Dr. Shannon Alford, Dr. Cherry Wan, Dr. Vernella Vickerman, Dr. Joseph Franses, Dr. Huyng-do Kim, Professor Chandrasekhar Kothapalli, Dr. Nate Hammond, Dr. Philip Bransford, Dr. Anusuya Das, Bill Polacheck, Sebastien Uzel, Jessie Jeon, Vivek Sivathanu, Jordan Whisler, Ran Li, Dr. Andrea Pavesi, Dr. Amir Aref, Dr. Juliana Chan, Tu Nguyen, Professor Sarit Das, and Professor Kenichi Funamoto. Administrative support from the wonderful assistants in Mechanical Engineering: Leslie Regan and in the Kamm lab: Sossy Megerdichian, Hannah Merrick and Annmarie Donnovan is also greatly appreciated. It has been a very rewarding experience to have worked with outstanding undergraduate students: Alice Brooks, Mengwen Zhang, Subhanu Samarajiva, Tim Chang and Eric Chang.

Many friends outside the lab have also supported me throughout my doctoral at MIT, with valuable advice during my early steps and spending fun times during extracurricular and academic activities: Dr. Sotiris Koutsopoulos, Suman Bose, Dimitris Tzeranis, Dr. Rosa Ng, Dr. Themis Sapsis, Ted Golfinopoulos, Dr. Manos Karagiannis, Dr. Ioanna Pagani, Professor Triantafyllos Stylianopoulos and Dr. Thales Papagiannakopoulos. I would also like to especially thank Dr. Eleni Maneta, who has always been encouraging and patiently supporting me during many stages of my PhD journey.

Funding from the Alexander S. Onassis Public Benefit Foundation in the form of a graduate student fellowship is gratefully acknowledged.

Finally, I would like to dedicate my thesis to my family in Greece, Eleni and Eirini Zervantonaki, Niko and Nitsa Kallitsa, my mother Aikaterini Kallitsa and especially to my father Konstantinos I. Zervantonakis, who left us early on October 12th 2009.

Table of Contents

Acknowledgements 3

Chapter 1: Introduction and Background 9

Cancer metastasis 9

Complexity in the tumor microenvironment 10

Tumor endothelium and endothelial cell phenotypes 11

Tumor vasculature 11

Tumor cell intravasation 12

Basal-to-apical transendothelial migration of neutrophils and macrophages 15

Targeted Cancer Therapies 16

Microfluidic cell culture 18

Thesis aims and overview 19

Chapter 2: Device Design, Characterization and Validation 21

2.1 Experimental approaches to investigate tumor-endothelial signaling 21

Tumor-endothelial cell interactions in vitro 21

In vivo models of tumor-endothelial cell interactions 24

2.2 Experimental methods to measure endothelial permeability 26

2.3 Assay development 27

2.4 Assay Validation 32

2.5. Assay comparison with other systems and discussion of limitations 35

Chapter 3: Tumor-Endothelial Interactions 39

3.1. Mechanisms of Tumor-Endothelial Cell Interactions 39

Tumor-endothelial cell interactions in the context of tumor cell invasion 40

Tumor-endothelial cell interactions in the context of extravasation 40

3.2. Analysis framework for characterizing tumor-endothelial interactions 45

3.3. Dynamics of Tumor-Endothelial Cell Interaction Events 47

3.4. Discussion of Tumor-Endothelial Cell Interaction events 50

Chapter 4: Role of Macrophages in tumor cell intravasation and endothelial barrier function 54

4.1 Macrophages in Cancer Metastasis 54

Macrophages in cancer 54

Endothelial barrier function regulation in the tumor microenvironment 55

Tumor cell intravasation and the tumor microenvironment 57

4.2. Methods for tumor-endothelial-macrophage culture 57

4.3 Tumor cell intravasation and endothelial permeability 59

4.4. Discussion 64

Chapter 5: Effects of biochemical factors on endothelial barrier function and intravasation 70

5.1.1 Endothelial barrier regulation via biochemical and biophysical factors 70

5.1.2 TNF-α signaling pathways 71

TNF-α effects on Tumor Cells 72

TNF-α effects on Endothelial Cells 73

TNF-α targeted therapy 75

5.2. Biochemical stimulation methods 75

5.3. Biochemical regulation of endothelial permeability and intravasation 75

5.4. Discussion of underlying mechanism and comparison with macrophage-induced intravasation 76

Chapter 6: Conclusions and Future work **80**
6.1 Conclusions and thesis contributions **80**
6.2 Implications **82**
6.3 Future research directions **83**
References **87**
APPENDIX **98**

LIST OF FIGURES

Figure 1: The invasion-metastasis cascade model illustrating the different sequential and interconnected steps that carcinoma cells need to complete in order to form a metastatic tumor [figure modified from (10)] 9
Figure 2: Complexity in the Tumor Microenvironment: different cell types and biological mechanisms that have been shown to have critical factions on dissemination of tumor cells [figure modified from (31)] 10
Figure 3: Schematic of structural characteristics in normal (A) and tumor blood vessels (B) showing inter- and intracellular gaps in the defective endothelial layer, as well as abnormal cytoskeletal projections (sprouts) inside the lumen and in the surrounding tissue. Immunofluorescence staining for endothelial cells (green: CD31) and pericyte markers (red: alpha-smooth muscle actinin or desmin) of a normal arteriole & venule (C), normal capillary (D), compared with abnormal vessels from MCa-IV (E) and LLC (F) tumors in mice. Scalebar: (C): 15um, (D): 80um, (E-F): 30um [figure adapted from (35) and (43)] 12
Figure 4: Active (left) and passive (right) mechanisms of tumor cell intravasation. Only a few single tumor cells (purple cells out of brown cells) invading from the left to the right in response to a chemokine gradient towards a blood vessel. A mass of tumor cells (green) collectively invading the blood vessel, passively shedding alive (green) and apoptotic/necrotic (gray) tumor cells into the circulation. [figure from (52)] 13
Figure 5: Milestones in the development of microfluidic technologies and cell culture [figure from (79)] 19
Figure 6: Different experimental assays to study tumor-endothelial cell interactions. [figure adapted from (55), (86), and (87)] 21
Figure 7: Microfluidic based assays to investigate tumor-endothelial cell interactions [figure adapted from (82), (102), (103) and (104)] 24
Figure 8: *In vitro* and *in vivo* systems for measuring endothelial diffusive permeability using fluorescent tracers. Left: Transwell assay monitoring the intensity time profile in the bottom chamber. Right: Single microvessel assay monitoring the intensity time profile inside a measurement window [figure modified from (114)] 27
Figure 9: Microfluidic Intravasation assay design. (A) Schematic of the PDMS-based device showing the two interconnected channels (green and red) via a Y-junction (black arrow) and the 3D ECM gel region (grey region). (B) Phase contrast image corresponding to the dashed black rectangle in (A) showing an invasive human tumor cell line (red) invading towards an endothelial monolayer (green). (C) A 3D rendering of a single gel region, corresponding to the white dashed rectangle in (B). scalebar: (a) 1.5mm, (b) 150um, (c) 50 um. 29

Figure 10: Fluorescence-based imaging method to measure endothelial permeability in the microfluidic assay. (A) Channel configuration with dextran and control (dextran-free) solutions to establish a diffusive mass flux across the endothelial monolayer. (B) Fluorescent image (top) and concentration profile (bottom) of 70kDa dextran distributubion inside a single gel region without an endothelial monolayer. (C) In the presence of an endothelial monolayer, there is a sharp drop in the intensity profile (bottom) and in the dextran distribution (top). 31
Figure 11: Validation of endothelial monolayer formation via immunofluorescence staining. (A) 3D rendering of endothelial cell-cell junctons in a single gel region (shown in white dashed rectangle in Figure 9B). (B) Formation of endothelial monolayer in the presence of invading fibrosarcoma cells. (C) A single confocal slice showing continuous endothelial Ve-cadherin junctions (green) in the presence of a single invading human HT1080 fibrosarcoma cell (red). (D) Confirmation of basement membrane deposition on the 3D ECM – channel interface by the HUVEC monolayers. Scalebar: (A-B) 50μm, (C-D) 30μm..... 32
Figure 12: Characterization of endothelial permeability. (A) Experimental measurement of 10kDa fluorescent dextran distribution in a single gel region (as outlined in Figures 9 and 10). Darker red color indicate high intensity, whereas blue color indicates low intensity. Scalebar: 50μm. (B) Computation simulation of the dextran distribution. (C) Intensity profile along the dashed line shown in (A). (D) Time plot of permeability evaluation after addition of TNF-α at t=0hr, demonstrating barrier selectivity (E) Endothelial permeability to 70kDa dextran dose response of TNF-α and to 0.5mM of cAMP for a HUVEC monolayer. Average values for n=12 regions per condition. (F) Characterization of different endothelial cell lines, HUVEC, HUVEC cell line knockdown for Perlecan (shPerl) and murine brain endothelial cell line. Average values for n=6 regions per condition. Error bars represent standard error of the mean. 33
Figure 13: (A) Schematic showing method to identify a tumor cell (TC) in contact with the endothelial barrier located on the basal surface and a TC that has intravasated and is on the apical surface (B) Single confocal slice showing a single fibrosarcoma cell (HT1080) that has intravasated across a HUVEC monolayer (white arrow). Scalebar: 25μm. (C) Quantification of HT1080 intravasation rates for microvascular (MVEC) and macrovascular (HUVEC) monolayers. Average values for n=3 devices per condition. Error bars represent standard error of the mean. 34
Figure 14: (A) Comparing bias in scoring intravasation events between different observers. (B) Raw data of confocal z-stack for scoring intravasation events. Average values for n=3 devices per observer. Error bars represent standard error of the mean. (C) Segmented z-stack of the original z-stack in (B) for automatic quantification. 37
Figure 15: An overview of studies that have investigated the role of altered signaling pathways in tumor cells, the role of endothelial cells and the role of cells in the tumor microenvironment [figure adapted from (27), (30), (42), (55), (64) and (67)] 42
Figure 16: Methods to characterize tumor-endothelial cell interactions. (A) 3D rendering of HT1080 cells (red) invading towards an endothelial monolayer at t=0hr. Insert shows the location inside the device. (B) 3D rendering at t=10hrs. (C) 2D projection of tumor cell centroids at t=0hr (black circles) and t=10hr (green squares) and location of endothelial barrier (blue line) interface. (D) Histogram of tumor cell centroid location along the x-axis in panel (C) at t=0 and 10hrs. (E) Wind-rose plot of tumor cell trajectories. (F) Distance of a

single tumor cell from the endothelial monolayer to quantify the time required to cross the endothelial barrier. 46
Figure 17: Tumor cell centroids and endothelial monolayer locations for the TNF-α stimulated endothelial barriers at t=0 (A) and t=10hrs (B). (C) Normalized change in 10kDa endothelial permeability of the endothelial barrier in the presence of tumor cells. (D) Quantification of the percentage of tumor cells that migrated beyond the EC-matrix interface (highlighted with the thick black line in panels A,B) for the control and TNF-α stimulated endothelial barriers. Average values for n=3 devices per condition. Error bars represent standard error of the mean. 48
Figure 18: (A) Time series of a single confocal slice showing a single HT1080 cell (red, black arrow) invading towards the endothelial monolayer. Trajectories of at least n=10 tumor cells under control (B) and TNF-α (C) stimulated endothelial barriers. (D) Quantification of the time to migrate beyond the EC-matrix interface using the methods described in figure 16F. Average values for n=10 trajectories per condition. Error bars represent standard error of the mean. 49
Figure 19: (A) Increase in endothelial permeability due to the presence of breast carcinoma cells inside the 3D ECM. Average values for n=12 regions per condition. Error bars represent standard error of the mean. (B,C) Immunofluorescence staining of endothelial VE-Cadherin junctions (green) in MVEC monolayers showing the remodeling of the endothelial cell junctions at the point of a fibrosarcoma cell contact (white and orange arrows) compared to distally located VE-Cadherin junctions (dashed white arrow) and the formation of gaps in the endothelial monolayer (purple arrow). Scalebars: (B) 5μm, (C) 10μm. 50
Figure 20: Diverse macrophage phenotypes: invasive, immunosuppressive and angiogenesis-related in cancer progression, invasion and metastasis [figure from (140)] 54
Figure 21: Macrophages facilitate tumor cell intravasation and impair endothelial barrier function. (A) Upper panel: Top and side views showing the device schematic with the endothelial monolayer and tumor cells. Lower panel: Breast carcinoma cell (green) that has intravasated across the endothelial monolayer (red). Scalebar: 30μm. (B) Tumor cells located on the basal side, unable to intravasate. (C) Time sequence of a single confocal slice showing a tumor cell (green) intravasating across an endothelial monolayer (magenta). The endothelial barrier location is highlighted with a white dashed line. Scalebar: 30μm. (D) Quantification of the percentage of tumor cell that had intravasated. Average values for n=3 devices per condition (E) Quantification of endothelial permeability. Average values for n=12 regions per condition. Error bars represent standard error of the mean. 60
Figure 22: (A) Localization of macrophages (magenta) on the luminal or subluminal sides of the endothelial monolayer (red) in the presence of tumor cells (green) in the intravasation experiments. Scalebar: 30μm. (B) Quantification of macrophage counts in the luminal and subluminal compartments. (C) Specificity of different cell types to impair endothelial barrier function (EC: endothelial cells only, Mφ: macrophages, TC: MDA231MenaINV tumor cells, 10A: MCF10A epithelial cells). Average values for n=12 regions per condition. Error bars represent standard error of the mean. 61
Figure 23: (A) Expression of actin binding proteins in the breast carcinoma cell lines can enhance tumor cell intravasation in the presence of macrophages. (B) Intravasation efficiency is regulated by the endothelial cell phenotype. HUVEC Perlecan knockdown cells showed increased baseline and macrophage-induced intravasation levels for the MDA231-MenaINV carcinoma cells. Average values for n=3 devices per condition. (C)

Stimulation with 0.5mM cAMP reduced endothelial permeability in the intravasation experiments with the breast carcinoma MDA231-MenaINV cell line in the presence of macrophages. Average values for n=6 regions per condition. (D) Small reduction in intravasation rate upon stimulation with cAMP. Average values for n=3 devices per condition. Error bars represent standard error of the mean. 62
Figure 24: Characterization of TNF-α (A) and IL10 (B) secretion rates under control, M1 and M2 macrophage polarization conditions. Average values and standard error of the mean for two independent experiments. (C) Immunofluorescence staining of M1 (IL12) and M2 (CD206) macrophage markers in the microfluidic device under macrophage monoculture, coculture with breast carcinoma and endothelial cells, and M2 (10ng/ml IL-4) and M1 (10ng/ml LPS) polarization conditions. (D,E) Quantification of fluorescent intensity of IL12 and CD206 markers under the conditions shown in panel (C). Average values for n=10 cells per condition. Error bars represent standard deviation. 64
Figure 25: TNF-α signal transduction pathway complexity [figure from (180)] 72
Figure 26: Diverse roles of TNF-α signaling on tumor cells and tumor-immune cell interactions in the tumor microenvironment [figure from (183)] 73
Figure 27: Signal transduction pathways activated in endothelial cells upon TNF-α/TNFR-1 binding. Multiple cellular functions are modulated including, apoptosis, cell surface adhesion molecule expression (e.g. ICAM1), tight junction and adherens junction reorganization, cytoskeletal changes and NF-κβ signaling [figure from (186)] 74
Figure 28: (A) TNF-α stimulation increases carcinoma cell intravasation in the absence of macrophages. Average values for n=3 devices per condition. (B) Absolute endothelial permeability to 70kDa dextran in the intravasation experiments. Average values for n=6 regions per condition. (C) Quantification of breast carcinoma mean migration speed. Average values for n=10 trajectories per condition. Error bars represent standard error of the mean. 76
Figure 29: Proposed mechanism of endothelial permeability - tumor cell intravasation association and macrophage-facilitated intravasation 82

LIST OF TABLES

Table 1: Summary of different mechanisms that have been implicated in cancer cell intravasation 15
Table 2: Comparison of different assays to investigate tumor-endothelial interactions... 25
Table 3: Mechanisms of tumor-endothelial cell interactions 44
Table 4: Roles of different cell types in endothelial permeability regulation 56
Table 5: Effects of different biochemical and biophysical factors on endothelial permeability 71

Chapter 1: Introduction and Background

Cancer metastasis

The number of individuals diagnosed with cancer is increasing every year, rendering cancer a major public health problem with estimations that one in 3 women and one in 2 men in the United States will develop cancer in their lifetime (1). Since, the declaration of "war" on cancer by US President Nixon in his State of the Union speech in 1971 (2), there has been significant and continued progress in understanding the biological mechanisms of cancer (3), in improving cancer treatment approaches and in developing targeted therapies (4). However, treating patients with metastatic disease remains a major challenge (5). Cancer metastasis, the process by which tumor cells migrate from the primary tumor to one or multiple distant organs, is responsible for 90% of all cancer-related deaths (6). In particular, in patients presenting distant cancer metastasis five-year survival rates are very low with 4%, 4%, 12%, 23%, 27% and 29% for liver, lung, colon, breast, ovarian and prostate cancer (7). In comparison, the five-year survival rates for breast cancer patients with localized ductal carcinoma in situ, is dramatically higher and is estimated to be 95% (8). The multi-step invasion-metastasis cascade (Figure 1) illustrates the different steps of cancer metastasis in solid tumors (9). This process consists of multiple sequential and interconnected steps: 1. vascularization of the primary tumor, 2. invasion through surrounding tissue, 3. intravasation, 4. extravasation, and 5. colonization at a distant organ.

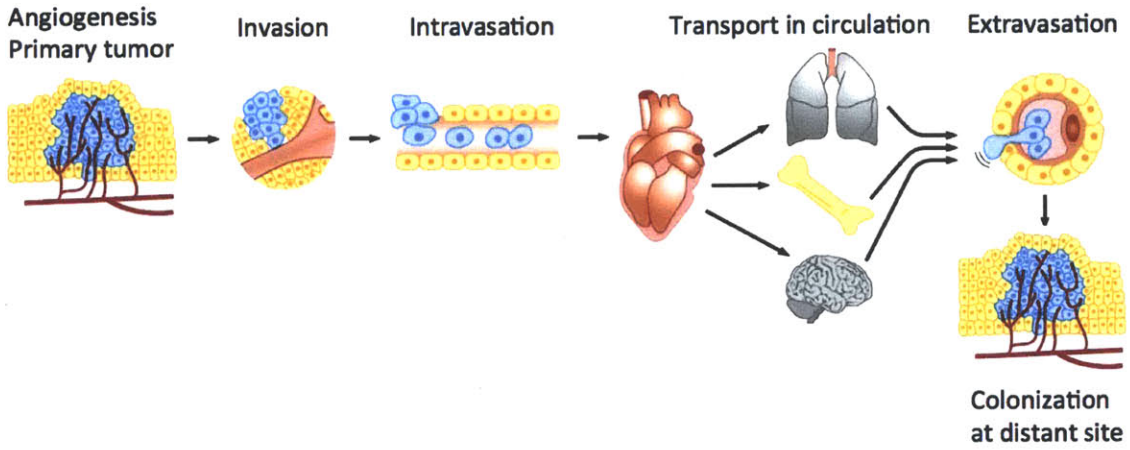

Figure 1: The invasion-metastasis cascade model illustrating the different sequential and interconnected steps that carcinoma cells need to complete in order to form a metastatic tumor [figure modified from (10)]

Ongoing research in the last years has succeeded in implicating specific molecules with different steps in the metastatic cascade (9). However, a number of fundamental questions regarding the nature of carcinoma metastases remain unanswered and research into its molecular basis is relatively limited compared to studies of oncogenic transformation (11). Understanding the mechanisms of cancer metastasis during each step of the metastatic cascade at the molecular, cellular, and cell population levels will significantly impact targeted cancer therapies.

Complexity in the tumor microenvironment

Tumor cells interact not only with biochemical and biophysical factors during each step of the metastatic cascade but also with other cell types known as stromal cells (Figure 2), resulting in a complex network of cell-cell interactions. Studies in human clinical specimens (12) and animal models (13) have shown that these interactions are critical for metastatic spread. Genetically engineered animal models and elegant *in vitro* assays have been helpful in highlighting the diversity of mechanisms tumor cells utilize to invade and their dependence on interactions with the tumor microenvironment (14). For example, cell-cell communication between tumor cells, macrophages and fibroblasts, has been shown to be essential for early tumor cell invasion into the surrounding tissue (15). Interestingly, the interactions of tumor cells with their microenvironment may play a supportive or inhibitory role during cancer cell metastasis and they have been identified as promising therapeutic targets. A complicating factor is that these interactions are dynamic and can evolved with tumor progression, since tumors recruit immune cells into the tumor microenvironment that can be "educated" to perform pro-invasive functions (16). Novel microfluidic-based assays are uniquely suited to model and dissect the complexity of the tumor microenvironment, via integration of culture of multiple cell types under precisely controlled biochemical and biophysical condition, enabling both basic discoveries in cancer research and allowing for high throughput drug screening.

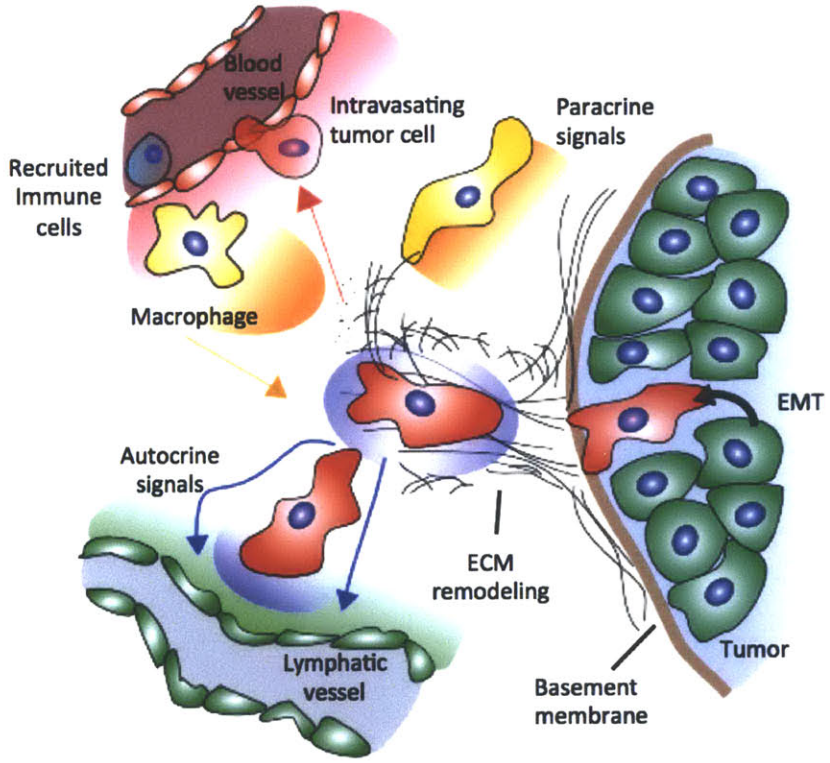

Figure 2: Complexity in the Tumor Microenvironment: different cell types and biological mechanisms that have been shown to have critical factions on dissemination of tumor cells [figure modified from (17)]

Tumor endothelium and endothelial cell phenotypes

Blood vessels are present in most human organs and consist of a single layer of endothelial cells, lining their inner surface. Functional studies of the vasculature originate in 1896 by Ernest Starling who also hypothesized that water and solute exchange movement across the vessel wall would cease when the forces governing fluid movement across the barrier are balanced (18). Successful culture and characterization of human endothelial cells was first established in 1973 (19, 20) and has been crucial for our understanding of the role of endothelial cells in healthy and diseased tissues. Endothelial cells play important roles in organ function, such as blood flow regulation through thrombosis, transport of nutrients, growth-factors and oxygen, and control of immune cell trafficking (21).

Franses et al discusses the evolution of the endothelial regulatory role in vascular disease, and the diverse endothelial cell functions in response to biochemical and biophysical signals originating from the blood or the tissue interstitium (22). Importantly, endothelial cells can have different properties depending on their organ of origin, whereas their phenotypic state can be critically influenced by different pathologies (23). Dudley et al provides an overview of studies that have characterized tumor-derived endothelial cells, with diverse patterns of altered gene expression depending on tumor type and stage (21). Understanding these abnormal patterns is critical for developing effective tumor therapies.

Tumor vasculature

Pioneering work from Dr. Judah Folkman established that growth of solid tumors requires the formation of new blood vessels (neovascularization), especially for tumors larger than 2 mm in size (24). Studying tumor vessels *in vivo* is challenging, because they comprise only a small fraction of the tumor, and also because vessel function is influenced by tumor-related inflammation and necrosis. Dvorak and colleagues developed a mouse model where VEGF-A^{164} is injected into different tissues and the structural and functional characteristics of the formed vessels are studied in detail (25). Later work from the same group, described the different types of tumor vessels formed in this system, and how they differ from the hierarchical arrangement of the artery-arteriole-capillary-venule-vein (Figure 3C) in healthy tissues (26). VEGF overexpression in these tumors resulted in enlargement of vessel circumference and total surface area in all the new vessels formed compared to the normal venules (Figure 3D, E and F). Moreover, among the different surrogate tumor vessels formed in this model, Nagy et al showed that the vessels with the largest diameter, termed as mother vessels, have thin walls, are hyperpermeable and have poor pericyte coverage.

Studies in clinical specimens from prostate cancer patients (27) have confirmed these structurally abnormal characteristics of tumor blood vessels (Figure 3) in experimental tumors in mice. Hashizume et al performed a detailed scanning electron microscopy study on tumor vasculature in mouse mammary carcinomas and characterized the cytoplasmic projections, transcellular and intercellular pores in tumor endothelial cells (28). The study findings demonstrated that tumor vessels are highly heterogeneous with about 14% of vessels having a defective cellular lining, composed of disorganized and loosely connected endothelial cells. Transcellular holes were measured in the range of 0.2 - 0.9μm and intercellular gaps in the range of 0.3 - 4.7μm. Later

studies from the same group examined the organization of the basement membrane in tumor vessels in mammary carcinomas (29). Although laminin coverage in tumor vessels was mostly complete, structural abnormalities were identified compared with normal blood vessels in agreement with the formation of endothelial sprouts in tumors. A comprehensive understanding of the tumor vessel structural and functional properties is critical for characterizing transport in the tumor and has important implications for cancer treatment, as reviewed by Goel et al (30).

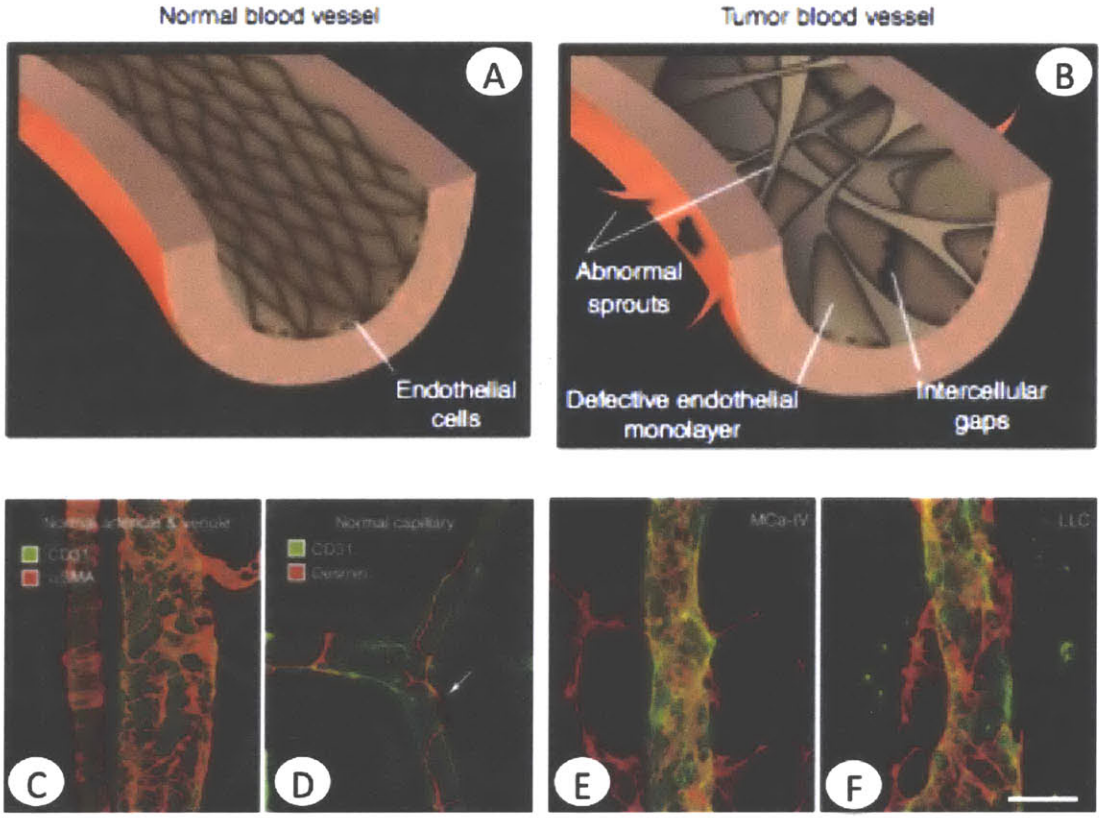

Figure 3: Schematic of structural characteristics in normal (A) and tumor blood vessels (B) showing inter- and intracellular gaps in the defective endothelial layer, as well as abnormal cytoskeletal projections (sprouts) inside the lumen and in the surrounding tissue. Immunofluorescence staining for endothelial cells (green: CD31) and pericyte markers (red: alpha-smooth muscle actinin or desmin) of a normal arteriole and venule (C), normal capillary (D), compared with abnormal vessels from MCa-IV (E) and LLC (F) tumors in mice. Scalebar: (C): 15um, (D): 80um, (E-F): 30um [figure adapted from (21) and (30)]

Tumor cell intravasation

Tumor cell intravasation, the process by which cancer cells enter into blood vessels (Figure 4), is one of the early rate-limiting steps in cancer metastasis (31). Increased tumor cell intravasation rates result in higher circulating tumor cell (CTC) numbers and increase the risk for the formation of lethal metastases (32). Clinically, lymphovascular invasion (LVI), which refers to tumor invasion of the lymphatic and blood vessels is a strong predictor of outcome in patients with invasive breast cancer and correlates both with breast cancer specific survival time and distant metastasis free survival time (33). Traditionally, metastatic dissemination is considered a late event in cancer development (34). Recent evidence, however, has raised an important question in cancer metastasis, as to whether tumors can shed tumor cells into the circulation

during early stages of cancer development (35). Enumeration of circulating tumor cells in Stage I-III breast cancer patients, having no clinically detectable metastases, revealed that an average of 60 CTC/ml were found in the blood, providing more evidence that intravasation is an early event. In comparison an average of 126 CTC/ml was found in patients with metastatic cancer (36).

Due to the challenges of studying tumor cell intravasation *in vivo* and the lack of physiologically relevant *in vitro* systems, a number of important issues remain poorly understood. In particular, although it is well established that entry of tumor cells into the circulatory system can occur both via the lymphatic and blood vessels, the mechanisms regulating the early steps in lymphatic metastasis (37) and hematogenous metastasis (11) are largely unknown, hampering the development of effective metastasis therapies. Regional lymph node metastasis represents the first step of tumor dissemination for many common cancers such as melanoma, breast and prostate cancers (37). However, it is debated whether lymphatic invasion is a driving force for distant organ metastasis (38), particularly since tumor cell entry into blood vessels is what allows direct access to distant organs. The differences between tumor cell invasion across blood and lymphatic barriers and their underlying mechanisms have only recently been investigated *in vitro*. Kerjaschki et al showed that tumor spheroids cultured on top of endothelial monolayers were significantly more effective in clearing lymphatic endothelial cells compared to blood vessel endothelial cells (39).

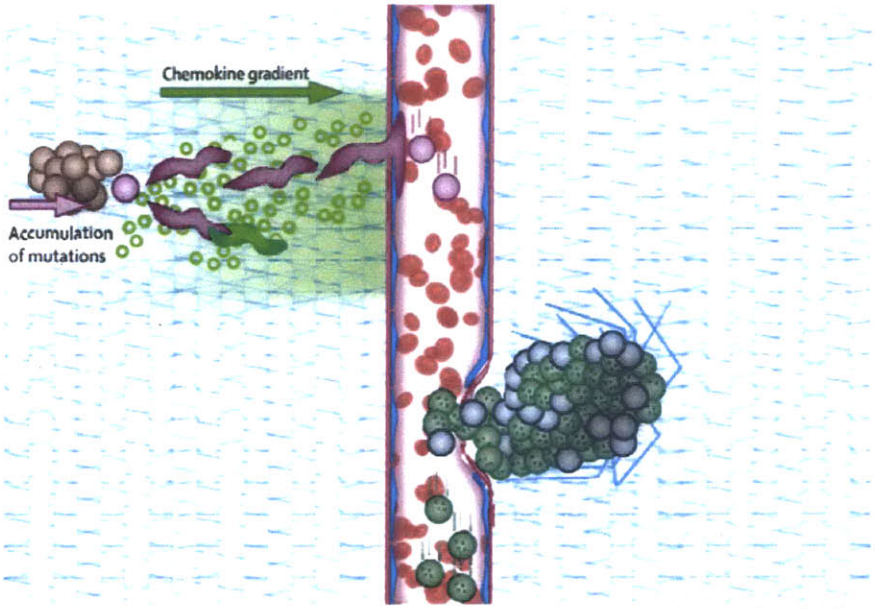

Figure 4: Active (left) and passive (right) mechanisms of tumor cell intravasation. Only a few single tumor cells (purple cells out of brown cells) invading from the left to the right in response to a chemokine gradient towards a blood vessel. A mass of tumor cells (green) collectively invading the blood vessel, passively shedding alive (green) and apoptotic/necrotic (gray) tumor cells into the circulation. [figure from (40)]

Another topic of debate in cancer cell intravasation is whether tumor cells migrate actively towards the blood vessels (Figure 4) or whether they are shed passively into the circulation (40). Multiphoton imaging studies in tumors *in vivo* support a model where intravasating tumor cells actively migrate towards signals present in the tumor microenvironment (13) and due to transient

activation of TGF-β signaling (41). On the contrary, there is also evidence supporting a collective mode of invasion, particularly into the lymphatic vessels, when TGF-β signaling is blocked (41). The mode of invasion will likely also depend on cell-cell and cell-extracellular matrix (ECM) adhesion molecule expression levels, expression of epithelial to mesenchymal transition (EMT) markers and interaction with the blood vessels.

Another important open question, is whether tumor cells invade into the vessels across the endothelial cell body (transcellular) or across endothelial cell-cell junctions (paracellular). Elegant recent studies of neutrophil transendothelial migration characterized the dynamics and involvement of endothelial junctional molecule (JAM-C) in paracellular and transcellular migration across the venular endothelium in inflamed tissue (42). *In vitro* studies on 2D surfaces showed that the mode of tumor cell transendothelial migration was dependent on the actomyosin contractile function of the endothelial cytoskeleton (43). Although these studies provide insight into the mechanisms of tumor cell intravasation, they did not recapitulate tumor-endothelial interactions in a physiologically relevant setting. Furthermore, although there has recently been progress in understanding the mechanism of transendothelial migration of leukocytes (44), it is unclear to what degree the adhesion molecules and paracrine signals critical for leukocytes may also be involved in tumor cell intravasation (45).

Despite progress in identifying regulators of tumor-cell autonomous intravasation mechanisms (46, 47), recent experimental evidence suggests that factors in the tumor microenvironment can also regulate tumor cell dissemination (31). In particular, recent studies have showed that macrophages (13) and neutrophils (16) promote tumor cell intravasation in murine mammary carcinomas. The association of macrophages with blood vessel invasion has also been confirmed by histologic examination of human tumors from breast cancer patients (12). Not surprisingly, characterization of tumor associated macrophages has revealed a heterogeneous macrophage population (48) with both pro- and anti-tumorigenic functions. Blood vessels in tumors are known to be hyperpermeable and become abnormal early during carcinogenesis (49). Although the functional and structural characteristics of these vessels have been characterized (50), it is not clear whether vascular remodeling is important in the process of intravasation and whether the ability of tumor cells to enter the blood stream depends on the endothelial barrier integrity. *In vivo* studies have found high tumor cell counts in the portal venous blood in tumors with higher blood vessel density (51), suggesting a positive correlation between tumor angiogenesis and tumor cell dissemination. In support of this hypothesis, studies using a zebrafish model (52) have also shown that the ability of tumor cells to induce vascular remodeling via secretion of angiogenic factors can facilitate vascular invasion.

A comprehensive understanding of the underlying biological mechanisms in cancer cell intravasation both at the intracellular and tumor microenvironment levels will be critical for the development of novel targeted therapies. *In vitro* systems, capable of dissecting the role of extrinsic signals and cell-autonomous programs would aid in reaching these goals. In Table 1, we summarize different mechanisms that have been linked with intravasation, and a more detailed discussion will be presented in the introductory sections of chapters 3 and 4.

Table 1: Summary of different mechanisms that have been implicated in cancer cell intravasation

Biological mechanisms involved in Cancer Cell Intravasation	Reference
Tumor cell autonomous mechanisms	
Human fibrosarcoma (HT1080) and squamous carcinoma (HEp3) cell intravasation and invasion in the chick embryo chorioallantoic membrane model (CAM) was reduced by inhibiting **CD151**	(53)
HEp3 intravasation into the CAM assay was reduced by **MMP** inhibition	(54)
siRNA silencing of **MMP-9** in HT1080 cells increased intravasation in CAM	(55)
Comparison of HT1080 variants in CAM assay showed: **TIMP-2** decreased, while **TF, JAM-C, NCAM-1** increased intravasation levels	(56)
VEGF and **uPA** expression correlated with intravasation and angiogenesis in prostate cancer (PC3) cells	(57)
miR-10b overexpressing SUM149 cells form metastases when orthotopically injected in mice	(58)
Twist silencing in 4T1 cells reduced tumor blood burden in orthotopically injected BALBc mice	(47)
VEGF and **RhoC** overexpression enhanced MDA-435 early intravasation in fish vessels. Fish vasculature was found to be permeable	(52)
MenaINV expression in MTLn3 cells increased tumor burden in murine mammary carcinomas	(46)
Knockdown of **N-WASP** reduced intravasation of MTLn3 cells in murine mammary carcinomas	(59)
MTLn3 cells overexpressing **EGFR** showed higher tumor blood burden in Rag gs -/- mice (lacking natural killer cells)	(60)
Transient **TGF-β** signaling is required for MTLn3 invasion into blood vessels	(41)
Tumor microenvironment dependent mechanisms	
Macrophage depletion and **EGFR** blocking reduced intravasation in a murine carcinoma model	(13)
PC-3 & HT1080 tumors recruited **MMP-9** positive **neutrophils**, increasing intravasation and angiogenesis	(16)

Basal-to-apical transendothelial migration of neutrophils and macrophages

In this section, we review studies that have investigated the intravasation of non-transformed cells. Intravasation is also sometimes described as "basal-to-apical transendothelial migration", where cells attached on the basal endothelial surface migrate across the endothelial barrier and attach on the apical surface. For example, neutrophils, which are the most abundant leukocyte cell type and are critical for defense against microbial infections, have been shown to be able to intravasate in zebrafish larvae (61) and in mice (42). This discovery is of particular interest in adaptive immunity, because unlike the classical view of neutrophil death in the site of wounding, it raises a very important question regarding the possible functions of these neutrophils once they enter back into the circulatory system (62). Mathias et al demonstrated intravasation, also termed as reverse migration, of neutrophils by tracking GFP expressing neutrophils in a transgenic zebrafish after a wound was formed. Interestingly, their results suggest that reverse transmigration was a robust active process, since both forward and reverse migration had similar velocity and directionality values (61). The studies in zebrafish however have raised criticism due to possible zebrafish embryo specific effects (e.g. developing vasculature). Woodfin et al performed intravital imaging of neutrophil transendothelial migration in a mouse model of intrascrotal inflammation and found that out of the total transendothelial migration events, 10%

were reverse transendothelial migration events (42). Woodfin et al also showed that this percentage increased to 50% in mice with endothelial cells lacking JAM-C. Interestingly, the mechanism by which JAM-C regulates neutrophil transendothelial migration remains unknown, however Woodfin et al suggest three different possible mechanisms: a) by regulating VE-Cadherin junctions and barrier integrity, b) by providing an adhesive ligand for neutrophil ligand Mac-1 and c) by regulating directionality of transmigration. *In vitro* studies using human cells have provided additional evidence for neutrophil reverse migration and showed that neutrophils that exhibited reverse transmigration expressed a distinct surface marker signature for $CD11b^{high}$, $CD54^{high}$ and $CXCR1^{low}$ compared to $CD11b^{high}$, $CD54^{high}$ and $CXCR1^{low}$ in freshly isolated neutrophils (63). Apart from neutrophils, monocyte derived mononuclear phagocytes have also been shown to undergo reverse transmigration across human umbilical vein endothelial cell (HUVEC) monolayer *in vitro* (64). The rate of reverse transmigration could be increased by treating HUVECs with IL-1 and was blocked by antibodies against ICAM-1.

Targeted Cancer Therapies

In this section, we review different targeted anti-cancer drugs that have been approved by the US Food and Drug Administration (FDA) for various cancer types against alterations in both tumor cells and the tumor microenvironment. We also discuss preclinical studies in animal models aimed to develop specific anti-cancer drugs for metastatic cancer. Despite the remarkable success of the targeted drug imatinib for chronic myelogenous leukemia (CML), with survival rates up to 96-99%, different small molecule kinase inhibitor drugs against human epidermal growth factor receptor (EGFR), human epidermal growth factor receptor 2 (HER2) and insulin-like growth factor I receptor in solid tumors have been far less successful (65). In particular, 70% of patients respond to imatinib (targets BCR-ABL) in CML compared with much lower rates for kinase inhibitors against solid tumors. For example, the response rates are 10% for Erlotinib (targets EGFR) in non small cell lung cancer and 15-26% for Trastuzumab (targets HER2) in metastatic breast cancer (66). In comparison, the response rates to non-specific cytotoxic chemotherapy for metastatic breast cancer are 27-69 % (66), however drug resistance and side effects are significant clinical problems.

In addition to interfering with mutations in tumor cells, targeting the tumor microenvironment is an emerging concept with the ultimate goal to isolate the cancer cells from their multiple supportive networks and kill them (31). Tumor anti-angiogenesis therapy, pioneered by Dr. Judah Folkman (24) is a promising approach to target blood vessels and starve tumors. Bevacizumab, a monoclonal antibody against Vascular Endothelial Growth Factor A (VEGF-A), was first approved by the US-FDA in 2004 for colorectal cancer and subsequently in 2006, 2008 and 2009 for non small cell lung carcinoma, HER2 negative breast cancer and glioblastoma respectively (65). Small molecule inhibitors have also been developed to target tyrosine kinase receptors, including the VEGF receptor, and a number of drugs (e.g. Sorafenitib, Sunitinib, Temsilolumus, Pazopanib) have received FDA approval for treating mainly renal cell carcinomas (67). Results from clinical trials have shown that clinical efficacy of targeted VEGF therapy requires addition of cytotoxic chemotherapy and the clinical benefits in progression free survival and response rate are low but encouraging (68). For example, in a 2003 clinical trial in metastatic renal-cell carcinoma patients, Bevacizumab prolonged the time to disease progression by 3-6 months and increased response rate by 8-30% (69). For a discussion on different classes of

targeted anticancer therapies along with other approaches targeting tumor vasculature we refer the reader to (67).

Although surgical resection and targeted or cytotoxic therapy are effective against localized primary tumors, metastatic cancers are largely incurable because of the cancer spread in distant organs and resistance to existing therapeutic agents (9). An important consideration for the development of anti-metastatic drugs is the requirement of targeting tumor cell proliferation and invasion at the distant site and potentially targeting the stromal cells as well. In the previous paragraph, we have mainly discussed already approved US-FDA drugs. Below we review preclinical studies that have focused on targeting molecular mechanisms of tumor-microenvironment interactions during both early and late steps in the metastatic cascade. Zijlstra showed that blocking the integrin-associated tetraspanin CD151 dramatically increased cell-extracellular matrix (ECM) adhesion, resulting in inhibition of intravasation and invasion in avian and murine models (53). Blocking Colony Stimulating Factor 1 (CSF-1) signaling in tumor-associated macrophages using CSF-1R antagonists, reduced macrophage recruitment and resulted in slower tumor growth and fewer pulmonary metastasis in a mouse mammary carcinoma model (70). Apart from immune cells, the role of other cell types interacting with the endothelial wall has been in investigated in cancer metastasis. Cooke et al showed that poor pericyte coverage of the blood vessels correlates with poor prognosis in breast cancer patients (71). Using a mammary carcinoma mouse model the same authors demonstrated that pericyte depletion increases pulmonary metastases. Another metatastatic cancer target that has received considerable attention is the vascular cell adhesion protein 1 (VCAM-1). This adhesion molecule is expressed on the breast tumor cell surface and mediates pro-metastatic tumor-stromal interaction at the distant organ (72). Blocking α4-integrin, receptor for VCAM-1, disrupted the tumor and bone marrow stromal cell interactions and had tumor suppressive effects in a mouse model of myeloma (73). A number of studies have also investigated the possibility of interfering with already established metastasis. Inhibition of the proto-oncogene tyrosine-protein kinase Src impaired the survival of already extravasated breast tumor cells in mouse xenografts and blocked the formation of distant bone metastases (74). Valastyan et al showed that miRNA miR-31 expression could prevent the outgrowth of established metastases via Akt-mediated signaling and induction of the pro-apoptotic signal Bim (75). For a recent review on different signaling pathways that are under investigation in clinical trials for treating metastatic disease we refer the reader to (6).

Bates et al emphasized that a very comprehensive understanding of the underlying biological mechanism is required for successful drug development. Despite significant progress in understanding the pathways that control the invasion-metastasis cascade and the identification of potentially clinically useful biomarkers to characterize metastatic efficiency, discovery of effective anti-metastatic targeted therapy lags behind (9). Poor understanding of the underlying biological mechanisms hampers effective treatment of metastatic cancers. For example, the role of stromal cells during each step of the metastatic cascade is just beginning to be appreciated (9). Hence, the development of physiologically relevant assays that can recreate the tumor microenvironment will not only aid in furthering our understanding of the underlying mechanisms, but will also provide powerful and versatile drug development platforms.

Microfluidic cell culture

Significant progress has been made in the area of microfluidic cell culture in the last 10 years, with constantly new biological assays being developed ranging from single-molecule (76) to whole organism (77) levels. An important milestone in the expansion of microfluidic cell culture platforms was the introduction of polydimethylsiloxane (PDMS) - based soft lithography microfluidics, which are easily fabricated and allow for the rapid development of cell culture compatible and easy to fabricate platforms (78). Berthier et al provide a historical timeline of microfluidics (Figure 5) and a very comprehensive comparison between traditional polystyrene-based cell culture and microsystems PDMS-based culture (79).

Tumor and stromal cell function in the tumor microenvironment is regulated by a variety of factors, such as biochemical signals secreted and sensed by the same cell type (autocrine) or by a different cell (paracrine) and biophysical signals, such as fluid flow and matrix mechanical properties (17). Microfluidic technology allows for the development of novel *in vitro* assays that enable the study of cellular behavior under tightly controlled microenvironments with high spatiotemporal resolution. Modeling the tumor microenvironment by integrating interactions among multiple cell types with biochemical and biophysical factors is a very attractive target for microfluidics. A number of microfluidic platforms have been developed to study growth-factor gradients in cancer cell migration (80), tumor-stromal cell interactions (81) and tumor-endothelial cell interactions (82). Studies employing transwell inserts do not allow for visualization of interaction events in real-time nor do they allow for user-defined control of growth-factor gradients (83).

On the other hand although live animal studies have demonstrated the highly dynamic interaction between tumor and endothelial cells (52), they require complex imaging setups and do not allow for accurate control of the tumor microenvironment factors in order to delineate the underlying mechanisms. At the same time and despite the advantages of (i) user-defined assay design, (ii) accurate control of intercellular distance and microenvironmental cues, (iii) excellent imaging and (iv) multiplex capabilities, a number of challenges also need to be taken into account. PDMS can adsorb small hydrophobic molecules into the material bulk and leaching of uncured PDMS oligomers can affect cellular phenotype (84). Future research is needed to address these challenges using integrated systems incorporating multiple cell types with integrated on-chip analysis and novel fabrication materials.

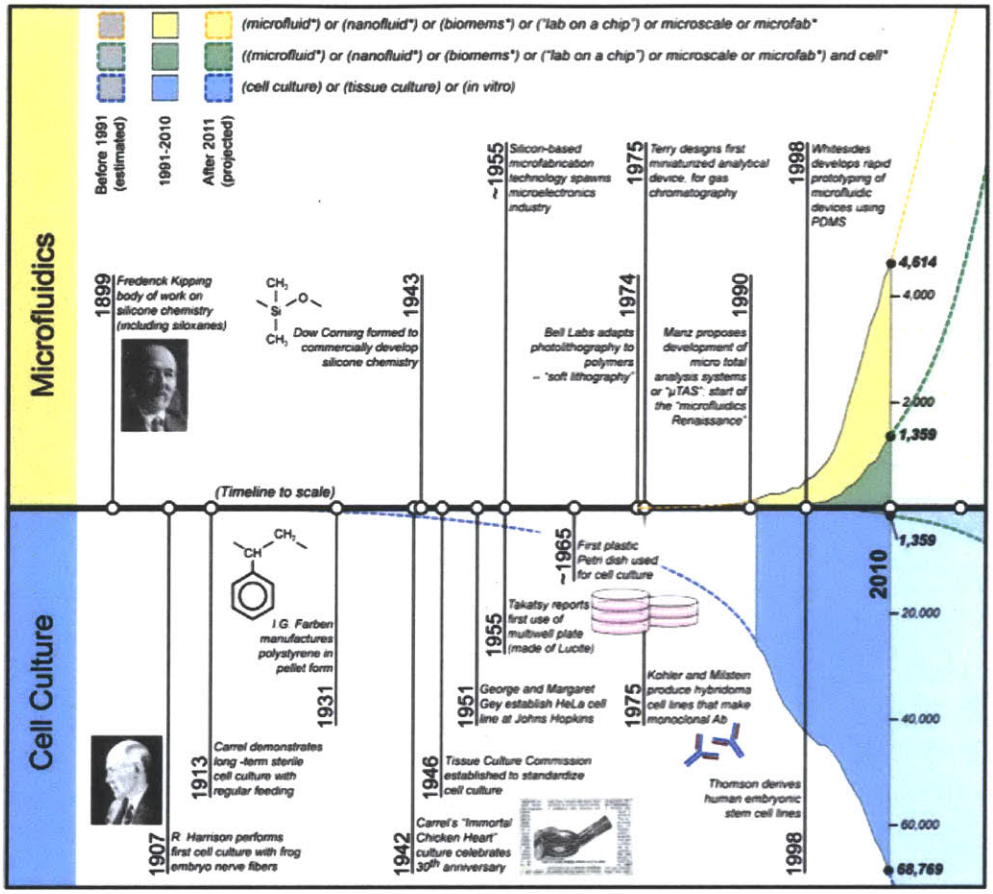

Figure 5: Milestones in the development of microfluidic technologies and cell culture [figure from (79)]

Thesis aims and overview

Thesis aims

This thesis is aimed to investigate the role of tumor microenvironmental factors on cancer cell intravasation. In particular, we employed a new microfluidic assay to test the hypothesis that cancer cell intravasation is regulated by factors present in the tumor microenvironment, such as macrophages and inflammatory cytokines. Addressing this question is not only important for understanding the molecular mechanisms and identifying potential targets for cancer therapy, but it also has implications for FDA approved vessel normalization drugs and cancer drug delivery. We developed, characterized and validated a microfluidic assay to model cancer – endothelial cell interactions in a physiologically relevant 3D microenvironment including macrophages, tumor and endothelial cells. The assay was designed to enable direct observation of tumor cells during intravasation across a well-characterized endothelial barrier and accurate control of biomolecular transport in the device.

Thesis overview

In the first chapter we introduce cancer metastasis, targeted therapies and discuss the critical players in the tumor microenvironment. We describe the functional and structural characteristics of tumor blood vessels, provide a review of recent work in tumor cell intravasation and relate it to studies of non-tumor cells that are also able to intravasate. Next, we describe the potential of microfluidic technology for engineering novel models of the tumor microenvironment.

Experimental methods to characterize tumor-endothelial interactions are described in detail in chapter 2. We compare different classes of *in vitro* and *in vivo* systems to model tumor-endothelial cell interactions. Experimental methods to characterize diffusive permeability of endothelial cells in culture and single microvessels are described next. The remaining part of the chapter is devoted to present the design considerations for the 3D microfluidic-based intravasation assay, along with validation studies of the endothelial monolayer functional and structural characteristics. Tumor cell intravasation studies with an aggressive fibrosarcoma cell line are presented and we discuss our assay and results in comparison with other *in vitro* assay, while also describing challenges and opportunities for further improvement.

A description of the molecular and cellular mechanisms of tumor-endothelial interactions is provided in chapter 3. In particular, we discuss critical molecular players that have been implicated in tumor invasion, tumor transendothelial migration and endothelial permeability. Next, we present the tumor-endothelial interaction analysis framework and our findings on the number and dynamics of tumor-endothelial interactions under conditions of endothelial barrier impairment. Chapter 4 is devoted to the role of macrophages in cancer metastasis and the regulation of endothelial permeability by different cell types in the tumor microenvironment. Characterization of macrophage secreted cytokines, localization and polarization status in the device were performed to investigate the role of these inflammatory cells in tumor cell intravasation. Blocking antibody experiments, and dosing with different concentrations of tumor necrosis factor alpha (TNF-α) were also carried out to assess the effects on the endothelial barrier function. We conclude this chapter with a systematic comparison of our results with *in vitro* and *in vivo* studies on the role of macrophages in cancer, while we also discuss the experimental limitations and suggest future experiments to address them.

In chapter 5, we discuss the role of TNF-α signaling in cancer metastasis and in endothelial phenotypes. To further explore the relationship between endothelial permeability and cancer cell intravasation, we present our experiments under conditions of altered endothelial permeability and compare them to our results in the previous chapter. Finally, in the last chapter we summarize our findings, discuss the implications for cancer metastasis and present a number of interesting directions for future research.

In summary, this thesis describes the development of a novel assay and approach to simultaneously investigate tumor cell invasion and endothelial permeability. This assay was employed to address a critical question in cancer research as to whether tumor cell can intravasate across an "intact" endothelial barrier. The results suggest that endothelial barrier function is critical during this process and that it can be modulated via factors in the tumor microenvironment to regulate intravasation.

Chapter 2: Device Design, Characterization and Validation

In chapter 2 we present a review of different experimental methods to investigate tumor-endothelial interactions. The design criteria for the 3D microfluidic assay are discussed next, together with validation studies of endothelial monolayer formation and intravasation of an aggressive human tumor cell line. The chapter concludes with a comparison of published *in vivo* and *in vitro* data.

2.1 Experimental approaches to investigate tumor-endothelial signaling

Tumor cell (TC) - endothelial cell (EC) interactions are involved in every step of the invasion-metastasis cascade (Figure 6). These interactions can occur via paracrine signaling, where soluble factors secreted by the growing tumor mass signal to the endothelial cells lining the pre-existing blood vessels, and/or via direct physical contact during the process of tumor cell entry into the blood vessels. Despite the effective results of the FDA approved anti-angiogenic drugs in targeting VEGF signaling in animal models, the results in the clinic are far less impressive (85). For successful translation into the clinic the underlying mechanisms of tumor-endothelial interactions in the context of tumor metastasis need to be better understood. Development of *in vitro* platforms that allow for physiologically relevant phenotypes to be assayed, combined with *in vivo* validation can enable the discovery of new drug targets.

Tumor-endothelial cell interactions in vitro

In vitro assays offer a valuable tool for investigation of cellular interactions in model systems amenable to tight experimental conditions. Furthermore, these systems are ideally suited for high throughput drug discovery due to lower experimentation costs. In the following sections we review the different classes of *in vitro* models that have been employed to investigate tumor-endothelial interactions in the context of cancer metastasis.

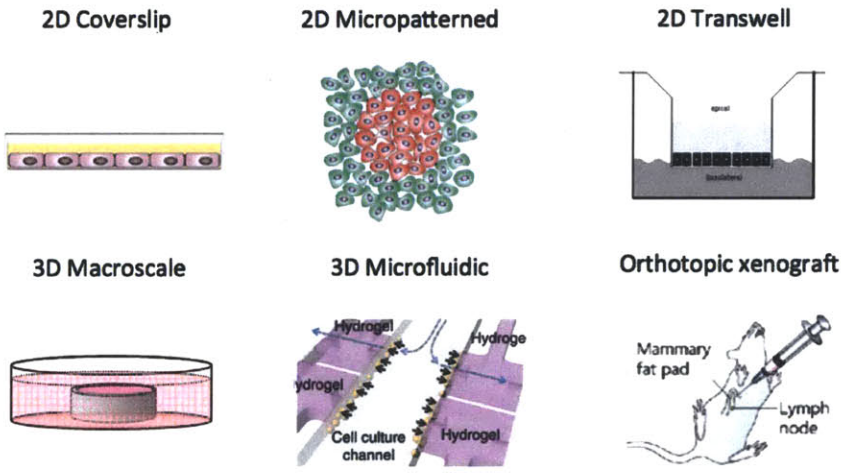

Figure 6: Experimental assays to study tumor-endothelial cell interactions. [figure adapted from (43), (86), and (87)]

Two-dimensional and conventional transwell assays

Tumor transendothelial migration is typically assayed using the transwell assay or Boyden chamber, which consists of a stiff filter located between an upper and a lower well. Endothelial cells are usually seeded on the top surface of the filter, which can be coated with a thin layer of a 3D ECM and subsequently tumor cells are seeded on the upper chamber (88). This configuration is used to investigate extravasation, since the tumor cells encounter the apical surface of the endothelial monolayer first. Less frequently investigators seed the endothelial cells on the lower surface to mimic intravasation, as the tumor cells will encounter the basal surface of the endothelial barrier first. Li et al (83) presented a modified Boyden assay by incorporating two endothelial monolayers on the top and bottom filter surfaces and used radioactive labeling to allow for accurate quantification of the transendothelial migration events. In contrast to the conventional assays that identify the tumor cells in contact with the endothelium by imaging, this system enabled the characterization of the tumor cells that detached from the endothelial monolayer and are typically not included in the imaging analysis discussed previously. To investigate the dynamics of tumor-endothelial cell interactions many investigators use a two-dimensional assay, where an endothelial monolayer is formed on a matrix-coated collagen glass-coverslip and tumor cells are added in suspension (89). A more physiologically relevant version of this assay includes forming the monolayers on a 3D ECM, typically collagen type I matrix, which allows one to also model tumor cell invasion in a 3D environment following transmigration in an apical to basal configuration (90).

Roussos et al described a transwell-based subluminal-to-luminal transendothelial migration assay, designed to characterize intravasation (46). In this system, a thin layer of ECM is placed on the bottom surface of the transwell filter and endothelial cells are seed on this basement membrane-like matrix. Subsequently tumor cells are seeded on the upper well of the filter and invade through the basement membrane and across the basal surface of the endothelial barrier. Despite the simplicity of this assay, it is not possible to visualize intravasation in real time, and the authors did not characterize endothelial barrier function. Ingthorsson (91) investigated the effects of endothelial cells on the formation of spheroid colonies of normal epithelial and tumor cell lines. Interestingly, under direct contact conditions in a reconstituted basement membrane endothelial cells consistently increased the spheroid size for normal epithelial and tumor cell lines, whereas under conditions of paracrine communication there was a mixed response. Spheroid sizes were smaller compared to those cultured in direct contact, with the largest difference for the normal epithelial cells (MCF10A and D382) and smaller or insignificant changes for malignant tumor cell lines (MCF7, T47-D and MDA231). Using a micro-patterning approach Stine et al investigated the effects of different tumor-endothelial interaction architectures on melanoma cell gene expression patterns and endothelial cell collective motility (86). Although this coculture model did not include any 3D ECM and biophysical stimuli, the system design allowed for simultaneous investigation of genotypic and phenotypic changes to reveal molecular mediators of these interactions.

Three-dimensional macroscale assays

Although 2D culture models have greatly advanced our understanding of many fundamental biological processes, *in vivo* cells are usually organized in three-dimensional environments.

Baker and Chen provide a recent review on how 3D cell culture conditions can alter cellular cues compared to 2D cultures (92). Novel 3D models integrating multiple cell types, biochemical and biophysical factors can help bridge the gap between conventional 2D cell culture assays and animal models (93). Pioneering work from the Bissel and Brugge labs in 3D culture models has demonstrated the role of oncogenic pathways and the changes in the ECM in maintaining tissue organization (94, 95). Importantly, compared to 2D the use of 3D models has been shown to mimic drug resistance to cytotoxic drugs (96) and targeted drug inhibition, which is also seen *in vivo*. Kenny et al performed a very comprehensive study comparing transcriptional profiles and cell morphologies of 27 breast cancer cell lines in 2D and 3D culture conditions (97). Although, future studies are required to characterize the changes on post transcriptional regulation (e.g. phosphorylation), the authors showed that there was a significantly altered gene expression signature involving 14 genes including, integrin β1. Fischbach investigated the role of 2D and 3D cultures on cancer cell angiogenic potential, and demonstrated that although VEGF secretion rates were insensitive to culture dimensionality, 3D culture enhanced secretion of IL-8 via an integrin dependent mechanisms (98). Khuon et al described a coculture assay, where breast carcinoma cells and endothelial cells were uniformly seeded in a 3D collagen type I matrix, and endothelial cytoskeleton activation pathways were investigated using FRET sensors (43). Although, this presents a simple 3D assay, it was not possible to establish gradients to guide cell migration in this culture model and it was unclear if tumor cells could intravasate across the single-cell vessel lumens.

Microfluidic assays

The advances in microfluidic systems have enabled the development of novel methods for studying in detail the effects of fluid flow, externally imposed cytokine gradients in endothelial cells and gradients established via coculture with other cell types (99). Tien and coworkers have described protocols for forming endothelial tubes into collagen gels, which contain open channels and allow for endothelial tube perfusion and transport characterization (100). Wong et al demonstrated that the use of cyclic adenosine monophosphate (cAMP) containing medium was critical for forming stable and intact endothelial tubes (101). Due to the capabilities of microfluidic technology to control intercellular distance, and integrate 3D ECM and high resolution imaging, a number of groups have developed microfluidic models (Figure 7) that mimic tumor-endothelial interactions in the context of angiogenesis, tumor cell adhesion and extravasation.

Chung et al described a microfluidic design incorporating 3D ECM, which enables the investigation of angiogenic sprouting in response to tumor cells that were seeded in a separate channel and secreted angiogenic factors (102). Using a dual layer microfluidic device Song et al fabricated a microfluidic device that incorporated fluid flow and was able to deliver spatially restricted cytokine stimulation to endothelial monolayers (82). The authors showed that cytokine activation and shear stress had synergistic effects on tumor cell adhesion. Kaji et al presented a co-culture assay to study the effect of tumor-endothelial cell paracrine signaling by controlling of the flow direction on cell migration (103). Interestingly, directing the flow from the endothelial cells to the tumor cells had no effect on the movement of either cell type, whereas switching the flow direction from the tumor cells to the endothelial cells resulted in a retraction of endothelial cells. These results suggest that tumor cells modulate endothelial migration by paracrine factors,

whereas endothelial cell derived factors did not have any effect on tumor cell motility. A similar design was presented recently by Zheng et al who used integrated microvalves to control the intercellular distance between tumor and endothelial cells in order to monitor cell migration (104). Shin et al described a microfluidic chip that integrates two cell culture chambers that are interconnected via valves to simultaneously assay intra- and extravasation. Although the authors demonstrated the device's ability to differentiate between aggressive and benign tumor cells, they did not investigate endothelial monolayer functional and structural characteristics (105).

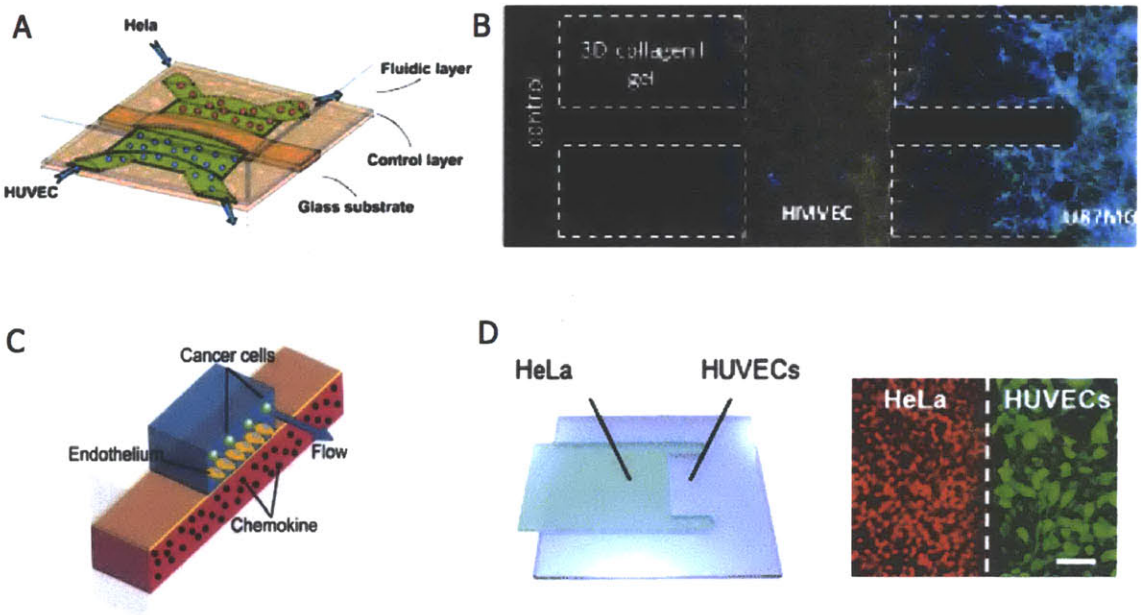

Figure 7: Microfluidic based assays to investigate tumor-endothelial cell interactions [figure adapted from (82), (102), (103) and (104)]

Despite significant progress in developing novel in vitro models to mimic the tumor microenvironment, there are still important challenges in terms of incorporating multiple physiologically relevant signals (e.g. fluid flow, 3D ECM and hypoxia) simultaneously and using more than only two cell types.

In vivo models of tumor-endothelial cell interactions

Findings from *in vitro* experiments need to be validated by comparing the observed phenotypes with *in vivo* studies, both with animal models in the pre-clinical setting, as well as with human tumors in patients in the clinical setting. Although, *in vivo* studies are more physiologically relevant, there are a number of challenges with studying the underlying mechanisms of tumor cell intravasation *in vivo*. Real-time intravital imaging typically requires specialized setups (e.g. dorsal skin window), which may perturb tumor pathophysiology (106). Dissecting the underlying molecular mechanisms of cellular interactions *in vivo* is further complicated due to the adaptive response of the microenvironment, such as recruitment of immune cells from distant organs. Furthermore, although many studies employing xenografts (subcutaneous or orthotopic) of human cancer cell lines in mice have shown similarities to human tumor histology, the chronic

evolution of stroma in human tumors and the usually compromised immune system in mice represent important differences (87). Genetically engineered mouse (GEM) models (e.g. the MMTV mammary tumor model) provide an improved model to study some types of tumors, but there are still notable differences in histology compared to human tumors and these models cannot recapitulate many aspects of human disease (87).

Most *in vivo* studies of tumor cell intravasation have been focused on mammary carcinomas utilizing orthotopic injection of rat adenocarcinoma MTLn3 or mouse carcinoma 4T1 into the mammary fat pat (46, 47, 60). Orthograft models in immunocompromised mice typically form spontaneous metastases through the invasion of the implanted tumor cells in the surrounding stroma, entry into the blood vessels and arrest in distant organs (e.g. lungs). The efficiency of tumor cell intravasation has been assayed with a number of different methods: a) by real-time multiphoton intravital imaging, b) by measuring the number of viable tumor cells in blood (tumor cell blood burden) and c) by histological examination of tumor sections at the primary tumor or at metastatic sites. Quigley and coworkers have developed the chick embryo chorioallantoic membrane (CAM) model, for comparative intravasation studies of different human tumor cell populations. In this model, tumor cells are grafted on the CAM membrane and tumor cell intravasation is assayed with live imaging, and collection of tumor cells from distant organs (55). The transparent zebrafish model is a useful model for studying the tumor invasion dynamics *in vivo*, where human tumor cells are injected in the fish peritoneal cavity, however, a fundamental limitation is that tumor cell size is larger than vessel size in this system (52). Another metastasis assay to study tumor-endothelial cell interactions in the context of extravasation is the experimental metastasis assay, where tumor cells are injected directly into the circulatory system of the animal through the tail vein (87). Intravasation in tumors in patients is characterized by histological examination of the biopsied tumor (12) and circulating tumor cell enumeration (51).

In Table 2 we summarize the previously described experimental systems, including their advantages and disadvantages.

Table 2: Comparison of different assays to investigate tumor-endothelial interactions

	Advantages	Disadvantages	References
2D cell culture	+Easy to use +High-throughput	-Physiological relevance -Live imaging (transwell) -Two cell types	(66)
3D cell culture	+Cell-ECM (integrin activation) +Drug resistance	- Confocal imaging - Modifications for spatial organization	(98) (96)
Microfluidic cell culture	+Cell-cell signaling +Gradients and Fluid Flow	- Low cell numbers - Biochemical assays	(107)
In Vivo	+Physiological relevance +Drug response	- Species difference - Tumor evolution	(87)

2.2 Experimental methods to measure endothelial permeability

Curry and collaborators (108) have pioneered methods (Figure 8) to measure the permeability of single capillaries *in vivo* in the frog mesentery using an apparatus including two micropipettes that switch immediately between clear and colored perfusates. The diffusive permeability (P_D [m/s]) of the endothelium is computed from the ratio of the area-normalized flux (J [moles / (sec x m^2)]) to the concentration drop (ΔC [moles/m^3]) across the endothelium:

$$P_D = J / \Delta C$$

The flux (J) is calculated using conservation of mass in a control volume around the capillary (Figure 8) and by monitoring the temporal changes in tracer intensity inside the tissue interstitium. Price and Tien describe a similar protocol for characterizing the diffusive permeability of single endothelial tubes formed in collagen gels using a fluorescent imaging method (100). The permeability coefficient P_D is computed in a similar way as described previously, by measuring the intensity drop across the endothelial barrier (ΔI, proportional to the tracer concentration) and the rate of intensity change inside the collagen gel dI/dt (see Appendix A1 and Supplementary Figure S7).

Different experimental methods have also been described to characterize endothelial permeability, which do not require real-time imaging of solute transport across the capillary wall. These methods are routinely employed to measure endothelial diffusive permeability in transwell systems and are based on sampling the temporal change of the soluble tracer (e.g. dextran) concentration in the upper and lower transwell (Figure 8) compartments (109). Recently, a number of microfabricated systems have been used to characterize endothelial permeability. An elegant two-layer membrane system was presented by Young et al, to measure diffusive permeability across an endothelial monolayer on a polycarbonate membrane using fluorescence imaging coupled with a convection-diffusion transport model (110). Douville et al described a low-cost, easy to fabricate PDMS-based device as an alternative to the transwell-based transendothelial resistance assay, which integrates commercial electrodes to measure transendothelial or transepithelial electrical resistance (111). However, both of the above systems utilize stiff substrates and the presence of the lower chamber makes real-time high-resolution imaging difficult.

An important consideration when studying endothelial permeability in cultured endothelial monolayers, is that the diffusive permeability values are typically one to two orders of magnitudes higher compared to values in intact capillaries *in vivo* (112). *In vivo* studies that investigated the effects of tumor growth on vascular permeability, used intravital imaging to characterize dextran distribution in the dorsal skin window in a mouse xenograft (113) and in a transparent zebrafish injected with human breast carcinoma cells (52).

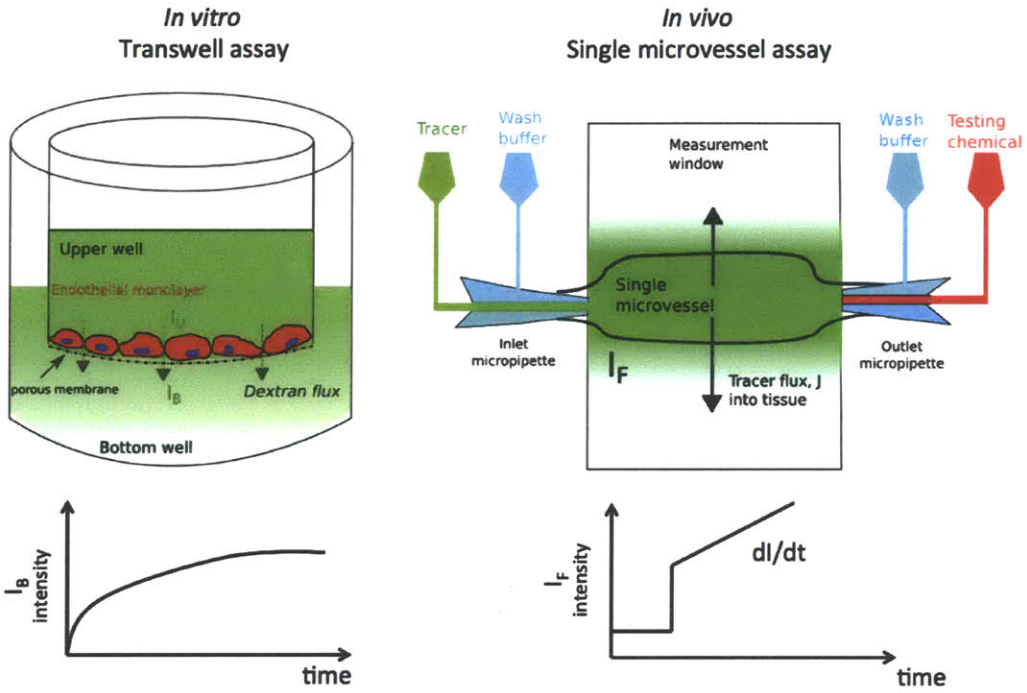

Figure 8: ***In vitro*** **and** ***in vivo*** **systems for measuring endothelial diffusive permeability using fluorescent tracers. Left: Transwell assay monitoring the intensity time profile in the bottom chamber. Right: Single microvessel assay monitoring the intensity time profile inside a measurement window [figure modified from (114)]**

The discussion of endothelial permeability in this thesis is focused on diffusive permeability, which accounts for transport of soluble molecules across the endothelial barrier through diffusion. Studies of endothelial barrier function have also investigated transport of water (hydraulic permeability) and electrical current (transendothelial resistance). Comparison of diffusive and hydraulic permeability values has shown that there is a positive correlation between them, suggesting that water and diffusible molecules share common transport routes across the endothelium (112).

2.3 Assay development

In this section we describe the design requirements for the microfluidic intravasation assay, the methods to measure endothelial permeability and the framework to quantify tumor cell intravasation.

Design requirements and proposed design

We considered the following points in order to model a physiologically relevant intravasation phenotype

1. Tumor cell invasion in a 3D ECM, that models the extravascular space in which tumor cells invade prior to entering into the blood vessels

2. Ability to perform live cell imaging at single cell resolution to investigate the underlying molecular mechanism (e.g. paracellular vs. transcellular) of tumor cell intravasation

3. Microchannel design to allow for access to the basal and apical endothelial surfaces for polarized cytokine stimulation and introduction of multiple cell types

4. Microchannel design to allow for the establishment of stable fluid flow and dextran gradients to quantify endothelial barrier transport properties. These gradients should be applied across the endothelium and the 3D ECM matrix and can be established via the secretion of soluble factors by a third cell type (e.g. macrophages) or exogenously applied (e.g. by addition of an EGF solution)

5. Large number (n>30) of experimental regions to increase the number of tumor cells in contact with the endothelium, which will enable reliable observation and quantification of rare, low probability intravasation events.

These design requirements were met by developing a device design in collaboration with Dr. Waleed Farahat and Dr. Levi Wood for the study of endothelial sprouting (115). This design includes two independently accessible microchannels (Figure 9A), where tumor and endothelial cells are seeded. These two channels (referred to as tumor and endothelial channels) are interconnected via a 3D ECM hydrogel, which includes 37 regions (each region is highlighted by a dashed window in Figure 9B) enabling multiple simultaneous observations within a single device. The tumor cells invade in 3D (Figure 9C) in response to externally applied growth-factor gradients (e.g. EGF, Figure 10B) or paracrine signals by other cell types (e.g. macrophages). On the 3D ECM-endothelial channel interface a continuous endothelial monolayer is formed, which enables the observation of cancer cell intravasation across a hollow vascular lumen and allows for access to the basal and apical surfaces through the microchannels. The endothelial monolayer is formed by seeding a single cell suspension of endothelial cells in the endothelial channel and allowing 48hours for cell attachment. The microfluidic intravasation assay may also be used to mimic different configurations of tumor cell invasion (Detailed protocols in Appendix A6 and Supplementary Figure 1). For example, the tumor cells can also be seeded as a single cell suspension or as a multicellular spheroid inside the 3D ECM, so that they are already in close proximity to the endothelial barrier at the beginning of the experiment.

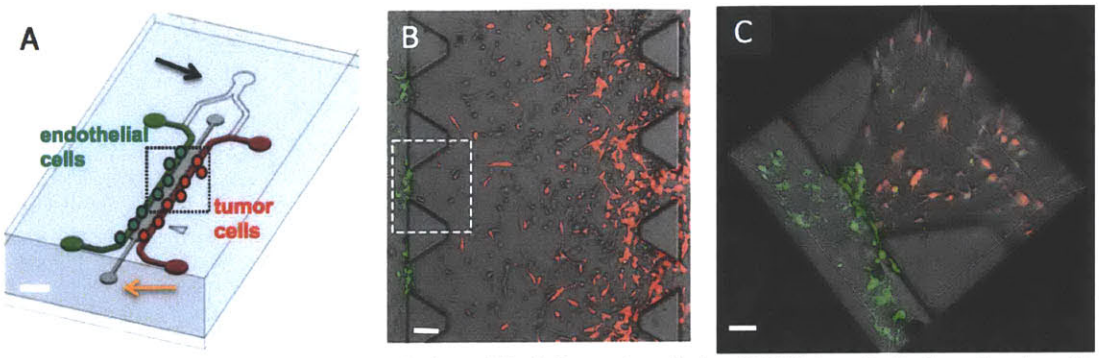

Figure 9: Microfluidic Intravasation assay design. (A) Schematic of the PDMS-based device showing the two interconnected channels (green and red) via a Y-junction (black arrow) and the 3D ECM gel region (grey region). (B) Phase contrast image corresponding to the dashed black rectangle in (A) showing an invasive human tumor cell line (red) invading towards an endothelial monolayer (green). (C) A 3D rendering of a single gel region, corresponding to the white dashed rectangle in (B). scalebar: (a) 1.5mm, (b) 150um, (c) 50 um.

Immunostaining of endothelial and tumor cells in the microfluidic device

After 48hours of tumor-endothelial cell interaction, devices were fixed with 4% PFA (Sigma-Aldrich) for 30minutes, washed twice with PBS (Invitrogen) for 1hour, permeabilized with 0.2% Triton-X (Sigma-Aldrich) for 10minutes, blocked with 10% Goat Serum (Invitrogen) in PBS for 2 hours and incubated overnight with primary detection antibodies. The next day, devices were washed twice with PBS for 1hour and a mixture of secondary antibodies (Alexa488, Alexa568, Alexa647), DAPI and Phalloidin were added and incubated for 2hours, after which devices were finally washed twice with PBS prior to confocal imaging. A detailed protocol is included in the Appendix A6.

Fluorescence-based imaging method to measure diffusive endothelial permeability

Apart from structurally characterizing the endothelial barrier, we also developed a method to characterize its function as a transport barrier, by monitoring diffusion of fluorescent dextran across the endothelial monolayer. This method is particularly important for the detailed investigation of the interplay between endothelial permeability and intravasation, and will become very useful for testing the hypothesis of increased tumor cell intravasation under conditions of impaired endothelial barrier function.

After confluent endothelial monolayers had been formed we used fluorescent dextran solutions at a concentration of 12.5 μg/ml to establish a diffusion-based mass flux across the endothelial monolayer (Figure 10A). Fluorescent images of dextran distribution were acquired using a Leica TCSPII confocal microscope equipped with a 10X NA=0.3 objective with live cell imaging capabilities (Figure 10B, C), for at least 10 gel regions per device. After adding the dextran solution in the endothelial channel only, devices were placed on the microscope stage and images were acquired after 30minutes to allow for thermal equilibration. Confocal z-stacks (15 z-slices with a Δz step of 10μm) were acquired every 10minutes for a duration of 2hours to ensure steady-state conditions for the evaluation of concentration profiles.

The endothelial diffusive permeability coefficient P_D was computed using:

$$P_D = \beta \cdot D \frac{dC/dx}{\Delta C}$$

where C is the dextran concentration (proportional to fluorescence intensity), ΔC is the change in concentration across the monolayer, β is an area correction factor, dC/dx is the slope of the concentration profile and D is the dextran diffusion coefficient in the ECM.

The equation $P_D = \beta \cdot D \frac{dC/dx}{\Delta C}$ was derived by considering mass conservation inside the ECM gel region at steady state, where the total dextran flux $P_D \cdot \Delta C \cdot A_{MONOLAYER}$ across the endothelial monolayer into the gel region is equal to the dextran outflux $D \cdot {}^{dC}/_{dx} \cdot A_{GEL}$. The area correction factor mentioned in the main text is given by $\beta = A_{GEL} / A_{MONOLAYER}$ and accounts for the change in cross-sectional area along the direction of dextran transport. The diffusion coefficients of the 10kDa and 70kDa dextrans were assumed to be 9×10^{-11} m^2/s and 4.5×10^{-11} m^2/s, based on a scaling law for soluble factor diffusion in buffer solutions (D_{BUFFER}) (116). These values are very similar (${}^{D_{GEL}}/_{D_{BUFFER}} \sim 0.94$) to the diffusion coefficients (D_{GEL}) in 2.5mg/ml collagen gels, that have a very large pore size (~0.1-1μm) compared to the hydrodynamic radius (~1-3nm) of the dextrans (117). The raw fluorescent intensity images were analyzed in MATLAB to compute the concentration gradient (${}^{dC}/_{dx}$) and step drop in concentration (ΔC) across the endothelium. To obtain a single value of ${}^{dC}/_{dx}$ and ΔC for each hydrogel region, we performed averaging across 30 pixel lines over the y-axis. The concentration gradient was evaluated at a distance 300μm away from the endothelial barrier where it was constant along the lateral direction, because of a constant cross-sectional area.

A finite element model was developed in COMSOL for analyzing transport across the endothelial monolayer within the microfluidic device and validating the evaluation framework. Constant concentration boundary conditions were defined at the inlet (C_{SOURCE}) and sink conditions at the outlet (C_{SINK}) of the control channel and at the gel filling port (Supplementary Figure 2). The numerical grid consisted of approximately 70 000 finite elements.

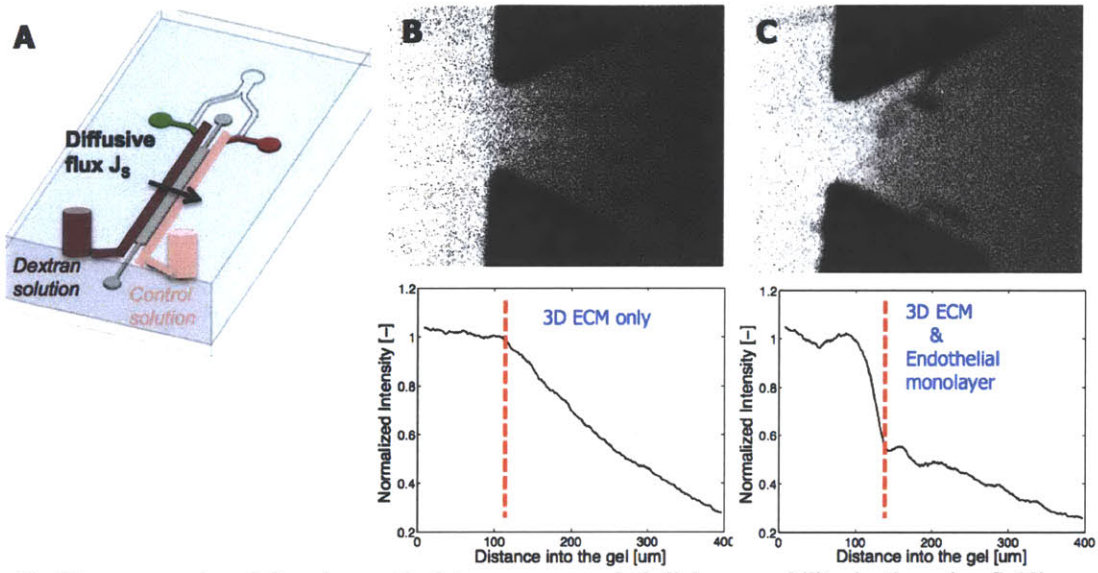

Figure 10: Fluorescence-based imaging method to measure endothelial permeability in the microfluidic assay. (A) Channel configuration with dextran and control (dextran-free) solutions to establish a diffusive mass flux across the endothelial monolayer. (B) Fluorescent image (top) and concentration profile (bottom) of 70kDa dextran distributubion inside a single gel region without an endothelial monolayer. (C) In the presence of an endothelial monolayer, there is a sharp drop in the intensity profile (bottom) and in the dextran distribution (top).

Intravasation metrics

Our assay allows for high-resolution real-time imaging of tumor cells located next to a hollow vascular lumen, enabling direct observation of tumor cell intravasation dynamics under a well-controlled microenvironment. For the intravasation studies, we used high-resolution confocal microscopy (63X water objective NA=1.2, Δz~2μm) to confirm the formation of an endothelial monolayer with continuous endothelial cell-cell junctions and to identify the exact location of tumor cells with respect to the endothelial monolayer (Figure 11A). We only analyzed tumor cells that where in contact with the endothelium (defined by a maximum distance of 10μm of the cell nucleus from the endothelial cell body), and manually identified whether the tumor cell was located on the basal or apical surface of the endothelial layer. Tumor cells that had adhered on the apical endothelial surface and were observed inside the vascular lumen were considered to have intravasated, whereas tumor cells that were in contact with the basal endothelial surface and were observed inside the 3D ECM were considered to be in the process of intravasation. This scoring scheme is schematically depicted in Figure 13A. We calculated the intravasation efficiency as the ratio of intravasated cells (cells on the apical surface) to the total cells in contact with the endothelial surface (sum of cells on apical and basal surfaces):

$$Intravasation\ efficiency = \frac{cells\ on\ apical\ surface}{total\ cells\ in\ contact}$$

This metric was computed for each device, by analyzing at least 20 gel regions, which corresponded to scoring at least 100 tumor cells. To minimize the experiment duration, we seeded human fibrosarcoma HT1080 tumor cells expressing an mCherry cytoplasmic marker inside the 2.5mg/ml collagen type I 3D matrix (seeding density 0.4 x 10^6 cells/ml) in order to

reduce the distance between tumor and endothelial cells and hence the time required for tumor cells to migrate towards the endothelial barrier. EGF gradients were established in these experiments to specifically bias tumor cell migration towards the endothelial barrier and to increase the number of intravasation events.

2.4 Assay Validation

In this chapter validation experiments are presented to characterize the intravasation efficiency of an aggressive tumor cell line, HT1080, which is already known to intravasate *in vivo* (56). The response of the endothelial barrier to different biochemical stimulation conditions was also investigated.

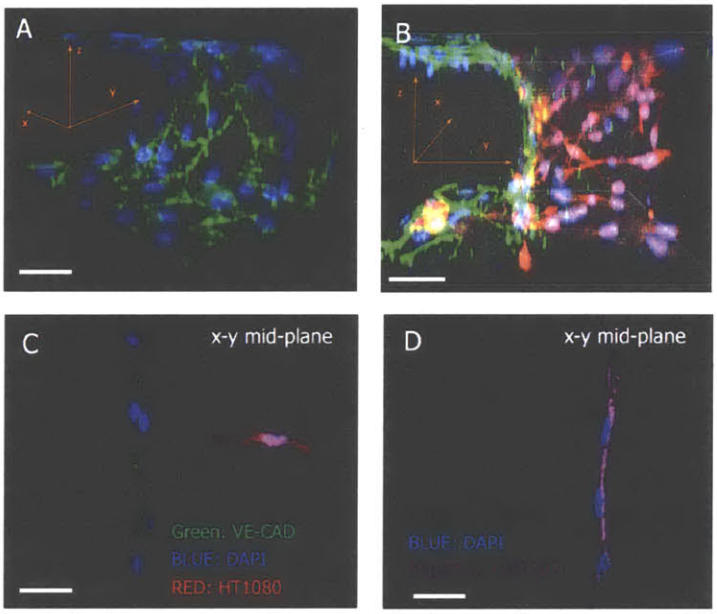

Figure 11: Validation of endothelial monolayer formation via immunofluorescence staining. (A) 3D rendering of endothelial cell-cell junctons in a single gel region (shown in white dashed rectangle in Figure 9B). (B) Formation of endothelial monolayer in the presence of invading fibrosarcoma cells. (C) A single confocal slice showing continuous endothelial Ve-cadherin junctions (green) in the presence of a single invading human HT1080 fibrosarcoma cell (red). (D) Confirmation of basement membrane deposition on the 3D ECM – channel interface by the HUVEC monolayers. Scalebar: (A-B) 50μm, (C-D) 30μm.

Formation of confluent monolayers and basement membrane deposition

To demonstrate the formation of confluent, 3D endothelial barriers (Figure 11A), we visualized the endothelial cell-cell junctions using a vascular endothelial cadherin antibody. We used two primary endothelial cell types, human microvascular dermal endothelial cells (HMVEC) and human umbilical vein endothelial cells (HUVEC), and demonstrated that they formed continuous cell-cell junctions spanning the full area of the microchannel surface and the 3D ECM – endothelial channel interface. These confluent endothelial monolayers formed in the presence of invading tumor cells in 3D (Figure 11B, C). To further demonstrate the structural integrity of the endothelial barrier, we also stained for the basement membrane deposited by the endothelial cells

on the 3D ECM-channel interface and found localized staining on the basal surface of the endothelial cells (Figure 11D).

Measurement of endothelial permeability for multiple endothelial cell types under different biochemical conditions and dynamic response to TNF-α

In order to validate the permeability measurement framework and to demonstrate the utility of our assay we performed diffusive permeability measurements for a number of different endothelial cell types and biochemical conditions. We compared the experimental distribution of fluorescent dextran at steady state (Figure 12A) with the computational simulations (Figure 12B) to validate our evaluation framework. A characteristic fluorescent intensity profile is shown in (Figure 12C) with the concentration step drop across the endothelial barrier and the concentration slope inside the 3D ECM. Endothelial permeability values were significantly lower for the high molecular weight dextran (70kDa) compared to the low molecular weight (10kDa), suggesting that the endothelial monolayer in the microfluidic device formed a size-selective barrier.

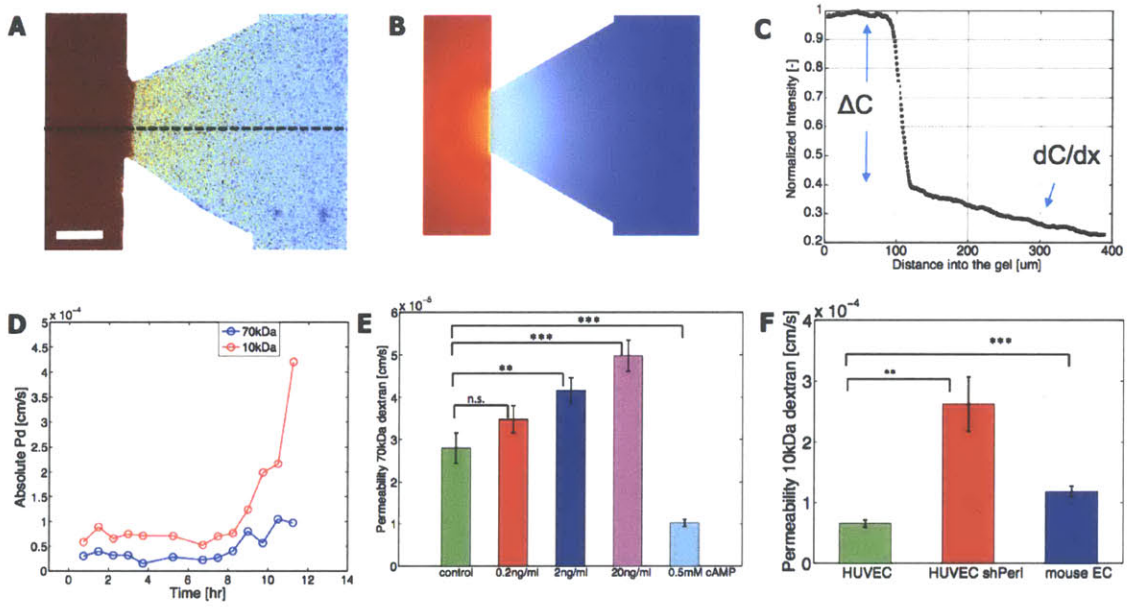

Figure 12: Characterization of endothelial permeability. (A) Experimental measurement of 10kDa fluorescent dextran distribution in a single gel region (as outlined in Figures 9 and 10). Darker red color indicate high intensity, whereas blue color indicates low intensity. Scalebar: 50μm. (B) Computation simulation of the dextran distribution. (C) Intensity profile along the dashed line shown in (A). (D) Time plot of permeability evaluation after addition of TNF-α at t=0hr, demonstrating barrier selectivity (E) Endothelial permeability to 70kDa dextran dose response of TNF-α and to 0.5mM of cAMP for a HUVEC monolayer. Average values for n=12 regions per condition. (F) Characterization of different endothelial cell lines, HUVEC, HUVEC cell line knockdown for Perlecan (shPerl) and murine brain endothelial cell line. Average values for n=6 regions per condition. Error bars represent standard error of the mean.

By monitoring the intensity profiles in time, we also measured the dynamics of endothelial permeability upon stimulation with TNF-α (at t=0hr). We found that permeability remained relatively constant for 8hrs and then gradually increased by approximately 4-fold and 2-fold for the 10 and 70kDa respectively (Figure 12D). Experiments to characterize the endothelial permeability response to biochemical factors that can impair (TNF-α) or enhance (cyclic

adenosine monophosphate [cAMP]) the endothelial barrier were performed to demonstrate the utility of our assay as a discovery platform (Figure 12E). Different doses of TNF-α (0, 0.2, 2 and 20 ng/ml) where applied to a confluent HUVEC endothelial monolayer for 48hours and the permeability to 70kDa molecular weight was measured. A graded response was measured, where stimulation with 0.2ng/ml did not result to significant changes ($p=0.16$) compared with the control, whereas stimulation with 2 and 20ng/ml resulted in significant differences ($p=0.008$ and $p=3x10^{-4}$). We also stimulated the endothelial barriers with cAMP to test whether we could enhance endothelial barrier function. Endothelial diffusive permeability in confluent HUVEC monolayers stimulated with cAMP (0.5mM) for 48hours was significantly ($p=4x10^{-4}$) decreased by 2.8fold compared to the control.

In Figure 12F we present the diffusive permeability to 10kDa dextrans for wild-type primary human endothelial cells (HUVEC), the same primary cells expressing lower levels of Perlecan (22) and mouse brain immortalized endothelial cells line (BrEnd3). We used the shPerlecan-HUVEC line as a model of "dysfunctional" endothelial cells, which may mimic tumor endothelial cells (22), and the mouse brain endothelial cells as a model of immortalized continuous cell lines. The wild-type HUVEC cells exhibited a significantly lower permeability (2.8×10^{-5} cm/s) compared to the mouse endothelial cells (1.2×10^{-4}cm/s, $p=7.1x10^{-4}$) and HUVEC-shPerlecan (2.6×10^{-4}cm/s, $p=0.0048$). Most of the experiments described in this thesis are conducted using HUVEC cells, given their lower permeability and their ability to form reliably monolayers.

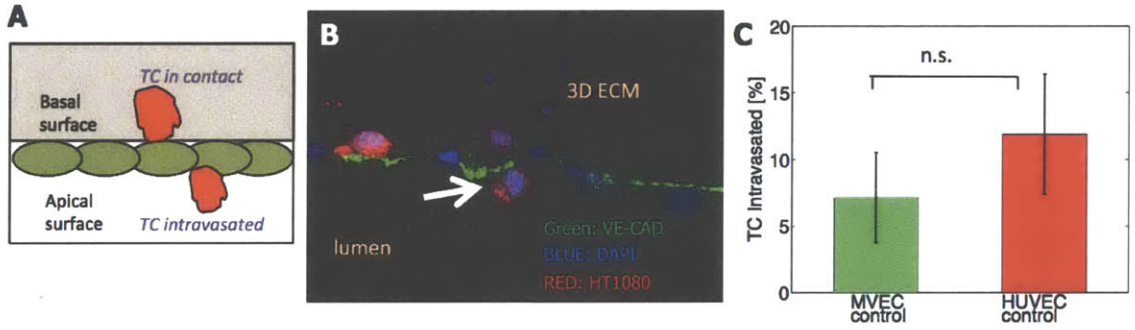

Figure 13: (A) Schematic showing method to identify a tumor cell (TC) in contact with the endothelial barrier located on the basal surface and a TC that has intravasated and is on the apical surface (B) Single confocal slice showing a single fibrosarcoma cell (HT1080) that has intravasated across a HUVEC monolayer (white arrow). Scalebar: 25μm. (C) Quantification of HT1080 intravasation rates for microvascular (MVEC) and macrovascular (HUVEC) monolayers. Average values for n=3 devices per condition. Error bars represent standard error of the mean.

Intravasation metrics for a human metastatic cancer cell line

To demonstrate the ability to observe tumor cell intravasation, we used a highly aggressive fibrosarcoma cell line (HT1080), which has been used previously for investigating the molecular mechanism of intravasation (53). Tumor cells (TC) were seeded inside the 3D ECM (2.5mg/ml collagen type I), allowed to interact with HUVEC and microvascular endothelial cells (MVEC), then fixated and confocal imaging was performed to identify intravasation events. A tumor cell that was located on the apical endothelial surface (Figure 13A, B) was scored as a tumor cell that has intravasated, whereas tumor cells that was located inside the 3D matrix and was in contact with the basal endothelial surface was identified as a tumor cell in contact. By calculating the

ratio of intravasated to total cells (percentage of TC that had intravasated Figure 13C) we showed that the cancer cells were able to cross the endothelial barrier at statistically similar (p=0.45) efficiencies with 7.14% and 11.9% for the MVEC and HUVEC monolayers.

2.5. Assay comparison with other systems and discussion of limitations

Due to the challenges of imaging tumor cell motility *in vivo* and recreating a physiologically relevant microenvironment *in vitro*, the underlying mechanisms of tumor cell intravasation remain largely unknown. Experimental systems to investigate tumor-endothelial interactions in the context of intravasation include the Boyden chamber and xenograft or transgenic animal models. These systems however, typically do not allow accurate control of important microenvironment factors and tumor cell imaging at single cell resolution. We have developed a microfluidic assay that enables real-time visualization and quantification of the interactions between tumor cells and an endothelial monolayer in the context of tumor cell invasion and intravasation. In this chapter we discussed the design considerations of our assay and presented experimental methods to investigate tumor cell intravasation and endothelial barrier function. We validated this microfluidic assay by characterizing structurally and functionally the transport properties of the endothelial barrier for different endothelial cell lines and under various biochemical conditions. Finally, we used a highly metastatic human fibrosarcoma cell line to demonstrate the assay's utility for studying intravasation.

Comparison with other tumor-endothelial cell interaction assays

Compared to other *in vitro* models of tumor-endothelial cell interactions, the assay presented in this thesis has the advantages of a well-characterized endothelial barrier with a hollow lumen on a 3D matrix and the inclusion of a third cell type (macrophages: see chapter 4). Previous microfabricated designs by Kaji et al (103), Zheng et al (104) and Stine et al (86) investigated tumor-endothelial interactions on 2D stiff substrates. Khuon et al (43) investigated tumor-endothelial cell interactions using a 3D collagen type I matrix, but did not include growth factor gradients and did not characterize the functionality of the endothelial barrier.

Permeability characterization method

Due to the use of a fluorescence-imaging based method to characterize diffusive transport of passive macromolecules across the endothelial barrier, we can acquire spatially resolved measurements of endothelial permeability in each gel region (out of the total 37). In contrast, the traditional transwell method provides a single measurement of P_D across the entire monolayer. The method presented in this thesis allows for a detailed regional investigation of endothelial barrier function with respect to different tumor cell numbers and also enables accurate measurements of endothelial permeability dynamics (in cm/s) for direct comparison of endothelial barrier function between different studies. Measuring P_D is an important consideration for studies employing the transwell assay, since the endothelial barrier function may critically influence tumor-endothelial interactions and intravasation.

The developed analysis framework in this thesis is based on a quasi steady state assumption to evaluate the intensity profiles. This assumption may introduce errors, especially for transient changes in local intensity values due to pressure-induced flow disturbances. To ensure steady state conditions, dextran transport was monitored for long durations (2hours or 20hours for the invasive growth experiments). A further improvement in the experimental system would be to integrate a fluid flow-based system to deliver constant concentration on the source and sink dextran channels and simplify experimental conditions (i.e. constant boundary condition) for analysis. Alternatively, a transient analysis framework could also be implemented to more accurately capture the dextran concentration profile changes in time. We also compared our analysis method with the method previously described by Curry et al (108) and found similar values of diffusive permeability (Appendix A1 and Supplementary Figure 7).

Endothelial permeability values

The endothelial monolayers formed in the microfluidic device exhibit size-selective transendothelial transport with a ratio of 5.5 for the low molecular weight (10kDa) to the high molecular weight (70kDa) permeability values. Previous measurements of this ratio for the same molecular weight dextrans showed lower ratios, 2.5 for HUVEC monolayers in vitro (101) and 3.5 for tumor blood vessels in mouse xenografts (113). The absolute P_D values for the larger molecular weight dextrans in our system (7.5×10^{-6}cm/s) is in the same order of magnitude with measurements for the same dextran size across bovine fetal aortic endothelial cells (5.6×10^{-6}cm/s) in transwell systems (109) and in engineered HUVEC monolayers (2×10^{-6}cm/s) in 3D matrices (118). However, the permeability values in our microfluidic device are significantly higher compared to measurements in normal intact venules (5×10^{-7}cm/s) *in vivo* (112), but are in the same order of magnitude with permeability values to 70kDa dextrans (1×10^{-6}cm/s) in mouse xenografts (113).

Our permeability measurements of TNF-α dose response are in agreement with previous measurements (119) of transendothelial electrical resistance that also showed a graded dose response to TNF-α. More specifically, the lowest TNF-α concentration (~2ng/ml) to induce a significant increase in endothelial permeability and the time (6-8hr) required to notice changes in endothelial permeability are in agreement with other studies on cultured endothelial monolayers (120). In addition, the 2.8-fold enhancement in endothelial barrier function to 70kDa dextran via the addition of cAMP is in agreement with measurements of engineered HUVEC monolayers in 3D matrices (101). Finally, the assay sensitivity is also highlighted by the permeability measurements of different endothelial cell lines.

Future work is required to investigate methods to reduce the endothelial permeability values to more closely mimic *in vivo* conditions. These experiments could include culture under serum-reduced and growth-factor reduced medium, since all endothelial growth cultures reported in this thesis were performed with complete EGM-2MV medium containing (5% fetal bovine serum) and relatively high (~10ng/ml) concentration of VEGF. Another factor to be investigated is whether the addition of EGF modulates endothelial permeability, although this is probably unlikely since a previous study has shown that human lung microvascular endothelial cells express low levels of EGF receptors (121). It would also be interesting to explore the structural

integrity of the endothelial basement membrane and whether it correlates with the permeability measurements.

Finally, another experiment that could be performed in this direction is to investigate whether the integration of a thin ECM coating that would mimic the basement membrane on the microchannels could lower the endothelial permeability. Although, it is unclear whether this addition will significantly impact permeability, it will be a step towards forming more physiologically relevant monolayers with a homogeneous basement membrane coating across the channel-gel-PDMS interfaces. Studies performed in transwell systems showed, that filter coating with collagen, fibronectin or gelatin had small effects on regulating endothelial permeability to dextran or albumin (122).

Quantification of intravasation events

Since the quantification method used in this thesis relies on the manual identification of the tumor cell position with respect to the endothelial monolayer, two independent observers were asked to analyze the same experimental dataset. Both observers were given the same criteria of how to identify an intravasation event and each observer did not know the results of the other observer's analysis in order to avoid bias in the quantification. Although, both observers identified intravasation events, there was a two-fold but statistically insignificant ($p=0.0675$) difference (5.33% vs. 9.8%) in the intravasation scores.

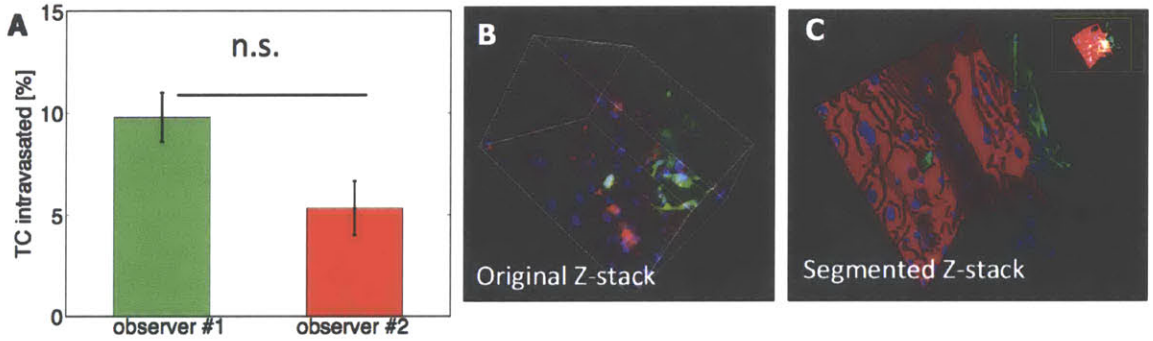

Figure 14: (A) Comparing bias in scoring intravasation events between different observers. (B) Raw data of confocal z-stack for scoring intravasation events. Average values for n=3 devices per observer. Error bars represent standard error of the mean. (C) Segmented z-stack of the original z-stack in (B) for automatic quantification.

To overcome the previously mentioned limitation we established a collaboration with Prof. Carlos Ortiz's group in University of Pamplona (Spain), to develop image analysis methods for automatically scoring intravasation events. This approach is based on segmenting the fluorescent confocal z-stacks to identify the tumor cells and the endothelial monolayer. Scoring of the intravasation events can be performed by computing the distance of the tumor cell centroid from the endothelial barrier interface, in a similar approach as the one presented in the next chapter to quantify tumor-endothelial interaction events.

Assay limitations and improvements

In the intravasation assay configuration, where tumor cells are already embedded in the 3D matrix, and therefore tumor cells may have already migrated on the endothelial channel during the process of endothelial monolayer formation. Even though, our results of low tumor cell numbers observed on the luminal endothelial surface suggest that this is unlikely, we propose a modification to the device design to overcome this limitation: the introduction of an additional cell-free 3D matrix between the existing gel region and the endothelial monolayer, that the tumor cells would have to invade prior to interacting with the endothelial barrier. It is noted that this issue is not applicable to the invasive growth assay configuration, where the endothelial monolayer is already formed prior to tumor cell seeding on the opposite channel.

Although, the role of edge effects on tumor cell migration and intravasation has not been investigated here, an important direction for future work is the development of microfluidic devices, which do not require in-plane PDMS posts to confine the 3D matrix between two media channels. Liu et al present a "post-less" design, which includes a stop-flow junction and is capable of incorporating a cell-laden 3D ECM next to a medium containing channel (123). The possibility that tumor cell invasion and intravasation could be influenced by the presence of the stiff 2-D surfaces (top PDMS wall and bottom glass coverslip) should also be investigated by designing devices of different channel heights. Interestingly, in the intravasation experiments, we observed that the tumor cells that had intravasated were located on multiple z-levels. Further quantification is required to investigate whether there are any trends on preferential intravasation along the top and bottom stiff substrates compared to the mid-plane z-levels.

Another important consideration is the large device-to-device (inter-device) variability among control permeability values. In the TNF-α dosing experiments we evaluated the diffusive permeability values for at least 10 regions per device and included data from at least 3 devices when reporting average permeability values to different TNF-α concentrations. This large inter-device variability could be explained by differences in endothelial seeding. To reduce inter-device variability, improved methods to accurately control the endothelial cell seeding density in the microchannel (e.g. using syringe pumps) and enhance the monolayer formation via timing of soluble factors delivery (e.g. growth signals, such as VEGF) would be necessary.

Translation of the device for use in the industrial setting by pharmaceutical companies would require that different fabrication materials be utilized. Small hydrophobic molecules that can be secreted by cells under control or drug testing conditions can be adsorbed by PDMS (84), and result in altered cellular responses compared to traditional cell cultures, since the available concentration of the various factors (e.g. autocrine factors) may be affected by PDMS. Ongoing work in the Kamm lab includes the development of microfluidic devices using hard plastic, which is the standard material for drug screening assays in the pharmaceutical industries.

Chapter 3: Tumor-Endothelial Interactions

The molecular and cellular mechanisms of the tumor-endothelial cell interactions in the context of tumor cell invasion, extravasation, intravasation and the effects of tumor cells on the endothelial monolayer structural and functional characteristics are discussed in this chapter. Experiments to investigate the effect of endothelial permeability on the number and dynamics of tumor-endothelial cell interactions are presented and compared with published results.

3.1. Mechanisms of Tumor-Endothelial Cell Interactions

Endothelial and tumor cell interactions involve bi-directional paracrine and juxtracrine signaling loops, with both cell types secreting and sensing soluble factors and modulating their migratory behavior. Importantly, apart from the well-established pro-angiogenic role of tumor cells, many studies suggest that endothelial cells have an active role in regulating tumor cell invasiveness, which can be mediated by the secretion of different soluble factors with both promoting (88) and inhibitory (22) functions.

Role of tumor-endothelial cell interaction on endothelial monolayer structure, endothelial phenotype and endothelial permeability

Endothelial junctional molecule expression of VE-Cadherin and PECAM-1 has been shown to be reduced during coculture with invasive breast tumor cells (MDA-MB-231) in a matrix metalloproteinase (MMP)-dependent mechanism, whereas less invasive breast carcinoma cells (MCF-7) did not affect endothelial cell junction expression (90). In these studies Mierke et al used a 3D extravasation assay and demonstrated that endothelial monolayers are not a passive barrier, but rather they become altered in the presence of tumor cells. Interestingly, magnetic bead based measurements of endothelial cell biomechanical properties, demonstrated that tumor cell contact reduced endothelial stiffness, which could play a critical role in transendothelial migration. Recently, Haidari et al investigated in detail the molecular mechanism of endothelial barrier disruption upon contact with invasive tumor cells *in vitro* (124). Contact of breast cancer cells (MDA-MB-231) with HUVEC monolayers induced tyrosine phosphorylation of VE-Cadherin, followed by dissociation of β-catenin from the cell-cell junctions and resulted in endothelial cell retraction. These phosphorylation events were mediated by activation of the H-Ras/Raf/MEK/ERK signaling pathway via the α2β1 integrin on the tumor cells while transendothelial migration was inhibited by blocking H-Ras and Myosin Light Chain (MLC). The authors also confirmed that this mechanism was involved in VE-Cadherin remodeling by different tumor cell lines, including prostate and ovarian cancer cells. This study however, was mainly focused on the biochemical pathways and immunofluorescence imaging of VE-Cadherin junctions and did not investigate functional changes of the endothelial barrier.

Studies by Voura et al (89) and Peng et al (125) have also shown that melanoma cells can induce remodeling of endothelial cell-cell junctions. Using a micropatterned coculture system, Stine et al showed that upon melanoma-endothelial cell coculture, melanoma cells upregulated Neuropilin 2, which resulted in enhanced tumor cell proliferation and promoted endothelial cell migration (86). The authors showed that the enhanced endothelial cell migration was inhibited by

a blocking antibody against Neuropilin 2, whereas tumor cell lines of different cancer types showed variability in their effects on endothelial cell migration. All the studies reviewed above, include interactions of single tumor cells with an endothelial barrier. Heyder et al showed that interaction of human bladder cancer spheroids with a HUVEC monolayer irreversibly damaged the endothelium at the site of extravasation, raising questions about potential differences between single cell and collective tumor cell behavior during tumor-endothelial interactions (126).

Role of tumor-endothelial cell interactions on endothelial barrier function

Endothelial permeability can be regulated by biochemical factors in the tumor microenvironment, which can be secreted from tumor cells. *In vitro* studies from different groups demonstrated that paracrine factors from ovarian cancer (127) and melanoma cells (128) can impair endothelial barrier function (see chapter 4 for detailed discussion). *In vivo* studies in zebrafish injected with VEGF overexpressing tumor cells (52) and in murine tumors (113) have confirmed these observations. Weis et al investigated the role of endothelial barrier function in extravasation (129). Tail vein injection of tumor cells overexpressing VEGF resulted in enhanced extravasation, and the effects of increased permeability were shown through intravenous injection of different VEGF doses.

Tumor-endothelial cell interactions in the context of tumor cell invasion

Apart from the well-established effects of tumor cell secreted factors (e.g. VEGF) on endothelial cell proliferation and migration, a number of studies have shown that endothelial cells can enhance tumor cell invasion via paracrine signaling. Kenig et al showed that Stromal Derived Factor 1 (SDF-1) secreted by endothelial cells resulted in increased invasion of glioblastoma cells via upregulation of MMP-9 (130). Mierke et al showed that endothelial cells show tumor pro-invasive effects in a 3D extravasation model mediated by endothelial cell specific secretion of IL-8 and Gro-β (131). Similar findings were reported by Issa et al who showed that lymphatic endothelial cells promoted melanoma cell proteolytic activity and cell motility via a paracrine loop involving tumor cell secreted VEGF-C and lymphatic endothelial cell secreted CCL21 (132). Franses et al showed that normal endothelial cells secrete factors that have inhibitory effects on tumor cell invasion and resulted in overexpression of MMP inhibitors in the tumor cells (22). Interestingly, in the same study, shRNA induced reduction in the expression of the basement membrane protein perlecan resulted in IL-6 overexpression in the endothelial cells which increased invasion in breast and lung carcinoma cells (22).

Tumor-endothelial cell interactions in the context of extravasation

Tumor-endothelial cell juxtracrine signaling and endothelial cell receptors are critical on tumor cell transmigration. Liang et al showed that lectin-like oxidized-low-density lipoprotein receptor 1 (LOX-1) promotes tumor cell adhesion and extravasation on TNF-α treated endothelial cells (133). This study however, did not investigate whether tumor cells specifically interacted with LOX-1 and whether endothelial barrier integrity was affected. A series of articles from Voura and colleagues have investigated the heterotypic cell-cell interactions during melanoma transendothelial migration. The first study from this group revealed that melanoma cells form heterotypic N-Cadherin contacts, which localized at the endothelial homotypic VE-Cadherin and PECAM1 junctions which were redistributed as the tumor cells extravasated (89). Further studies

investigated the role of PECAM1, which is required for leukocyte extravasation, and found that antibody blocking of PECAM1 did not affect melanoma cell extravasation (134). Finally, the role of melanoma cell α5β3 expression was shown to be critical for successful melanoma extravasation (135). Further studies on heterotypic cell-cell junctions have shown that inhibition of tetraspanin CD9, which was found to localize in tumor-endothelial cell regions of contact, reduced the ability of melanoma cells to transmigrate. Kargozaran et al showed that endothelial cells can have a permissive role in facilitating tumor cell extravasation via secretion of MMP-2 (88). Although, the authors showed that siRNA knockdown or pharmacologic inhibition of endothelial secreted MMP-2 reduced the ability of aggressive MDA-MB-231 carcinoma cells to transmigrate, they did not investigate the mechanism of MMP-2 upregulation and whether MMP-2 impaired endothelial cell-cell junctions or basement membrane architecture.

Tumor-endothelial cell interactions in the context of intravasation

Most studies of tumor cell intravasation have taken a tumor cell centric approach, focusing on genetic and transcriptional changes on tumor cells only. Twist, a critical regulator of epithelial to mesenchymal transition has been shown to be essential for metastasis formation in an orthotropic murine mammary xenograft (47). Yang et al showed that siRNA mediated silencing of the transcription factor Twist, which is critical for embryonic morphogenesis, reduced the tumor blood burden and also increased cell migration when expressed in normal epithelial cells. Another study by the Weinberg lab, further demonstrated the role of epithelial to mesenchymal transition regulators in facilitating tumor cell entry into the blood stream. Tumor cells induced to overexpress the microRNA miR-10b showed increased invasion *in vivo* and formed lung metastases (58). Investigation of the underlying molecular mechanism showed that Twist induces miR-10b, which resulted in overexpression of the pro-metastatic gene RhoC. I*n vivo* and *in vitro* studies from the Condeelis group have investigated the role of different actin regulatory proteins on tumor cell migration and intravasation in murine mammary tumors. In particular, it was shown that N-WASP is required for intravasation, since N-WASP silencing or overexpression of a dominant negative form resulted in a marked decrease in invadopodia formation and intravasation (59). In a relevant study, the role of the actin binding protein MenaINV was investigated and it was shown that expression of MenaINV increased tumor cell sensitivity to EGF and was associated with increased invasion and intravasation (46). The critical role of EGF pathways in intravasation has also been demonstrated by Le Devecek et al who demonstrated that rat adenocarcinoma MTLn3 cells overexpressing the epidermal growth factor receptor ErbB1 showed increased tumor blood burden when injected orthotopically in $Rag2^{-/-}$ $\gamma c^{-/-}$ mice lacking natural killer cells (60).

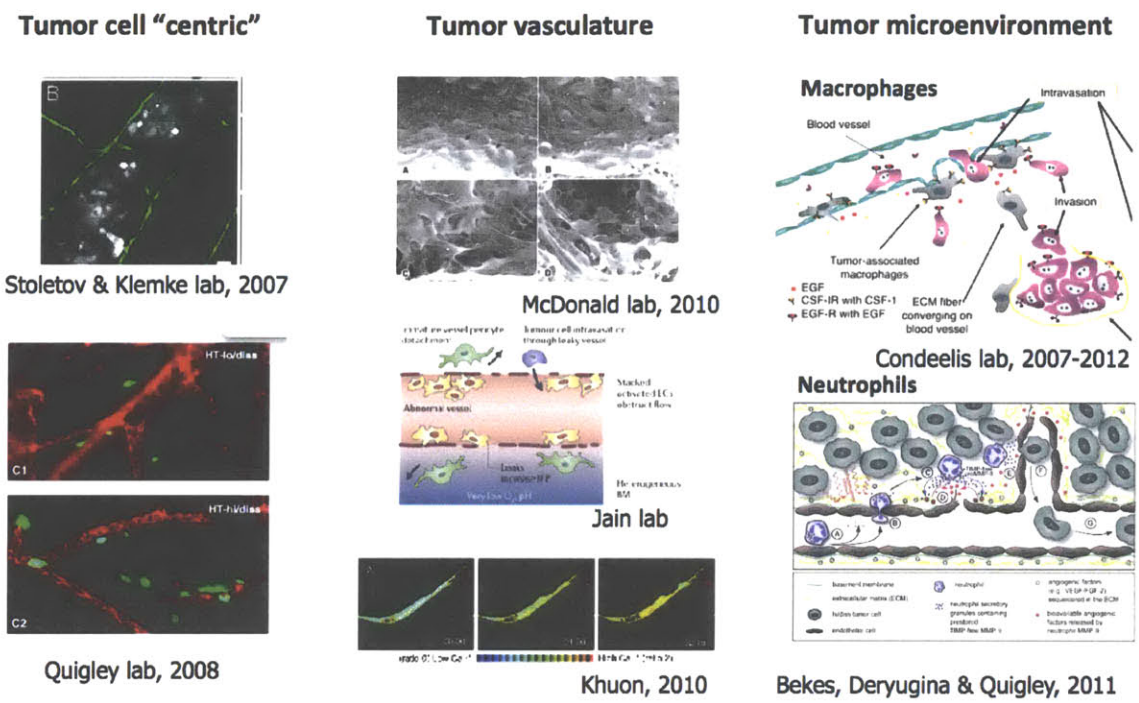

Figure 15: An overview of studies that have investigated the role of altered signaling pathways in tumor cells, the role of endothelial cells and the role of cells in the tumor microenvironment [figure adapted from (13), (16), (29), (43), (52) and (56)]

In addition to the previously discussed studies on EMT pathways and actin regulatory proteins, Kim et al investigated the role of proteases in intravasation using the chorioallantoic membrane assay (54). Using human cancer cell lines (HEp3, HT1080, MCF7, MDA231) of different metastatic capacities they showed that MMP inhibition resulted in reduced intravasation in the chick embryo CAM assay. Studies from the Quigley group reported an unexpected effect of increased intravasation for MMP-9 siRNA silenced human fibrosarcoma cells (55), suggesting that tumor-derived MMPs may have different effects than stromal cell derived MMPs and raising important questions about the mechanisms of intercellular MMP regulation in the tumor microenvironment. Quigley et al serially cultured HT1080 cells in the CAM assay to select for tumor cells that displayed high intravasation efficiency and compare the expression of cell surface proteins between high and low intravasation efficiency populations (56). Comparison of the two populations demonstrated that TIMP-2 expression reduced intravasation efficiency, whereas the surface proteins NCAM-1, JAM-C and TF increased intravasation efficiency. Interestingly TIMP-2 has also been linked with tumor cell transendothelial migration by Peyri et al in a breast cancer cell line (136). Apart from the previously described pathways, a comprehensive study from the Quigley group investigated the effects of Tetraspanin CD151 on tumor cell intravasation (53). *In vivo* studies of human tumor cells in mouse and avian models showed that blocking the integrin-associated CD151 reduced intravasation efficiency in a mechanism associated with increasing cell-ECM adhesion and therefore impaired tumor cell migration. Elegant intravital imaging studies from Sahai and coworkers have also shown the critical role of cell motility in intravasation (41). Using a TGF-β live cell reporter, it was shown that transient TGF-β activation promoted single cell motility and invasion into the blood vessels, whereas cohesively migrating cells that were only able to invade the lymphatic vessels did not

express active TGF-β signaling. Quigley and coworkers also performed comparative analyses of cell populations with different intravasation efficiencies in prostate cancer cells (57). Expression of VEGF and the serine protease urokinase-type plasminogen activator (uPA) correlated with higher intravasation levels, and this cell population also showed increased angiogenic and invasive potentials. Stoletov et al also showed that overexpression of VEGF enhanced the early intravasation steps of human breast cancer cells injected in zebrafish (52). Also, in relation to the actin cytoskeleton regulation studies reviewed previously, Stoletov et al also investigated the role of RhoC, a member of the small family of GTPases involved in actomyosin contractility, and found that in combination with VEGF it significantly increased the ability of tumor cells to complete early intravasation steps. The association between pro-angiogenic effects and highly efficient tumor cell intravasation is also supported by studies in human colorectal tumors that show a positive correlation between tumor vessel density and circulating tumor cell counts (51).

Apart from the important role of tumor cell intrinsic factors in intravasation, elegant work from the Condeelis group has shown that perivascular macrophages are also associated with tumor cell intravasation (13). Experiments in mice defective for CSF-1 production, showed a six-fold decrease in tumor associated perivascular macrophages and a 16-fold reduction in tumor cells in the blood, indicating the critical role of macrophages in intravasation. A less dramatic, five-fold reduction was observed when an EGFR inhibitor was used in the presence of macrophages to interfere with the EGF/CSF-1 paracrine loop. The involvement of macrophages in facilitating increased intravasation has also been demonstrated in human tumors using immunohistochemical staining in tumor sections from patients with metastatic breast cancer (12). Bekes et al investigated the role of another immune cell type, neutrophils (16). HT1080 and PC-3 tumors grown in murine and avian models recruited MMP-9 expressing neutrophils, which released a TIMP-free proMMP-9 to enhance tumor angiogenesis and facilitate intravasation. In addition to the *in vivo* studies described previously, Khuon et al used a 3D coculture *in vitro* assay to investigate the role of endothelial myosin light chain kinase (MLCK) and myosin II-regulatory light chain (RLC) during transendothelial migration (43). The authors found that tumor-endothelial contact resulted in upregulation of endothelial MLCK, while RLC activity was elevated during transcellular transendothelial migration. Although the authors suggested that this assay modeled intravasation, the transcellular invasion assays were performed on 2D surfaces, which is not necessarily physiologically relevant. Furthermore, in the 3D experiments it was unclear whether tumor cells could completely intravasate across the vessel-like endothelial networks.

Taken together, the above described studies indicate that tumor cell intravasation can be regulated by diverse signal transduction pathways and tumor microenvironment modifications, including actin cytoskeleton regulatory (MenaINV and RhoC) proteins, chemotactic pathways (EGF), invadopodium formation (N-WASP), EMT regulators (Twist and TGF-β), proteases (TIMP-2, MMP-9 and uPA), ECM adhesion (CD151), macrophages, neutrophils and blood vessel remodeling (VEGF). However, most of these studies did not address the question of whether these regulators are also involved in remodeling the tumor microenvironment. This is an important question that can be addressed with the *in vitro* microfluidic assay developed in this thesis, to elucidate mechanisms of tumor-microenvironment interactions in tumor cell intravasation.

Table 3: Mechanisms of tumor-endothelial cell interactions

	Phenotypic change	Mechanism	References
Tumor cell secreted factors	Endothelial hyperpermeability by **paracrine tumor cell factors**	VEGF secreted by TC	(127)
Tumor cell secreted factors	Endothelial cell migration regulated by **paracrine tumor cell factors**	Neuropilin-2 overexpressed by tumor cells upon coculture enhanced	(86)
Tumor cells secreted factors	Endothelial cell migration regulated by **paracrine tumor cell factors**	Tumor-secreted factors, specific factors not identified	(103)
Tumor cell contact	Tumor cell transendothelial migration by modulating **endothelial cell-cell junction**	TC bound to EC via α2β1 integrin induced H-Ras pathway activation leading to VE-Cad phosphorylation resulting in b-catenin dissociation	(124)
Tumor cell contact	Enhanced **tumor cell extravasation** by TC overexpressing **integrins**	$\alpha5\beta1^{high}$ TC extravasated more effectively	(90)
	Tumor cell contact regulate **endothelial cell-cell junction expression** via **proteolysis**	Reduction in VE-Cadherin and PECAM-1 expression via an MMP-dependent and tumor cell type specific mechanism	(90)
Tumor cell contact	Trans- vs paracellular invasion route determined via endothelial cell **cytoskeletal contraction**	Endothelial MLCK and RLC mediated	(43)
Tumor cell Cytoskeletal	MenaINV tumor cells show **coordinated cell invasion** and intravasate more efficiently *in vivo*	Higher sensitivity to EGF	(46)
Tumor cell Cytoskeletal	N-WASP controls **invadopodium formation** and intravasation	Reorganization of actin cytoskeleton	(59)
Tumor cell adhesion and extravasation	Tumor cell **adhesion** and **extravasation** across TNF-α treated endothelial monolayers	LOX-1 mediated	(133)
	Tumor cell **extravasation**	Inhibiting α5β3 integrin reduced extravasation	(135)
Tumor cell extravasation	VEGF overexpressing colon cancer cells enhanced **extravasation**	VEGF impaired endothelial barrier via activation of Src to disrupt VE-Cadherin	(129)
Endothelial cell secreted factors	Increased tumor cell **invasion** by dysfunctional endothelial cells	Normal EC medium upregulated TIMP2 expression in TC. Dysfunctional EC secreted IL-6	(22)
Endothelial cell secreted factors	Increased tumor cell **invasion**	HUVEC, MVEC secreted IL-8 and Gro-β	(131)
Endothelial cell secreted factors	TC-EC paracrine interactions **inhibit TC proteolytic activity** and can be perturbed by **EC basement membrane integrity**	TC secreted VEGF-C induced lymphatic EC secreted CCL21, driving CCR-7 TC chemoinvasion	(132)
Endothelial cell secreted factors	Increased tumor cell transendothelial migration	MMP-2 secretion by EC	(88)
Endothelial cell secreted factors	TC-EC paracrine interactions increase tumor cell **proteolytic activity and tumor invasion**	EC secreted SDF-1 induces upregulation of TC derived MMP-9	(130)

3.2. Analysis framework for characterizing tumor-endothelial interactions

Tumor-endothelial cell interaction experiments

To investigate the effects of endothelial permeability on tumor-endothelial cell interactions, we used a highly invasive human fibrosarcoma (HT1080) cell line in order to observe single cell migration after tumor cells were seeded in the tumor channel. On the contrary, when breast tumor cells (MDA231) of epithelial origin were used, they invaded collectively and drastically remodeled the 3D ECM, resulting in gel contraction that made characterization of tumor-endothelial cell interaction events challenging.

Tumor cells were seeded at a density of $3x10^6$ cells/ml inside the tumor channel and cultured for 3 days under a 20ng/ml/mm EGF gradient to enhance cell invasion. Endothelial monolayers were formed using the same method described in chapter 2 and the devices were prepared for live cell imaging 48hours after endothelial cell seeding, when tumor cells were located at approximately 500μm away from the endothelial barrier. In the biochemical stimulation experiments, TNF-α at 2ng/ml in complete medium containing 20ng/ml EGF was added to the endothelial channel only. Confocal z-stacks were acquired every 1hour for more than 10hours to monitor tumor cell invasion dynamics (Figure 16A, B) and dextran transport across the endothelial barrier. Tumor cells were transfected with a pMSCV-mCherry vector (Gertler lab, MIT) and were sorted using Flow Cytometry to ensure the presence of a cell population with homogeneous expression of fluorescent intensity, while endothelial cells were stained with 5μM green cell tracker 5-chloromethylfluorescein diacetate (Invitrogen) each time a new experiment was performed. The fixation, staining and image acquisition protocols for both live and end-point high resolution staining are described in chapter 2.

Quantifying tumor-endothelial cell interactions

To quantify the tumor-endothelial interaction events and their dynamics, we characterized the location of each tumor cell with respect to the endothelial barrier interface (Figure 16). Semi-automatic tracking (Figure 16E) of tumor cells was performed in 3D using the Spot Tracking module in Imaris (Bitplane) using a spot diameter of 10μm. Since, tumor cells were infected with a cytosolic fluorescent marker and exhibited significant shape changes, manual editing of the spot tracking in Imaris was necessary in some cases to correct for errors in spot detection (i.e. whenever cell shape deviated significantly from a spherical shape and multiple spots were assigned to a single cell). The interface of the endothelial barrier with the 3D ECM was detected in Imaris also using the Spot Tracking module by identifying the CellTracker stained endothelial cells located on the gel interface. We constrained our analysis to 2D (only the X-Y-, coordinates of the tumor cell centroid and endothelial interface spot locations), since tumor cells were predominantly observed in one confocal z-plane. The Matlab script calculated the distance (Figure 16D) of each tumor cell centroid from the endothelial monolayer at each time point and a tumor-endothelial interaction event was defined when the tumor cell had migrated beyond the 3D ECM-endothelial channel interface. To characterize these tumor-endothelial cell interaction events we counted the number of tumor cells that were within a distance of 250μm from the endothelium and the number of tumor cells that had already migrated beyond the tumor-endothelial cell interface and interacted with the endothelial barrier (Figure 16D).

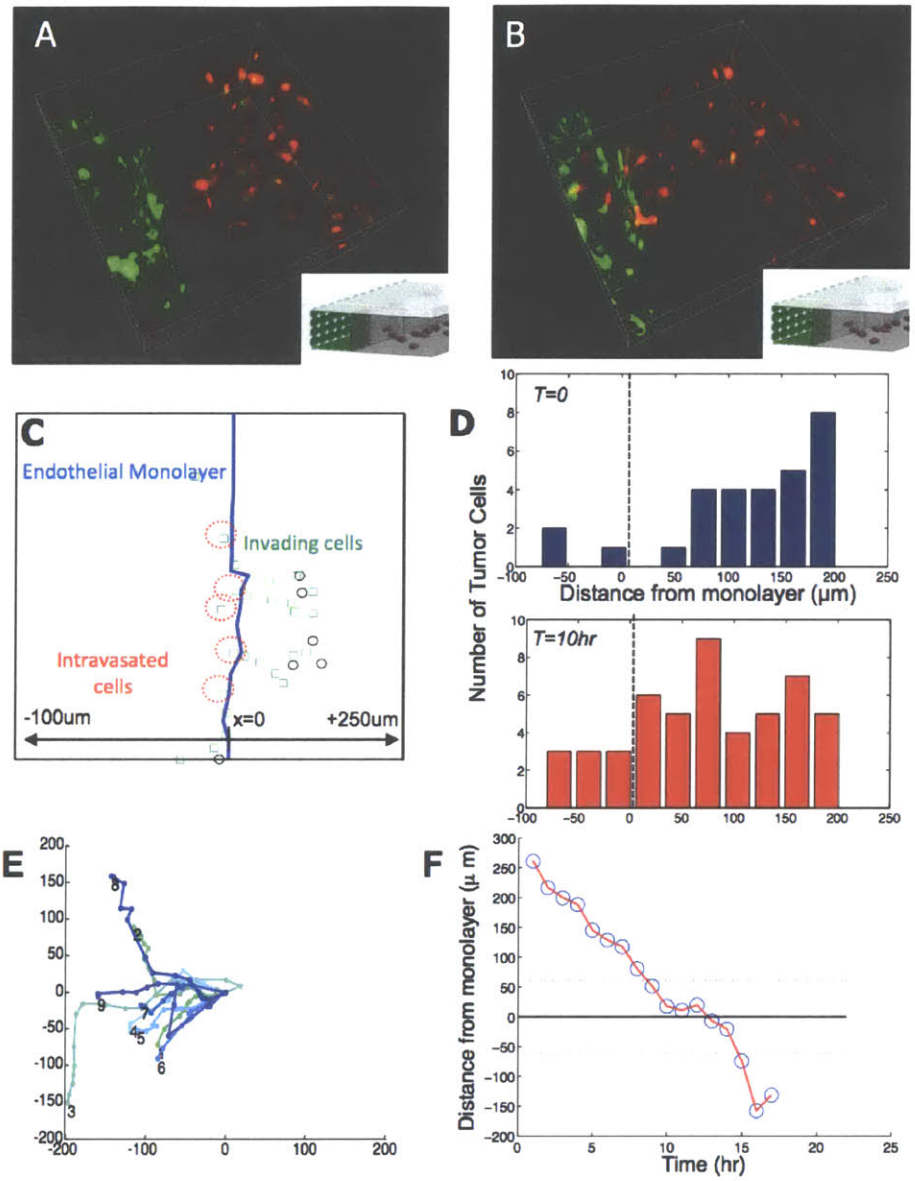

Figure 16: Methods to characterize tumor-endothelial cell interactions. (A) 3D rendering of HT1080 cells (red) invading towards an endothelial monolayer at t=0hr. Insert shows the location inside the device. (B) 3D rendering at t=10hrs. (C) 2D projection of tumor cell centroids at t=0hr (black circles) and t=10hr (green squares) and location of endothelial barrier (blue line) interface. (D) Histogram of tumor cell centroid location along the x-axis in panel (C) at t=0 and 10hrs. (E) Wind-rose plot of tumor cell trajectories. (F) Distance of a single tumor cell from the endothelial monolayer to quantify the time required to cross the endothelial barrier.

To characterize the dynamics of tumor-endothelial cell interactions, the time required for each tumor cell to migrate 60μm across the ECM-endothelial channel interface was computed (Figure 16F). The migration dynamics of tumor cells inside the 3D ECM were also analyzed by computing the average migration speed (v_{RMS})

$$v_{RMS} = \frac{total\ \text{distance}\ travelled}{time\ observed} = \frac{\sum\sqrt{\left(x_{i+1}-x_i\right)^2+\left(y_{i+1}-y_i\right)^2+\left(z_{i+1}-z_i\right)^2}}{\sum \delta t}$$

where x_i,y_i,z_i are the coordinates [μm] of the tumor centroid at the i-th time-step and δt [sec] is the time-step of observation.

3.3. Dynamics of Tumor-Endothelial Cell Interaction Events

Tumor-endothelial cell interaction events

To mimic the microenvironment of highly aggressive tumors, tumor cells were seeded on the non-endothelial cell coated channel (red channel in Figure 9A), which formed an invasive and growing tumor mass in the 3D collagen type I matrix in the presence of endothelial monolayers (green channel in Figure 9A). Single tumor cells were observed to invade in 3D with a characteristic "spindle-like" fibroblastic morphology (Figure 11C) and tumor cell shape and endothelial monolayer cell-cell junction morphology could be monitored. Confocal z-stacks of tumor cells invading towards the endothelial barrier were acquired and the number of tumor cells within a single gel region, their centroid location and the endothelial monolayer location were quantified. A tumor-endothelial cell interaction event is defined as a tumor cell in direct physical contact with the endothelial monolayer in the endothelial channel. These interaction events occurred either in the endothelial channel where the tumor cells could be located on the basal or apical surface of the endothelial monolayer or on the ECM-endothelial channel interface, while tumor cells were in the process of migrating out of the 3D matrix onto the endothelial channel. The number of tumor cells that were located within 250μm from the endothelium and the number of TC-EC interactions increased from T=0 (Figure 16A) to T=10hours (Figure 16B), as the tumor cells were migrating in response to the EGF gradient (Figure 16C, D).

Effects of biochemical stimulation with TNF-α on tumor-endothelial cell interaction events

We hypothesized that the high permeability values of the tumor blood vessels could regulate the number of tumor cells interacting with the endothelial monolayer. To perturb the endothelial barrier function the endothelial monolayer was stimulated with 2ng/ml TNF-α in the presence of tumor cells. Under these conditions the barrier impairment was confirmed by measuring significantly higher (p=0.0017) permeability values (Figure 17C) compared to the control, which is in agreement with the endothelial cell monoculture studies (chapter 2). Under these conditions, the number of tumor-endothelial cell interaction events increased significantly (p=0.006) by 1.7-fold compared to the control condition (Figure 17D). A similar number of tumor cells located 250μm from the endothelium under both conditions was identified, confirming that the observed difference was due to an enhanced ability to interact with the endothelium on the channel (Supplementary Figure 3). The dose of 2ng/ml TNF-α was selected to ensure the presence of a confluent monolayer 24 hours after stimulation (Supplementary Figure 3).

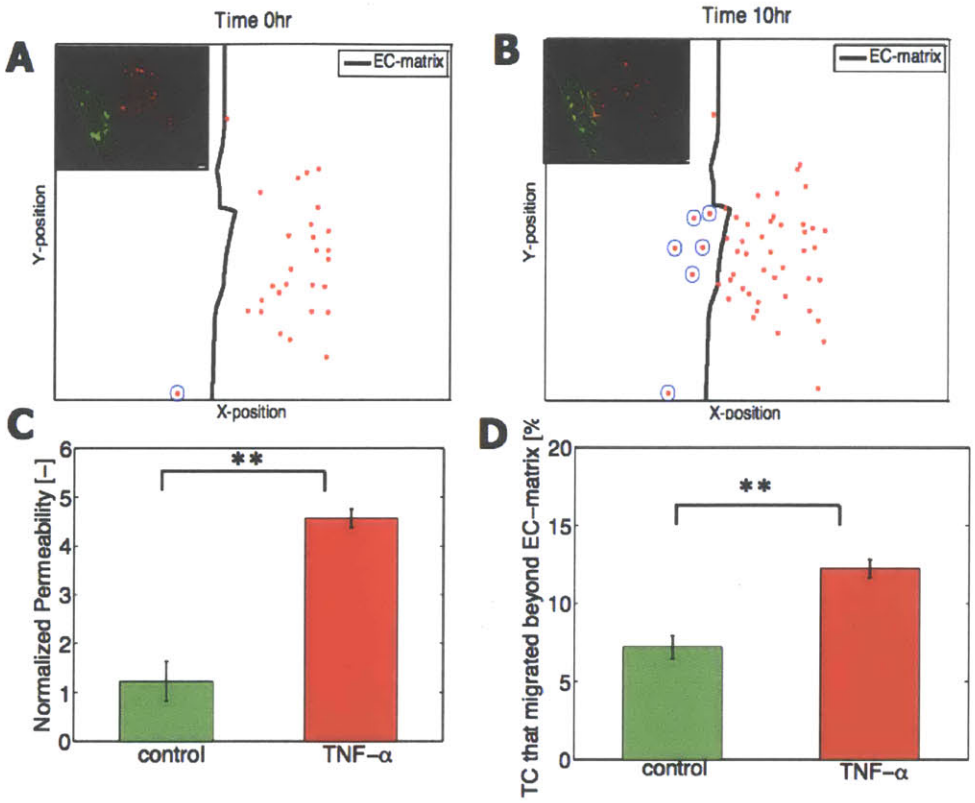

Figure 17: Tumor cell centroids and endothelial monolayer locations for the TNF-α stimulated endothelial barriers at t=0 (A) and t=10hrs (B). (C) Normalized change in 10kDa endothelial permeability of the endothelial barrier in the presence of tumor cells. (D) Quantification of the percentage of tumor cells that migrated beyond the EC-matrix interface (highlighted with the thick black line in panels A,B) for the control and TNF-α stimulated endothelial barriers. Average values for n=3 devices per condition. Error bars represent standard error of the mean.

Tumor-endothelial cell interaction dynamics

Imaging the tumor-endothelial cell interactions in the context of intravasation is critical for gaining mechanistic insight into the underlying mechanism. For example, it is particularly important to investigate whether tumor cells transmigrate through endothelial cell-cell junctions or through the cell body. The microfluidic-based intravasation assay allows for high-resolution real-time imaging of tumor-endothelial cell interactions, due to the height (< 200μm) of the microfabricated channels, which is compatible with high numerical aperture objectives.

Qualitative characterization of tumor cell migration at a 3D endothelial monolayer with a well-defined lumen can offer insight into the timescales, spatial organization and mechanism of tumor cell intravasation. The human fibrosarcoma HT1080 cell line was used due to its ability to invade in 3D with high migration speeds compared to the MDA231 cancer cells of epithelial origin. Analysis of time-series images of single tumor cells located within 60μm of the endothelium (Figure 18) led to a number of interesting observations:

(i) Tumor cells formed dynamic protrusions to probe their surrounding microenvironment

(ii) The shape of tumor cells changed significantly as they migrated from the 3D matrix, adhered to the endothelial barrier and migrated across it on the endothelial channel

(iii) Tumor cells migrated preferentially towards remodeled regions of the endothelial monolayer

To further investigate the effects of endothelial barrier function on tumor-endothelial interaction dynamics the time required for tumor cells to migrate a total distance of 60μm across the endothelial monolayer was quantified. We found that TNF-α-induced endothelial barrier impairment led to significantly (p=0.024) faster (Figure 18D) tumor cell migration (1.35 ± 0.25h) compared to the control condition (2.42 ± 0.38h). On the other hand, we quantified tumor cell migration in the 3D matrix prior to interactions with the endothelial barrier and found no significant difference in cell migration speeds (29.59 ± 2.57 μm/h vs. 29.53 ± 4.16 μm/h, Supplementary Figure 3) under control and TNF-α treated conditions.

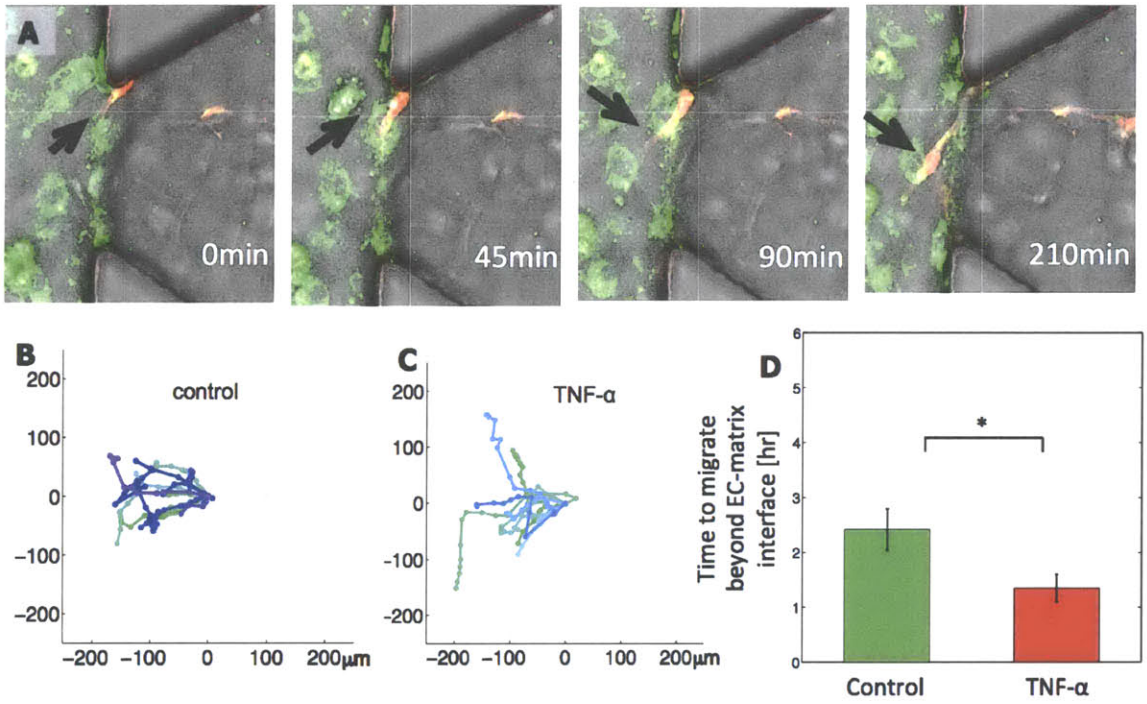

Figure 18: (A) Time series of a single confocal slice showing a single HT1080 cell (red, black arrow) invading towards the endothelial monolayer. Trajectories of at least n=10 tumor cells under control (B) and TNF-α (C) stimulated endothelial barriers. (D) Quantification of the time to migrate beyond the EC-matrix interface using the methods described in figure 16F. Average values for n=10 trajectories per condition. Error bars represent standard error of the mean.

Tumor cell - induced endothelial permeability impairment and endothelial cell-cell junction remodeling

To address the question of whether the presence of tumor cells induced vessel leakiness, we performed endothelial permeability measurements under endothelial monoculture and coculture with tumor cells in the absence of any biochemical stimulation. HUVEC monolayers in devices seeded with breast carcinoma cells (Figure 19A) were found to have a significantly (p=0.036) higher permeability value of 3.89×10^{-5} cm/s compared to 2.80×10^{-5} cm/s for control devices. In addition to the live cell imaging described in the previous section, we also performed detailed end-point immunofluorescence staining to visualize endothelial cell-cell junction integrity and actin cytoskeleton (Figure 19B, C). Interestingly, endothelial cell-cell junctions appeared

remodeled with an irregular morphology when tumor cells were located in close contact to these junctions compared with continuous undisturbed endothelial cell-cell junctions distally from the tumor cell (Figure 19B). Staining of the actin cytoskeleton also showed patterns of local actin remodeling in locations of VE-Cadherin gap formation (Figure 19C). Although in the present analysis (Figure 19C) it is not possible to distinguish between tumor and endothelial cell actin, we hypothesize that actin remodeling in both cell types is critical. In particular, endothelial cell-cell junction will likely need to be remodeled and tumor cell shape may change as the tumor cell transmigrates across small gaps in the endothelial monolayer.

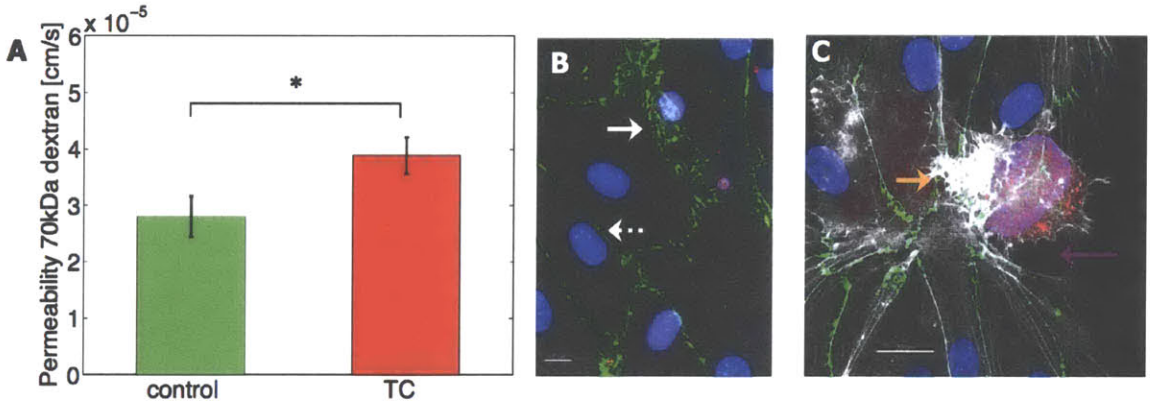

Figure 19: (A) Increase in endothelial permeability due to the presence of breast carcinoma cells inside the 3D ECM. Average values for n=12 regions per condition. Error bars represent standard error of the mean. (B,C) Immunofluorescence staining of endothelial VE-Cadherin junctions (green) in MVEC monolayers showing the remodeling of the actin cytoskeleton and the endothelial cell junctions at the point of a fibrosarcoma cell contact (white and orange arrows) compared to distally located VE-Cadherin junctions (dashed white arrow) and the formation of gaps in the endothelial monolayer (purple arrow). Scalebars: (B) 5μm, (C) 10μm.

3.4. Discussion of Tumor-Endothelial Cell Interaction events

The ability to image tumor cell migration in real-time in combination with monitoring transendothelial transport allowed us to investigated the role of endothelial permeability on tumor-endothelial cell interactions. We also visualized the diverse array of tumor cell phenotypes: 3D invasion in response to growth-factor gradients, direct physical contact with, and migration on the endothelial monolayer. In addition to our measurements in chapter 2 of endothelial permeability and tumor cell intravasation, the results in this chapter on the effects of endothelial permeability on tumor cell invasion provide insight into the role of the tumor microenvironment on tumor-endothelial cell interactions.

Metrics of tumor-endothelial cell interactions

Using single-cell tracking we followed the migratory paths of these invasive tumor cells and characterized the timescales of tumor-endothelial cell interactions. Interestingly, we found that under conditions of perturbed endothelial barrier function, tumor cells migrated faster and in larger numbers across the endothelial barrier. These results are in agreement with *in vivo* studies in a zebrafish tumor model, where the ability of human tumor cells to extend invasive protrusions into the fish vasculature was increased when tumor cells overexpressed angiogenic

factors, such as VEGF (52). Furthermore, the time-scales of tumor cell migration on the endothelial channel are comparable with *in vivo* measurements in transgenic murine mammary tumors using intravital microscopy (13). Comparison of the tumor cell migration speed (29 μm/hr) inside the 3D collagen type I matrices in our devices is in the same order of magnitude with measurement of the same cell type in the chicken embryo assay (23 μm/hr) by Zijlstra et al (53). Although, we did not investigate the variability in the tumor-endothelial cell metrics, this is an interesting direction for future work. Different factors can contribute to this variability. For example, Dubois et al showed that in a 3D migration assay the cell migration speeds ranged from 14 to 52 μm/hr, which is in the same order of magnitude as our measurements (137). Our results of a 1.7-fold increase in tumor-endothelial cell interactions in the presence of TNF-α is in agreement with a transwell study which found a 2-fold increase in the number of HT1080 that invaded across TNF-α (1ng/ml) stimulated HUVEC coated transwell filters (138). Along these lines, it would be interesting to investigate whether endothelial cells can influence tumor cell migration, since previous studies (see Table 3) have shown that it can occur via growth-factor and protease secretion. Not surprisingly, preliminary comparison of tumor cell migration speeds in the 3D matrix and on the endothelial channels showed differences in the migration speed magnitude (Supplementary Figure 3).

Quantification of tumor-endothelial cell interactions

The accurate tracking of tumor cells required manual editing of trajectories, especially in regions with high tumor cell density, where tumor cell trajectories merged and identification of a single tumor cell was challenging. This is an important point for the design of experiments on invasive growth and should be considered in future studies. In particular, we selected experimental conditions (collagen gel density, EGF gradient and timing of cell seeding) so that we could easily track the tumor cells. *In vivo* tumor cells are highly packed and this might affect tumor-endothelial cell interactions as well. A possible way to overcome this challenge is to use tumor cells that express fluorescently tagged H2B (fluorescent nuclei), which would make tracking of single cell easier. We used this cell line in preliminary experiments and single cell tracking was more straightforward, further studies are needed to demonstrate the ability to track tumor cell migration at higher cell densities, which may better mimic *in vivo* tumor conditions.

To simplify the analysis of tumor-endothelial cell interactions, we only analyzed the x-y-components of the tumor cell migration tracks and assumed that the endothelial barrier location did not vary along the vertical z-axis. Our methods could be easily extended to perform a 3D analysis, by using the segmentation methods described in the discussion section of chapter 2, or by simply tracking the endothelial barrier interface for every z-slice and computing an in-plane tumor-endothelial cell distance for more accurate tumor-endothelial interaction metrics.

Interaction of tumor cells with the endothelial monolayer

Our microfluidic assay offers a unique platform to investigate the role of paracrine and juxtracrine tumor-endothelial cell interactions on tumor cell invasion, and intravasation and on endothelial permeability. This is of particular importance for a detailed understanding of the critical molecular players involved, which is required to design effective targeted cancer therapies. Interestingly, qualitative observation of the tumor cell phenotypes during interaction

with the endothelial barrier indicated that tumor cell migration beyond the endothelial barrier showed preferential migration along pre-existing paths that were taken by leader tumor cells (Supplementary Figure 3). This observation of "hotspots" of tumor-endothelial cell interactions suggests possible tumor-tumor cell cooperation during endothelial monolayer invasion and active tumor-endothelial signaling which could be mediated by various mechanisms. One possibility is that tumor cells can induce VE-Cadherin remodeling in a β1-integrin dependent mechanism as described by Haidari et al (124). To specifically investigate tumor-induced endothelial remodeling, VE-Cadherin junction remodeling should be quantitatively characterized by analyzing their morphology and the gap area formed.

Further studies are required to investigate this interesting observation of "hotspots" and assess whether there are specific ligand-receptor interactions between the two cell types. This is particularly important in the context of tumor cell intravasation, where it is unknown whether tumor cell utilize specific receptors on the apical endothelial surface for adhering and transmigrating. The microchannel design allows for high-resolution imaging of tumor-endothelial contact to investigate the possible role tumor-endothelial cell adhesion molecules.

It would also be interesting to test whether tumor cell secreted factors (growth factors or proteases) can remodel the endothelial monolayer. Our results of increased endothelial permeability in the presence of tumor cells suggest that paracrine factors can modulate endothelial barrier integrity, and are in agreement with other *in vitro* studies (127). Interestingly, preliminary analysis of the effects of tumor cell growth on endothelial permeability has shown that within a single microfluidic device, gel regions with higher tumor cell counts tend to show higher permeability values. An important direction for future investigation would be to study the role of juxtracrine interactions on endothelial permeability and whether these changes are reversible. These results would have important implications for clinical studies aimed to normalize tumor vasculature as a therapeutic strategy (30). Engineering tumor cells to express fluorescent actin would allow for a detailed investigation of juxtracrine tumor-endothelial interactions and would elucidate the dynamics and mechanism of endothelial cell-cell junction remodeling (Figure 19C). Elegant work from Khuon et al has shown that tumor cell contact with the endothelial actin cytoskeleton resulted in endothelial MLCK phosphorylation and actin contraction (43), however the role of physical forces generated via the tumor actin cytoskeleton in transendothelial migration has not been explored.

One of the challenges with characterizing the ability of tumor cells to intravasate as they interact with the endothelial barrier, is the requirement for finely resolved confocal slice sampling in the z-axis to accurately determine whether tumor cells have migrated through the endothelial barrier or whether they are simply migrating along the endothelial cells without crossing the barrier. To address this question, a high numerical aperture objective is required (NA>0.8), similar to the one used for the end-point confocal imaging in chapter 2 and 4 (see Figure 13 and Figure 21). The experiments to investigate tumor-endothelial interaction dynamics were performed with a 10X NA=0.3 objective making it challenging to identify whether tumor cells had crossed the endothelial barrier. Hence, we refer to the tumor cells that have migrated beyond the ECM-EC channel interface as tumor cells interacting with the endothelial barrier.

Finally, one improvement of the experimental protocol for monitoring more physiologically relevant tumor-endothelial interactions would be the integration of a thin ECM coating on the microchannel and ECM-channel interface, as discussed in the previous chapter. The advantage of this modification would be to promote adhesion of the endothelial cells on the PDMS interfaces, resulting in a more homogeneous endothelial barrier with the aim to reduce the frequent endothelial monolayer remodeling observed towards the edges of the PDMS-3D matrix interface, especially under TNF-α stimulation.

Interactions of other cell types with endothelial monolayers

Preliminary experiments with a number of different cell types were performed to demonstrate that the tumor-endothelial interaction assay can also be employed for studying invasive growth and interactions of various cell types with endothelial monolayers, such as different cancer cell lines (fibrosarcoma and breast cancer cells), human mesenchymal stem cells and human dermal fibroblasts (Supplementary Figure 4).

Chapter 4: Role of Macrophages in tumor cell intravasation and endothelial barrier function

The role of different cellular and acellular factors in the tumor microenvironment on cancer cell invasion, intravasation and endothelial permeability are described in this chapter. Next, the methods developed to culture tumor-endothelial-macrophages in 3D matrices and to characterize tumor cell intravasation in the presence of macrophages are presented. A series of experiments designed to identify and investigate the role of macrophage-secreted factor on endothelial permeability and intravasation are discussed. Finally, we compare our results with studies in the literature and discuss the underlying biological mechanisms.

4.1 Macrophages in Cancer Metastasis

Macrophages in cancer

Cancer related inflammation is a critical component of the tumor microenvironment, where immune cells infiltrate into the solid tumor and regulate tumor progression (139). Macrophages are derived from monocyte differentiation and have been shown to play diverse roles (Figure 20) in many aspects of cancer, ranging from inflammation-induced mutagenesis to metastasis (140). Macrophage subsets can be broadly classified in the "classically activated" M1 state and "alternatively activated" M2 state (48). M1 macrophages are classically activated by exposure to interferon-γ or lipopolysaccharides (LPS) and elicit tissue destructive activities by secreting high levels of cytokines such as TNF-α, IL-12 and IL-1. M2 macrophages secrete high levels of VEGF, MMPs and IL-10 and have tissue remodeling and immunosuppressive activities.

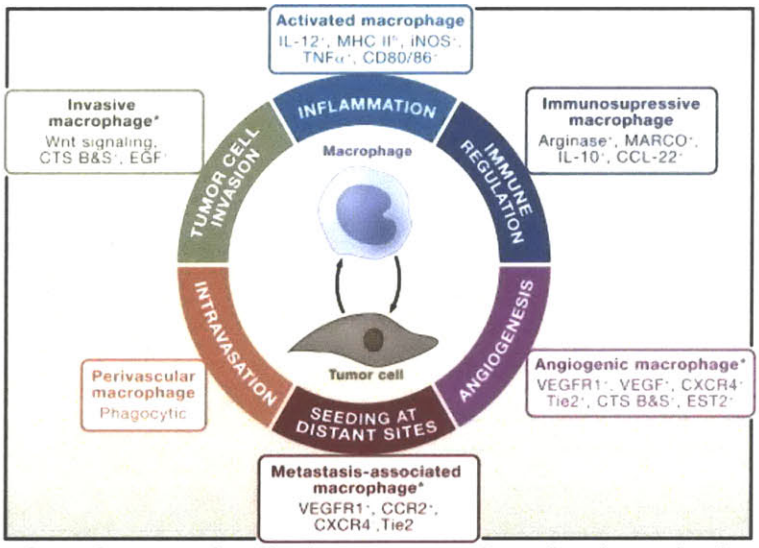

Figure 20: Diverse macrophage phenotypes: invasive, immunosuppressive and angiogenesis-related in cancer progression, invasion and metastasis [figure from (140)]

Hagemann using an *in vitro* transwell assay showed that macrophages promoted invasion of aggressive tumor cell lines only, via secretion of the inflammatory cytokine TNF-α and MMP

enzymes (141). Wang et al showed that coculture of tumor cells with macrophages resulted in IL-6 overexpression in the macrophages, which in turn acted in an autocrine fashion to polarize macrophages (142). Although, the authors showed that macrophages were polarized towards an M2 phenotype, they did not investigate the mechanism by which tumor cells promoted IL-6 overexpression in the macrophages. Zhang et al showed that M2 macrophages enhance lymphangiogenesis in a mouse lung adenocarcinoma model *in vivo* and increased lymphatic endothelial cell migration *in vitro* (143).

Targeting macrophages in the tumor microenvironment has been proposed as a therapeutic approach (144), and therefore, a comprehensive understanding of the underlying tumor-endothelial-macrophage interactions in the context of tumor cell dissemination is needed. The effects of macrophages in modulating endothelial barrier function remain largely unknown, and because macrophage can secrete both pro-inflammatory and anti-inflammatory cytokines, macrophage-endothelial interactions will likely depend on macrophage polarization status.

Endothelial barrier function regulation in the tumor microenvironment

Interaction of endothelial cells with stromal cells in the microenvironment of each organ is critical for proper organ function and may be differentially regulated under physiological and pathological conditions. One example of endothelial-stromal cell interactions in healthy tissues is the blood-brain barrier, which has been shown to be regulated by endothelial-astrocyte interactions resulting in high transendothelial resistance and enhanced endothelial barrier function (145). In the tumor microenvironment, the barrier function of the endothelium can be controlled by biochemical factors, which can be secreted by different cell types. In particular, tumor-secreted VEGF has been shown to result in increased permeability values in a coculture model of ovarian cancer cells with HUVEC monolayers and these effects could be inhibited by VEGF neutralization (127). Tumor cell mediated changes to endothelial permeability have also been demonstrated for melanoma cell conditioned medium (128). Zenker et al used a transwell system to perform coculture of brain capillary endothelial cells with human blood-derived macrophages (146). Surprisingly, the presence of macrophages resulted in endothelial barrier function enhancement, measured by increased transendothelial resistance, even under pro-inflammatory conditions when macrophages were stimulated with LPS. In contrast to these results, two other studies showed that macrophages impaired the endothelial barrier in a mechanism dependent on activation status and nitric oxide signaling. Wakamoto et al showed that conditioned medium from peripheral blood mononuclear monocytes, stimulated with plasma containing HLA Class II antibodies resulted in high endothelial permeability values, which could be inhibited by blocking antibodies against TNF-α and IL-1β (147). Farley et al showed that high macrophage/endothelial cell ratios and alveolar macrophages expressing inducible nitric oxide synthase resulted in increased endothelial permeability (148). On the contrary, bone marrow derived progenitor cells have been shown to have a reversing effect on thrombin-induced barrier impairment via a mechanism involving MLC phosphorylation and strengthening of cell-cell junctions via Cdc42 (149).

Not surprisingly, apart from immune cells and mesenchymal cells, red blood cells and platelets have also been shown to regulate endothelial permeability. Treatment of bovine endothelial cells with platelet-conditioned medium resulted in enhanced endothelial barrier function, measured by

an increased transendothelial resistance in a cAMP/PKA and cGMP/PKG independent mechanism (150). Curry et al showed that diffusive and hydraulic permeability in rat microvessels *in vivo* was decreased by erythrocyte containing or erythrocyte conditioned medium, via a sphingosine 1-phosphate (S1P) dependent mechanism (151). Interestingly, S1P was also shown to be involved in the protective role of pericytes in enhancing endothelial barrier function (152). Furthermore, the barrier enhancing effects of paracrine mediated S1P signaling was also recently demonstrated in dendritic cell – endothelial cell interactions (153).

A more detailed description of endothelial barrier regulation by different biochemical and biophysical factors is presented in chapter 5. In the next table we summarize the role of different cell types on endothelial permeability (on vascular endothelial cells only). Based on the above studies, an important direction for future exploration is the investigation of the relative role of juxtracrine and paracrine endothelial-stromal cell interactions.

Table 4: Roles of different cell types in endothelial permeability regulation

Cell Type	Effects on permeability	Mechanism	References
Tumor cells	[+] Breast carcinoma cells increase diffusive permeability	Paracrine and juxtracrine (needs to be confirmed)	(154)
	[+] Ovarian cancer cells increase diffusive permeability	VEGF	(127)
	[+] Melanoma cell conditioned medium increased endothelial permeability	Paracrine (needs to be confirmed)	(128)
Macrophages	[+/o] Diffusive Permeability increase by paracrine factors from monocyte activated with plasma containing HLA Class II antibodies	TNF-α and IL-1β	(147)
	[+/o] Dependent on alveolar macrophage number and iNOS expression	Inducible nitric oxide synthase	(148)
	[+] Diffusive Permeability Increase	TNF-α	(154)
	[-] Blood-derived macrophages decreased transendothelial resistance	Paracrine factors	(146)
Epithelial cells	[+] Diffusive Permeability Increase	Paracrine and juxtracrine (needs to be confirmed)	(154)
Dendritic cells	[-] Diffusive permeability reduced by paracrine factors from dendritic cells	S1P secreted by dendritic cells	(153)
Astrocytes	[-] Contact transwell coculture resulted in increased transendothelial resistance	Tight junctions reinforcement.	(145)
Red blood cells	[-] Decreased hydraulic and diffusive permeability in rat microvessels *in vivo*	S1P secreted by red blood cells	(151)
Platelets	[-] Enhance barrier function via increased transendothelial resistance	Unknown, but independent of cAMP/PKA and cGMP/PKG	(150)
Pericytes	[-] Enhanced barrier function via increased transendothelial resistance	S1P secreted by pericytes	(152)
[+]: increased, [-]: decreased, [o]: no change in permeability. All studies are performed *in vitro*, unless otherwise noted. No studies with fibroblast- or neutrophil-endothelial coculture and measurements of permeability were found in PubMed (search on 10/15/2012)			

Role of cAMP in endothelial permeability

Growth factors and hormones binding to receptors on the cellular plasma membrane can stimulate target cells via second messenger pathways. These mechanisms involve activation of receptor coupled GTP-binding proteins which can stimulate the enzyme adenylyl cyclase and thus convert ATP to cyclic adenosine monophosphate (cAMP) (155). The second messenger cAMP has been shown to regulate many physiologic processes (156) and is well known for its role in enhancing endothelial barrier function (112). Intracellular cAMP levels are regulated by cAMP-dependent protein kinase (PKA), the exchange protein activated by cAMP (Epac) and by the enzyme phosphodiesterase (157). Beese et al investigated the role of cAMP and its derivatives on tight junction formation and paracellular permeability to 10 and 70 kDa dextrans (158). Treatment of HUVEC monolayers with pCPT-cAMP and 8-Br-cAMP/Na derivatives improved formation of continuous tight junctions (Zona occluden-1 and Claudin5) and reduced paracellular permeability.

Tumor cell intravasation and the tumor microenvironment

To enter into the circulatory system, tumor cells must first successfully navigate a complex microenvironment comprised of biochemical and biophysical signals and ultimately transmigrate across the blood vessel wall. An important question in cancer research is whether the barrier function of the endothelium plays a role in tumor cell intravasation. Interestingly, immune cells such as neutrophils (16) and macrophages (13) that have a pro-inflammatory role have been associated with intravasation. However it is not clear whether these immune cells also regulate endothelial permeability. In addition to the tumor cell autonomous programs described in chapter 3 (e.g. EMT), we designed experiments to investigate the interplay between tumor cell intravasation and endothelial permeability in the presence of extrinsic tumor cell factors, such as macrophages.

4.2. Methods for tumor-endothelial-macrophage culture

Intravasation experiments

To investigate the role of macrophages, we used the highly aggressive breast carcinoma cell line MDA231 engineered to express the MenaINV actin binding protein for two reasons: a) to recreate a physiologically relevant phenotype, since macrophages have a critical role in breast cancer (139) b) to increase the incidence of intravasation (12). In order to minimize the tumor-endothelial cell distance, a 3D collagen type I ECM (2.5mg/ml) seeded with breast carcinoma cells and murine macrophages (RAW264.7) at a cell seeding density of 0.8×10^6 cells/ml and 0.4×10^6 cells/ml respectively was injected into the gel regions. Endothelial cells were seeded in the endothelial channel (2×10^6 cells/ml) to form monolayers 24hours after filling the ECM containing tumor and macrophage cells, and all three cell types were allowed to interact for 48hours. EGF gradients (20ng/ml/mm) were established in all experiments and in the devices with macrophages we also seeded macrophages at a 0.25×10^6 cells/ml density in the endothelial

channel. The same intravasation experiments were also performed with a human fibrosarcoma cell line and the results were described in chapter 2.

Staining, imaging protocols and the methods for confocal stack visualization and quantification of the intravasation events are described in chapter 2. Briefly, macrophages were stained with a PE/Cy5 anti-mouse CD11b (Clone M1/80; Biolegend) antibody and the characterization of their localization with respect to the endothelial surface was performed with the same approach as that used for the identification of an intravasation event. Blocking antibody experiments were performed to investigate the role of macrophage secreted TNF-α. We used an antibody against murine soluble TNF-α (polyclonal; R&D Systems) and an IgG conrol antibody (R&D Systems). We selected the antibody concentration to be 2μg/ml, corresponding to a 10 times higher dose than the ND_{50} supplier suggested neutralization dose. To confirm the intravasation events observed in the end-point imaging, we also performed live cell imaging to monitor macrophages, tumor cells and endothelial cells in real-time. All intravasation metrics were calculated as averages from at least three independent devices (n=3).

Effect of macrophages on endothelial permeability

Endothelial permeability to 70kDa dextran was measured in all the intravasation experiments, using the method described in chapter 2, after 48hours of tumor-macrophage-endothelial interactions and right before fixation of the devices. To investigate whether the macrophage-associated endothelial impairment is specific to this cell type we compared the ability of macrophages, breast carcinoma and epithelial (MCF10A) cells to regulate endothelial permeability. 24 hours prior to endothelial cell seeding, the different cell types were seed at a density of 0.4 x 10^6 cells/ml inside the 3D ECM (collagen I, 2.5mg/ml), similar to the conditions in the intravasation experiments. We allowed interactions for 48hours after the endothelium had formed before measuring endothelial permeability to 70kDa dextran. The same experimental protocol and quantification framework were used, as the ones described in chapter 2. Due to device-to-device variability, the reported permeability values were calculated as an average from twelve (n=12) gel regions, where each gel region was treated as an independent experiment and data from at least two independent devices were included.

Characterization of macrophage secreted factors and macrophage polarization

To further validate the ability of macrophages to increase endothelial permeability, we characterized the macrophage-secreted cytokines. RAW264.7 cells were seeded in a 24 well plate, at 100 000 cells/well in 400μl of medium and were stimulated with 10ng/ml LPS (Sigma) or 10ng/ml IL-4 (PeproTech) to polarize the cells in a M1 or M2 phenotype. 24hours after cell seeding and stimulation, culture medium supernatant was collected, centrifuged to remove cell debris and stored at -80C. We used the Bio-Plex bead-based cytokine array (BioPlex) for the murine cytokine TNF-α (M1 marker) and IL-10 (M2 marker) and experiments were repeated twice.

To investigate whether intravasation and endothelial permeability impairment is associated with a specific macrophage phenotype, we also studied macrophage polarization upon interaction with tumor and endothelial cells. M1 or M2 polarization status was assessed by immunostaining

against IL-12 (Clone C17.8; eBiosciences) and CD206 (Clone MR5D3; Santa Cruz Biotech). Macrophages were seeded in 3D ECM under conditions of: a) control monoculture (RAW264.7 only), b) monoculture with LPS, c) IL-4 stimulation as described above and d) tumor-macrophage-endothelial coculture, similar to the intravasation experiments. Imaging was performed with the same protocol as described in chapter 2 and the expression of M1 (IL-12) and M2 (CD206) markers was quantified for at least 10 cells per condition using ImageJ and a previously described method (159).

4.3 Tumor cell intravasation and endothelial permeability

Role of macrophages in tumor cell intravasation and endothelial permeability

Previous work from the Condeelis lab has shown that macrophages increased the invasiveness of murine carcinoma cells and facilitated higher intravasation rates through an EGF/CSF-1 paracrine loop (160). Experiments were designed to investigate the role of the endothelial barrier during intravasation and test the hypothesis that macrophages may regulate endothelial barrier function. Breast carcinoma cells and macrophages were seeded inside a 3D collagen type I matrix to mimic a physiologically relevant intravasation phenotype (Figure 21). An EGF gradient was applied across the endothelial barrier and macrophages were also seeded in the endothelial channel to bias tumor cell invasion towards the endothelium in order to maximize the number of possible intravasation events that could be observed. The presence of macrophages resulted in endothelial barrier impairment, as measured by a 2.83 fold increase ($p=0.03$) in endothelial permeability to 70kDa dextran (Figure 21E). A nine-fold increase ($p=0.048$) was measured in the number of tumor cells (Figure 21D) that had intravasated (13 out of 289 cells) and intravasation efficiency (4.08 ± 0.87 %) compared to control conditions (2 out of 304 cells; 0.45 ± 0.28 %). We also quantified the number of tumor cells in contact with the endothelium and found a similar number under both conditions (Supplementary Figure 5), which confirmed that our results were not biased by a difference in the number of tumor cells interacting with the endothelium. Intravasation events were also validated by performing live cell imaging (Figure 21C), where tumor and endothelial cells were labeled with fluorescent markers and macrophages could be identified based on their distinct spherical morphology.

Characterization of macrophage secreted factors and TNF-α blocking

To gain insight into the mechanism of macrophage-induced increases in intravasation and endothelial barrier function, we characterized the macrophage-secreted factors using a cytokine array. We confirmed that the RAW264.7 secreted significant levels of TNF-α that could also be modulated by stimulation with IL-4 and LPS. Antibody neutralization experiments against the soluble murine TNF-α were performed to investigate the role of macrophage secreted TNF-α in intravasation and endothelial permeability. Blocking TNF-α resulted in a significant 2.45 fold ($p=0.03$) reduction in intravasation, and a significant 1.67 fold ($p=0.04$) reduction in endothelial permeability to 70kDa dextran compared to stimulation with the control IgG antibody (Figure 21E).

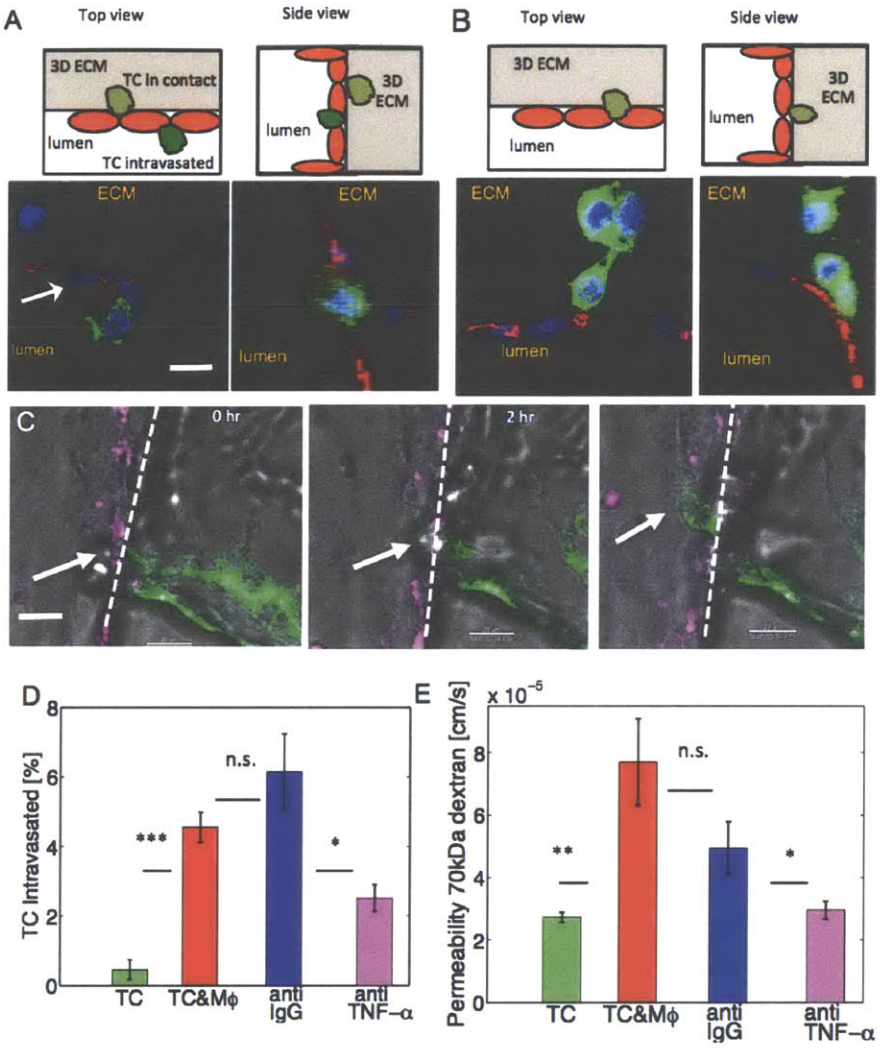

Figure 21: Macrophages facilitate tumor cell intravasation and impair endothelial barrier function. (A) Upper panel: Top and side views showing the device schematic with the endothelial monolayer and tumor cells. Lower panel: Breast carcinoma cell (green) that has intravasated across the endothelial monolayer (red). Scalebar: 30μm. (B) Tumor cells located on the basal side, unable to intravasate. (C) Time sequence of a single confocal slice showing a tumor cell (green) intravasating across an endothelial monolayer (magenta). The endothelial barrier location is highlighted with a white dashed line. Scalebar: 30μm. (D) Quantification of the percentage of tumor cell that had intravasated. Average values for n=3 devices per condition (E) Quantification of endothelial permeability. Average values for n=12 regions per condition. Error bars represent standard error of the mean.

Macrophage localization in the intravasation experiments and specificity of macrophage-induced endothelial impairment

To investigate whether macrophages preferentially localized to the apical or basal endothelial surfaces, we characterized their localization (Figure 22A). Similar (p=0.61) numbers of macrophages attached on both surfaces, with 6.42 ± 1.88 macrophages located in subluminal compartments and 5.29 ± 1.00 in the luminal compartment (Figure 22B). To further investigate whether the observed endothelial permeability increases were specific to macrophages, permeability measurements for endothelial monolayers that interacted with different cell types were performed. In particular, devices were prepared with 3D ECM seeded with macrophages

only, tumor cells only and mammary epithelial cells only. Not surprisingly, the presence of all cell types resulted in different levels of endothelial barrier impairment (Figure 22C). The presence of macrophages resulted in the highest permeability value (5.6 x 10^{-5} cm/s), 24% and 44% higher than the values for the mammary cell (4.5 x 10^{-5} cm/s) and tumor cell (3.9 x 10^{-5} cm/s) conditions.

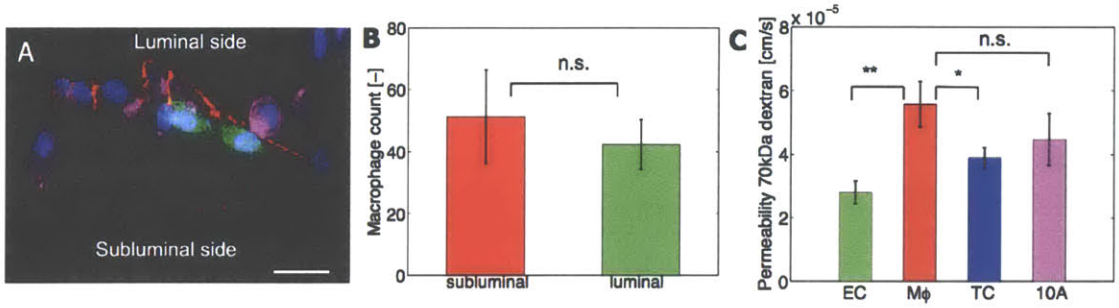

Figure 22: (A) Localization of macrophages (magenta) on the luminal or subluminal sides of the endothelial monolayer (red) in the presence of tumor cells (green) in the intravasation experiments. Scalebar: 30μm. (B) Quantification of macrophage counts in the luminal and subluminal compartments. (C) Specificity of different cell types to impair endothelial barrier function (EC: endothelial cells only, Mφ: macrophages, TC: MDA231MenaINV tumor cells, 10A: MCF10A epithelial cells). Average values for n=12 regions per condition. Error bars represent standard error of the mean.

Macrophage ability to modulate intravasation for different tumor cell lines

To further investigate whether carcinoma cells of different invasive potential would also exhibit differences in intravasation efficiency in the presence of macrophages, the intravasation assay was performed for the parental MDA231GFP cells and the same cell line expressing the MenaINV protein (Figure 23A). The breast cancer cells expressing the MenaINV were more efficient in intravasating (13 of 289 cells, 4.08%) compared to the parental cells (5 of 196 cells, 2.32%). The presence of macrophages in the parental cells also led to a significant increase (p=0.019) in intravasation levels, when compared with intravasation in the absence of macrophages (2 of 304, 0.53%).

Intravasation for endothelial cell of different origin and with defective basement membrane

The intravasation assay was carried out with different endothelial cell lines to investigate whether the endothelial cell phenotype plays a role in tumor cell intravasation. The differences in endothelial permeability among the different endothelial cell lines were described in chapter 2. We did not find a significant difference in intravasation rates between the control HUVEC and MVEC line (Supplementary Figure 5). On the contrary, endothelial monolayers that displayed basement membrane defects (HUVEC-shPerlecan) resulted in increased (p=0.39) intravasation levels with a rate of 4.32% (6 out of 212 cells) compared to wild type HUVEC that had a low intravasation rate of 0.45% (2 out of 304 cells) for the MDA231 parental cell line (Figure 23B). Similar results were observed in the presence of macrophages, where the intravasation rate was increased (p=0.0021) by 2.65-fold with 6.61% (28 out of 458) for the shPerlecan-HUVEC cells compared to only 2.31% (5 out of 196) for the control HUVEC monolayers.

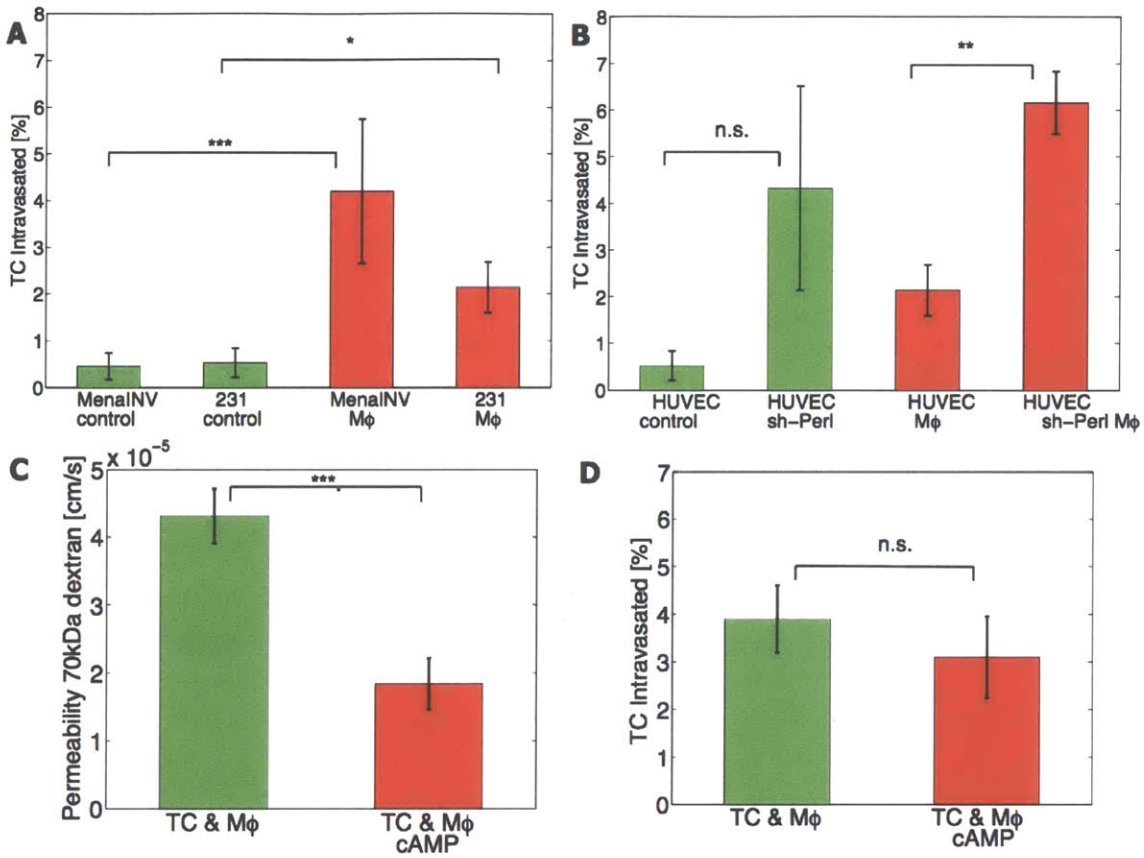

Figure 23: (A) Expression of actin binding proteins in the breast carcinoma cell lines can enhance tumor cell intravasation in the presence of macrophages. (B) Intravasation efficiency is regulated by the endothelial cell phenotype. HUVEC Perlecan knockdown cells showed increased baseline and macrophage-induced intravasation levels for the MDA231-MenaINV carcinoma cells. Average values for n=3 devices per condition. (C) Stimulation with 0.5mM cAMP reduced endothelial permeability in the intravasation experiments with the breast carcinoma MDA231-MenaINV cell line in the presence of macrophages. Average values for n=6 regions per condition. (D) Small reduction in intravasation rate upon stimulation with cAMP. Average values for n=3 devices per condition. Error bars represent standard error of the mean.

Effects of cAMP-induced endothelial barrier enhancement on intravasation

To further investigate the hypothesis that endothelial permeability regulates tumor cell intravasation, we designed experiments to enhance barrier function and measure any changes in the tumor cell intravasation rates. In these experiments, we used the coculture condition with macrophages as a control, which demonstrated high intravasation rates and endothelial permeability, and added a high concentration (500μM) of cAMP to the endothelial channel only. P_D measurements to 70kDa confirmed that endothelial permeability was reduced (Figure 23C) and the number of tumor cells that had intravasated was also reduced (Figure 23D). However, despite the 2.34-fold reduction ($p=1.9 \times 10^{-4}$) in permeability, the intravasation rate was only reduced by 21.5% ($p=0.95$).

Characterization of macrophage polarization state

The polarization of macrophages into an M1 or M2 phenotype has important implications on the mechanism by which macrophages may regulate cancer metastasis. To characterize the

macrophage phenotype in the intravasation experiments we measured the cytokine secretion levels and expression of M1 and M2 markers using immunostaining. Under control conditions TNF-α concentration in the supernatant was 2.97 pg/ml. This secretion rate was decreased to 0.16 pg/ml when macrophages were stimulated with 10ng/ml IL-4 to become polarized towards an M2 phenotype, whereas it could be increased to 38.91 pg/ml by activating macrophages using 10ng/ml LPS towards an M1 phenotype (Figure 24A). We also characterized macrophage secreted IL-10 under control, IL-4 and LPS conditions and measured secretion rates of 47.75 pg/ml, 258.55 pg/ml and 65.92 pg/ml respectively.

Under the conditions described above, the ability to polarize macrophages in the microfluidic device towards M1 or M2 phenotypes was confirmed using immunostaining against IL-12 and CD206 (Figure 24). More specifically, under stimulation with 10ng/ml LPS to polarize cells in an M1 phenotype, expression of the M1 marker IL-12 and secretion of TNF-α increased by 9.53-fold and 13.10-fold respectively (Figure 24A, D), while these markers were downregulated when the cells were stimulated with 10ng/ml IL-4 to drive cells into an M2 phenotype (Figure 24B, E). Similarly, during IL-4 stimulation, expression of CD206 and secretion of IL-10 were increased by 9.10-fold and 5.41-fold, while the expression of M1 markers and secretion of M1 associated cytokines was reduced. However, there was no significant difference in M1 and M2 marker expression under macrophage coculture with tumor and endothelial cells compared with the macrophage monoculture condition. Furthermore, macrophages in the microfluidic device showed a heterogeneous population with respect to M1 and M2 marker expression.

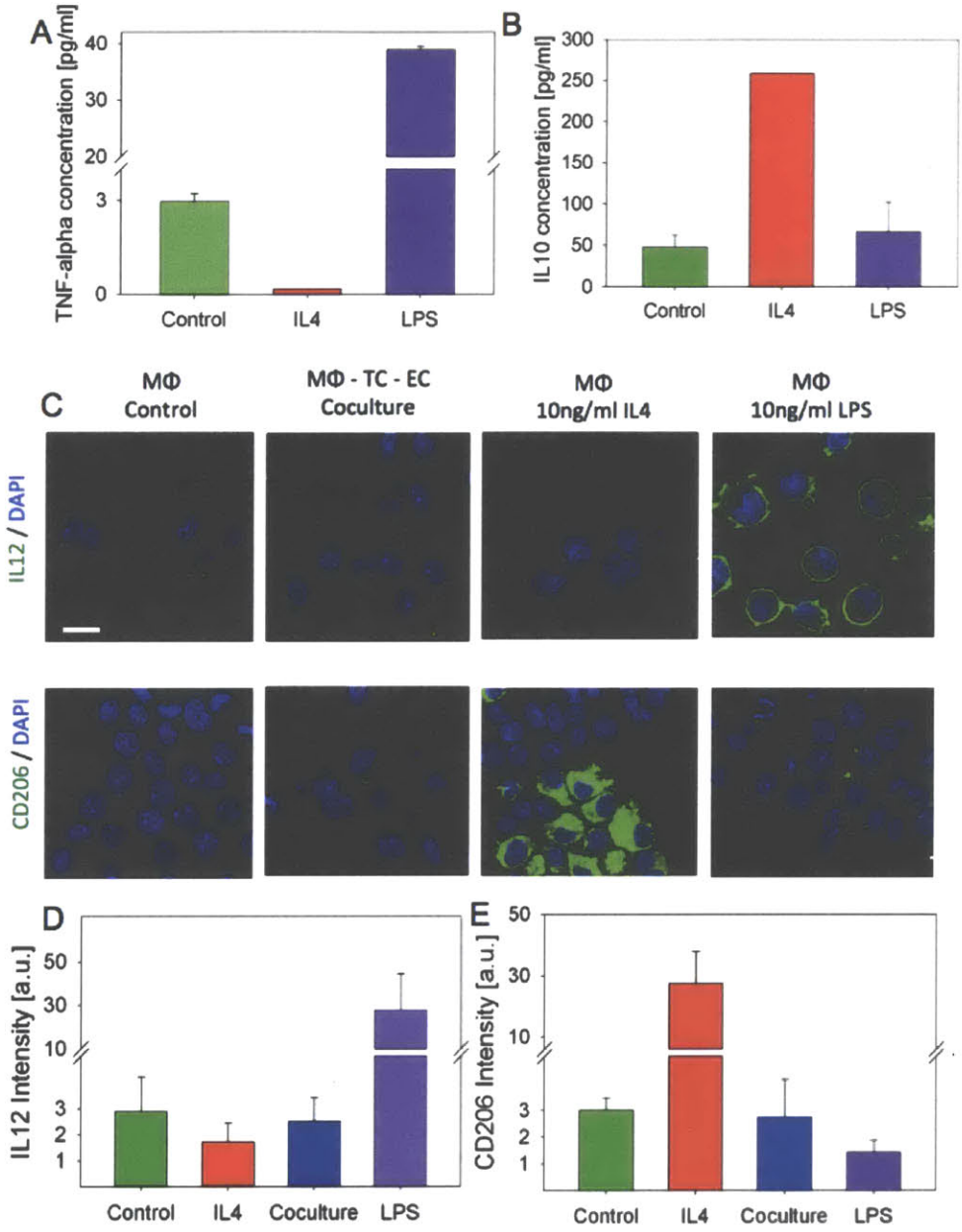

Figure 24: Characterization of TNF-α (A) and IL10 (B) secretion rates under control, M1 and M2 macrophage polarization conditions. Average values and standard error of the mean for two independent experiments. (C) Immunofluorescence staining of M1 (IL12) and M2 (CD206) macrophage markers in the microfluidic device under macrophage monoculture, coculture with breast carcinoma and endothelial cells, and M2 (10ng/ml IL-4) and M1 (10ng/ml LPS) polarization conditions. (D,E) Quantification of fluorescent intensity of IL12 and CD206 markers under the conditions shown in panel (C). Average values for n=10 cells per condition. Error bars represent standard deviation.

4.4. Discussion

We employed our intravasation assay to investigate a critical question in cancer research, as to whether macrophages can promote cancer cell intravasation. Studies using different cancer and endothelial cell lines demonstrated that the presence of macrophages resulted in a significant

increase in the number of tumor cells that intravasated and was associated with a leaky endothelial barrier. Blocking antibody studies demonstrated that macrophage-secreted TNF-α is involved in the macrophage-mediated intravasation increase, and characterization of macrophage polarization status demonstrated that they form a heterogeneous M1/M2 population. To further investigate the ability of macrophages to impair endothelial barrier function, we compared their potency in increasing endothelial permeability with human tumor and epithelial cells and found that macrophage coculture resulted in the largest permeability values.

The results of macrophage-mediated barrier impairment and the associated increase in intravasation taken together with our findings of increased tumor-endothelial interactions by TNF-α stimulation (chapter 3) highlight the role of the endothelium as a barrier to tumor invasion. Interestingly, although cAMP stimulation resulted in enhancement of endothelial barrier function, intravasation rates were only slightly reduced. Moreover, qualitative observations of macrophages being proximal to the intravasation site suggested that apart from soluble signals, juxtracrine macrophage-endothelial interactions may also regulate tumor cell transendothelial migration.

Intravasation efficiency

An important finding of our work is that, under conditions of intact endothelial barrier function, breast carcinoma cell intravasation is a rare event, with less than 1% being able to migrate across the endothelial barrier. This was a very challenging aspect in the beginning of our work, since we had very few events to quantify and we were looking for ways to increase the intravasation efficiency. One possible way to increase the number of tumor cells intravasating over a specific time period was to reduce the 3D matrix collagen density. However, reducing the collagen gel density led to matrix contraction, which distorted the interface and made it difficult to observe intravasation events. Although a structurally irregular endothelial barrier might be more physiologically relevant, we chose experimental conditions (2.5mg/ml collagen type I matrix, tumor cell seeding density and endothelial monolayer seeding protocol) to ensure a flat endothelial monolayer – 3D matrix interface.

Our observation of low intravasation rates are in agreement with previously published *in vitro* and *in vivo* data. Stoletov et al showed that in a zebrafish model of tumor cell invasion, only 1.7% of human breast carcinoma cells sent protrusions inside the fish vasculature (52). Similarly, studies from the Condeelis group have found that in an *in vitro* transwell model less than 1% of tumor cells (46) completely transversed the endothelial monolayer and *in vivo* only 18 of 96 fields contained single intravasation events as recorded by intravital imaging (13).

To test the utility of our assay as a discovery platform we tested the intravasation efficiency of two different breast carcinoma lines, the parental cell line and the same cells expressing the MenaINV actin binding protein. The MDA231MenaINV were more potent in intravasating compared to the MDA231GFP l cells. In particular, the presence of macrophages resulted in a 9-fold increase for the MDA231MenaINV cells compared to a 4.5-fold increase for the MDA231GFP parental cells. *In vivo* studies in mouse xenografts with rat breast carcinoma cells (MTLn3) expressing the same MenaINV protein showed a 4-fold difference in the number of circulating tumor cells between the two cells lines (46). Our measurements on fibrosarcoma

tumor cell intravasation efficiency (chapter 2) demonstrated higher intravasation rates (7% and 10% for MVEC and HUVEC cell lines respectively) compared to the carcinoma cell lines.

Role of macrophages and macrophage polarization in intravasation

Our findings have shown that macrophages can facilitate intravasation for different breast carcinoma cell lines and for different endothelial cell lines. Interestingly, blocking the macrophage-secreted TNF-α did not reduce intravasation rates back to the control condition, without macrophages, suggesting that there are additional factors regulating intravasation. In our experiments macrophages were present both in the endothelial channel and inside the 3D matrix, suggesting that juxtracrine interactions between macrophages-tumor-endothelial cells may also be involved in facilitating intravasation. Hence, an important question to be investigated is whether tumor cell intravasation requires macrophages to be in contact with the tumor cells at the location of intravasation. This is an open question in cancer metastasis and has critical implications for the mechanism of intravasation. To address this question, experiments should be performed to identify whether macrophages located distally from the endothelial barrier (e.g. seeded in a separate microchannel rather than the endothelial channel) can facilitate intravasation via the secretion of paracrine factors.

In addition to the end-point characterization of macrophage localization (Figure 22), it would be very interesting to analyze macrophage localization and transmigration during the process of an intravasation event. Macrophage presence on different sides (apical vs. basal) of the endothelial surface, could signal via different mechanisms to the endothelial cells and the tumor cells. Elegant work from the Condeelis group showed that in transgenic breast cancer tumors in mice, macrophages were found in the perivascular tissue compartment and resulted in increased tumor cell invasion (13). Our results of macrophage-induced intravasation are in agreement with both *in vitro* (46) and *in vivo* studies (13), as well as with clinical specimens from metastatic breast tumors (12).

With respect to the juxtracrine macrophage-tumor-endothelial interactions, interestingly, the macrophage cell line (RAW264.7) used in our study has been shown to undergo transendothelial migration across HUVEC monolayers *in vitro* in macrophage-endothelial cell cocultures (161). Hence, this raises an interesting question of whether macrophages also transmigrate during tumor cell intravasation and whether this actually enhances tumor cell intravasation. Our findings of the lack of complete inhibition of tumor cell intravasation upon TNF-α blocking raises the possibility that juxtracrine interactions are also critical in tumor cell intravasation. Further experiments are required to test this hypothesis.

Characterization of M1 and M2 marker expression via immunofluorescence showed that although we could polarize the macrophages towards an M1 or M2 phenotype using biochemical stimulation, coculture conditions with tumor and endothelial cells did not polarize macrophages towards either an M1 or M2 phenotype. Our results of a mixed M1/M2 population are consistent with the central hallmark of macrophage plasticity (48) and are consistent with *in vivo* (162) and *in vitro* (163) studies. Also, our measurements of TNF-α and IL-10 secretion rates under control and stimulation with IL-4 and LPS are consistent with the M1/M2 polarization model and the associated regulation of secreted factors (48).

Conflicting results, however, are reported in the literature with respect to the tumor-induced macrophage polarization. Hagemann et al used a transwell system and showed that coculture of macrophages with tumor cells resulted in increased TNF-α and MMP expression, suggesting that macrophage polarization was biased towards an M1 phenotype (141). On the contrary, the results of macrophage IL-6 upregulation by Wang et al suggest polarization towards an M2 phenotype (142). Future studies to investigate in detail the M1/M2 polarization status of macrophages and their role in tumor invasion and endothelial barrier function regulation are necessary.

Role of endothelial cell phenotype in intravasation

An important consideration in studying tumor cell intravasation is the type of endothelial cells used to form the endothelial barrier. Nagy et al characterized the barrier function of "tumor-like" blood vessels in the mouse dorsal ear skin after injection of a VEGF adenovirus and demonstrated that these vessels are hyperpermeable by tracing ferritin transport across the vessel wall (25). Compared to normal vessels, tumor blood vessels were estimated to be 4-10 times more permeable. Furthermore, studies on tumor endothelial cells have shown significant differences in gene expression patterns compared to normal endothelial endothelial cells (21).

To explore the role of the endothelial cell phenotype in intravasation we compared the intravasation efficiency of microvascular endothelial cells and two cell lines of macrovascular endothelial cells, a wild-type control and a HUVEC line (shPerlecan-HUVEC) that expressed lower levels of Perlecan. The shPerlecan-HUVEC line has been previously used as a model of "dysfunctional" endothelial cells, which may mimic tumor endothelial cells (22). We found that these dysfunctional endothelial cells were significantly leakier compared to the wild-type controls and also tumor cells intravasated more readily across them. An interesting observation here, is that the presence of macrophages resulted in a 1.4-fold increase in intravasation for the dysfunctional HUVEC cells compared to the much higher 4.4-fold increase for the wild-type endothelial cells. An important point however, which could complicate this comparison, is that Franses et al showed that dysfunctional endothelial cells also promoted tumor cell invasion (22). Additional studies are required to determine whether the increase in intravasation was due to the increased permeability or due to enhancement of tumor cell invasiveness.

The results with the dysfunctional HUVEC cell line provide additional evidence that the endothelium poses an active barrier to tumor cell intravasation and its impairment results in a significant increase in the number cells that migrate through. Future work, should investigate the barrier function of endothelial monolayers using endothelial cells derived from tumors. These endothelial cells would have been adapted to the tumor microenvironment and it is critical to understand whether the origin of the cells can influence tumor cell transmigration. Elucidation of differences between normal and tumor endothelial cells will have important implications for therapeutic targeting of tumor blood vessels.

Enhancement of endothelial barrier function via cAMP

In the presence of macrophages, addition of high cAMP concentration in the endothelial channel resulted in a significant enhancement of endothelial barrier function, which is in agreement with

studies on endothelial monoculture (101). Under these conditions of significantly lower permeability values, interestingly, however, tumor cell intravasation rate was only mildly reduced (Figure 23). To interpret this result, we propose two different hypotheses: a) the high cAMP concentration (0.5mM) used to normalize the endothelial barrier may also result in pro-invasive effects on tumor cells or macrophages and in turn result in higher tumor cell invasiveness and b) Normalization of barrier function with cAMP may not interfere with the expression of surface adhesion molecules induced via TNF–α stimulation on endothelial cells, which then facilitate intravasation.

The low molecular weight (<500 Da) of cAMP would be associated with small diffusive permeability values, which can result in high cAMP concentrations on the basal endothelial surface and thus may stimulate cAMP-related signaling pathways in tumor cells and macrophages. Yamashita et al showed that MDA231 cells, treated with forskolin that lead to high intracellular cAMP concentrations, exhibited larger membrane protrusions associated with enhanced tumor cell motility (164). According to this study, however, cAMP stimulation may also affect tumor cell motility, and therefore this represents an ambiguous method to investigate the relationship between permeability and intravasation.

To investigate the second possible explanation, further studies on endothelial cell adhesion molecules (e.g. using immunofluorescence methods and biochemical assays) are necessary. In particular, it would be interesting to design experiments using endothelial cell lines that could be induced to express different levels of cell-cell adherens junctions (resulting in different permeability) to investigate the correlation and causal role of endothelial permeability and tumor cell intravasation. Furthermore, to test whether tumor cell intravasation is linearly correlated with endothelial permeability, experiments where a dose-dependent perturbation of endothelial permeability would be induced and intravasation rate would be measured are necessary. It is possible, that tumor cell intravasation and permeability are non-linearly related. For example, this could be a threshold behavior, where intravasation may increase until a threshold value of endothelial permeability, corresponding to sufficient changes on endothelial cell-cell junctions that facilitate high intravasation rates.

Specificity of macrophage-induced endothelial permeability

Not surprisingly, multiple cell types in the tumor microenvironment can regulate endothelial barrier function. Our results show that although macrophages are the most potent cell type in increasing endothelial permeability, the presence of both tumor and normal epithelial cells could also increase endothelial permeability values. This could be explained by secretion of angiogenic factors (e.g. VEGF) by the tumor and mammary epithelial cells (165). In a relevant study of endothelial barrier function impairment via tumor cells, Hu et al found that ovarian cancer cells induced a 3-fold increase in transport of 10kDa dextran across a HUVEC monolayer in a VEGF and VE-Cadherin dependent mechanism (127).

In the presence of macrophages, the observed two-fold increase in endothelial permeability is in agreement with a transwell based study by Wakamoto et al, who showed that conditioned medium from HLA Class II antibody stimulated peripheral blood mononuclear cells induced a 3-fold increase in transport of 40kDa dextran across HUVEC monolayers (147). Contrary to these

results, Zenker et al reported an enhancement of endothelial barrier function in a non-contact transwell coculture with human blood derived macrophages and brain endothelial cells (146).

Different cell sources

Finally, an important note when investigating tumor-endothelial cell interactions is the source of the endothelial and tumor cells. Investigators have utilized both primary human endothelial cells (HUVEC, (43)) as well as established cell lines (HMEC, (46)) to form endothelial monolayers. Bouis et al provide a thorough review of different established endothelial cells lines and their limitations (166). As we discussed earlier in this chapter, future work should systematically compare intravasation efficiency across different endothelial cell lines, and also investigate the role of human derived macrophages (the RAW264.7 macrophage-like cell line used in all the experiments in this thesis is of murine origin).

Chapter 5: Effects of biochemical factors on endothelial barrier function and intravasation

To further investigate the role of macrophage-secreted factors in tumor cell intravasation, we review the role of the inflammatory biochemical factor TNF-α on tumor cell invasion and endothelial cell biology. Next, we present experimental evidence of intravasation enhancement in TNF-α stimulated endothelial monolayers in the absence of macrophages. We conclude this chapter by comparing our results with different studies on cytokine stimulated endothelial barriers and discuss the molecular mechanism.

5.1.1 Endothelial barrier regulation via biochemical and biophysical factors

Alterations in endothelial barrier function are important for regulating transport of water, oxygen, plasma proteins, solutes and cells (167). Michel and Curry (112) present an excellent comprehensive description of different permeability coefficients (hydraulic permeability, diffusive permeability, ultrafiltration coefficient and osmotic reflection coefficient). The permeability coefficients depend on the molecular size of the solute transport, and intact vessels show a decline in the ratio of the diffusive permeability coefficient to the diffusion coefficient (P_D/D) with increasing molecular size due to the reduction in free area available for diffusion (168). Transport across a continuous intact endothelium can occur either via transcytosis (transcellular route) for macromolecules with a radius larger than 3nm or via interendothelial cell-cell junctions (paracellular route) for smaller macromolecules (169). Paracellular transport is maintained by the endothelial cell-cell junctions which are organized into two distinct groups: tight junctions and adherens junctions (169). Members of the cadherin family form adherens junctions and Dejana et al provide a detailed review on the role of VE-Cadherin on vascular permeability control (170).

DeMaio et al used a transwell-based assay and showed that VEGF stimulation (50ng/ml) of bovine retinal endothelial cells resulted in increased endothelial permeability to 70kDa dextran and water (171). Endothelial stimulation with TNF-α results in robust endothelial barrier impairment (172), and similar effects have been reported for other cytokines and proteases such as Interleukin-1β (173) and thrombin (149). Apart from the well-established role of cytokines in endothelial cell activation, Sahni et al showed that endothelial permeability can also be regulated by fibrinogen, a 340kDa glycoprotein presented in the blood plasma and produced by hepatocytes, via VE-Cadherin binding (174). A detailed review of the molecular mechanisms of biochemical mediators that increase and decrease endothelial permeability is provided by Komarova et al (169).

Abnormal blood vessel architecture and ECM remodeling in tumors may result in altered blood flow patterns and in increased interstitial fluid pressure, which can lead to transendothelial flow across the endothelium. Using a transwell-based transendothelial flow system Miteva et al demonstrated that basal to apical flow in lymphatic endothelial cells resulted in increased endothelial permeability to 3kDa dextran (175). Warboys et al investigated the effects of exposure to acute (1hour) versus chronic (7days) shear stress on endothelial permeability to labeled albumin (176). Interestingly, acute exposure increased endothelial permeability, whereas

chronic exposure resulted in endothelial barrier enhancement. Recently, Huynh et al investigated the role of substrate stiffening on endothelial permeability by forming bovine aortic endothelial monolayers on polyacrylimade matrices of varying stiffness (177). Stiffer substrates resulted in higher diffusive permeability values and wider VE-Cadherin junctions in a ROCK-dependent mechanism. In the table below we summarize the effects of different acellular factors on endothelial permeability, and we also refer the reader to chapter 4 for the effects of different cell types on endothelial permeability.

Table 5: Effects of different biochemical and biophysical factors on endothelial permeability

Biochemical / Biophysical factor	Effects on permeability	Mechanism	References
Cyclic AMP	[-] Decrease diffusive permeability	ERM proteins redistribution	(158)
TNF-α	[+] Increased diffusive permeability	Tight junctions redistribution	(172)
VEGF	[+] Increased diffusive permeability	Src-mediated signaling of VE-Cadherin internalization	(171)
Fibrinogen	[+] Increased diffusive permeability	VE-Cadherin binding	(174)
Thrombin	[+] Increased diffusive permeability	Cleaves and activates PAR-1	(149)
Shear stress	[+/-] Increased / decreased depending on exposure duration	Nitric oxide, PI3K and cGMP mediated	(176)
Interstitial flow	[+] Increased diffusive permeability in lymphatic endothelial cells	ICAM-1 dependent	(175)
Matrix stiffness	[+] Increased diffusive permeability	Cellular contractility (ROCK)	(177)

5.1.2 TNF-α signaling pathways

TNF-α is a member of the TNF ligand superfamily which has highly diversified roles in cell signaling (178). This pro-inflammatory protein has a molecular weight of 17kDa and was first discovered in 1985 in the human promyelomonocytic cell line HL60 conditioned medium (179). TNF-α interacts with two cell surface receptors TNF-R1, which is expressed on every cell type studied to date, and TNF-R2, which is limited to immune, endothelial and nerve cells (180). Binding of TNF-α to these receptors can result in activation of diverse signal transduction pathways including apoptotic, proliferative and pro-inflammatory pathways. More specifically, at least 5 different intracellular signaling complexes can be activated including Caspase-3, NF-kβ, extracellular signal regulated kinase (ERK), p38 mitogen-activated protein kinase (p38MAPK) and c-Jun N-terminal kinase (JNK).

TNF-α has been shown to have both beneficial and potential harmful effects, as it has been linked with physiologic proliferation of B cells and with many diseases, such as cancer (180). This paradoxical role of TNF-α can be explained by the complexity and diversity of the signal transduction pathways that it is involved in (Figure 25). In the next section we review studies that have highlighted the diversity of TNF-α effects in tumor and endothelial cells. In addition to the discussion in the previous chapter on the effects of cellular interactions on endothelial permeability, we review the effects of different biochemical factors on endothelial barrier function.

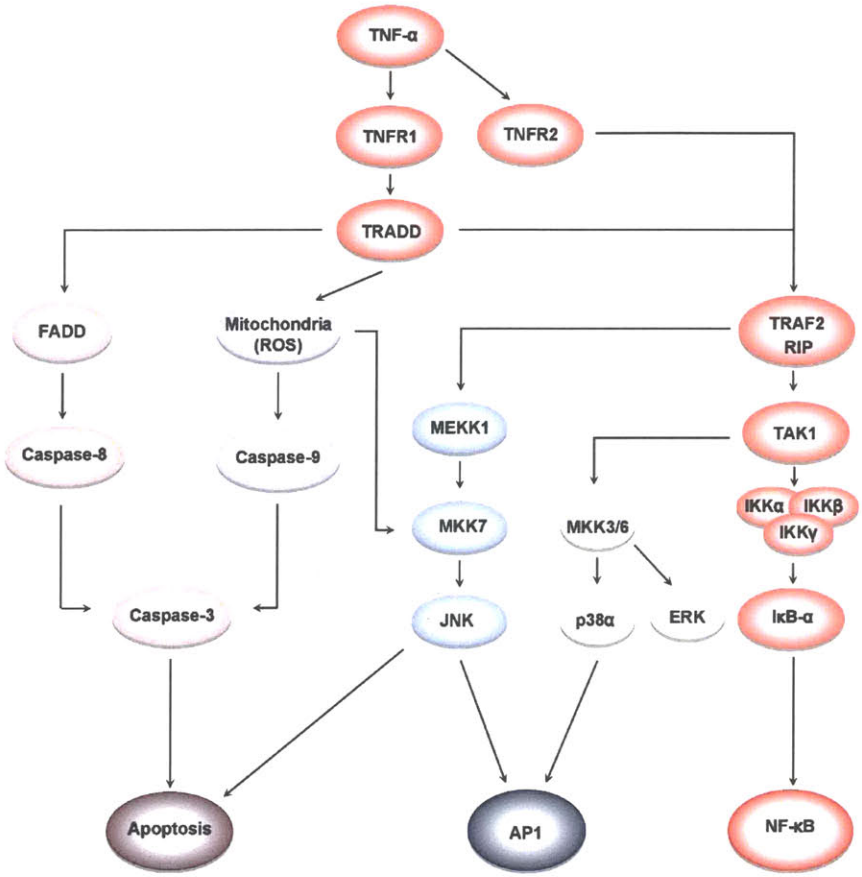

Figure 25: TNF-α signal transduction pathway complexity [figure from (180)]

TNF-α effects on Tumor Cells

TNF-α acquired originally its name as tumor necrosis factor alpha because of its ability to induce necrosis of subcutaneous tumors transplanted in mice (181). Interestingly TNF-α has been shown to exert both powerful anticancer activity for melanoma metastases (182) and to be associated with poor prognosis in human tumors (183). Montesano et al showed that TNF-α stimulation of epithelial spheroids enhanced single cell dispersion in 3D collagen type I gels and on two dimensional substrates (184). TNF-α has also been shown to be implicated in EMT via Snail and β-catenin protein stabilization (185). In the tumor microenvironment, macrophages act as a source of TNF-α, which can in turn enhance cancer cell invasiveness (Figure 26). Hagemann et al, used a transwell assay to show that macrophage coculture increased invasion in human breast cancer cell lines, whereas migration of benign epithelial cells remained unchanged (141). This enhanced invasion was mediated by an increase in macrophage secreted TNF-α and MMPs.

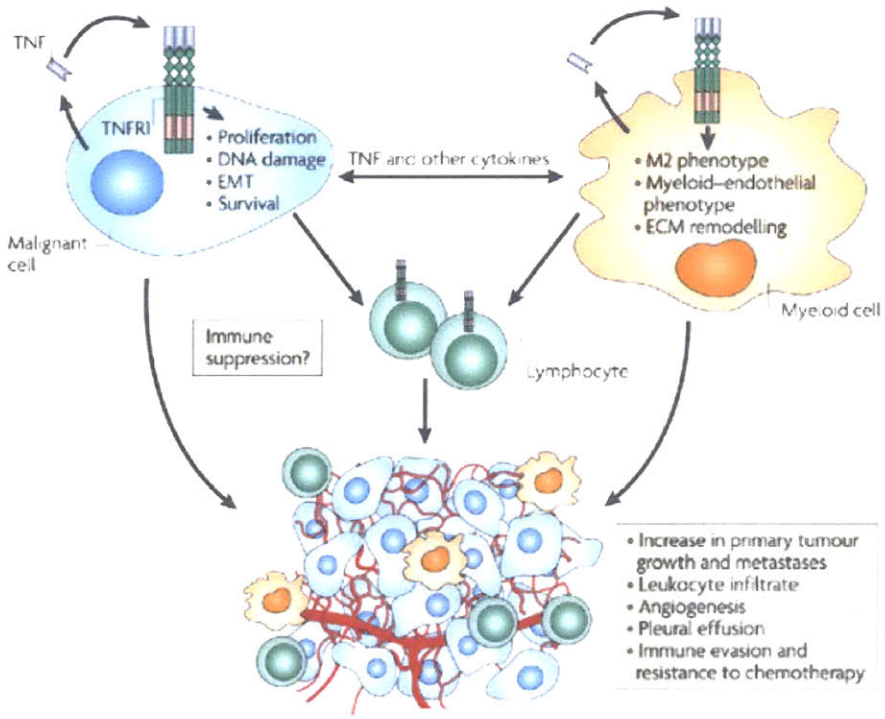

Figure 26: Diverse roles of TNF-α signaling on tumor cells and tumor-immune cell interactions in the tumor microenvironment [figure from (183)]

TNF-α effects on Endothelial Cells

Pober and Cotran proposed a framework to classify the response of endothelial cells to cytokines in three ways: (a) injury during immune response (b) angiogenic sprouting via invasion and proliferation and (c) activation. Endothelial activation, is defined as the ability to perform new functions without endothelial cell death (injury) or proliferation (167). Endothelial cell activation via TNF-α (Figure 27) leads to upregulation of pro-inflammatory signals with increased cell surface adhesion molecule expression, which are also associated with vascular leak (186). Both *in vivo* and *in vitro* studies (120) have shown that TNF-α induces endothelial barrier impairment. Mark et al showed that endothelial cell exposure to TNF-α resulted in a time-dependent, reversible and graded endothelial permeability response (120).

Many studies have shown that surface adhesion molecules (VCAM-1, ICAM-1 and E-Selectin) are upregulated in TNF-α treated endothelial monolayers (187) in a time and dose-dependent manner for both macrovascular and microvascular endothelial cells (188). Endothelial monolayers treated with high TNF-α doses (100ng/ml) exhibited morphological changes, such as membrane ruffling and extension of filopodia, which were mediated via Rho, Rac and Cdc42, resulting in formation of intercellular gaps (189). These morphological changes are correlated with changes in endothelial permeability, and VE-Cadherin redistribution. Not surprisingly, the effects of TNF-α are concentration dependent, with low concentrations (1ng/ml) leading to increased paracellular permeability and redistribution of junctional proteins, whereas higher concentrations (10 and 100ng/ml) result in caspace-3/7 activation and cell death by apoptosis (190). Activation of endothelial monolayers with TNF-α also influences he secretion of basement

membrane proteoglycan proteins and results in altered proteoglycan metabolism (191). In a related study, Partridge et al showed that the TNF-α-induced endothelial permeability increases were associated with loss of deposited fibronectin and ECM remodeling.

McKenzie and Ridley demonstrated that short-term exposure to TNF-α activated RhoA and phosphorylated myosin light chain kinase, however only small changes to cortical actin were observed and there were no significant changes in permeability (172). Prolonged exposure to TNF-α caused a progressive increase in endothelial permeability, cell elongation and intercellular gap formation. A redistribution of the tight junction protein ZO-1, and a removal of Occludin and JAM-A from tight junctions were also observed consistent with the measured increases in permeability. The molecular mechanism underlying endothelial permeability increases after TNF-α treatment involves reorganization of tight junction proteins (172) and reorganization of ezrin/radixin/moesin (ERM) proteins through p38 MAPK activation (192). These ERM proteins function as membrane-cytoskeletal linkers and are required for cytoskeletal rearrangements(193). Koss et al showed that endothelial permeability was not increased in TNF-α stimulated endothelial barriers in the presence of a p38 MAPK specific inhibitor or treatment with siRNA for the ERM proteins (192).

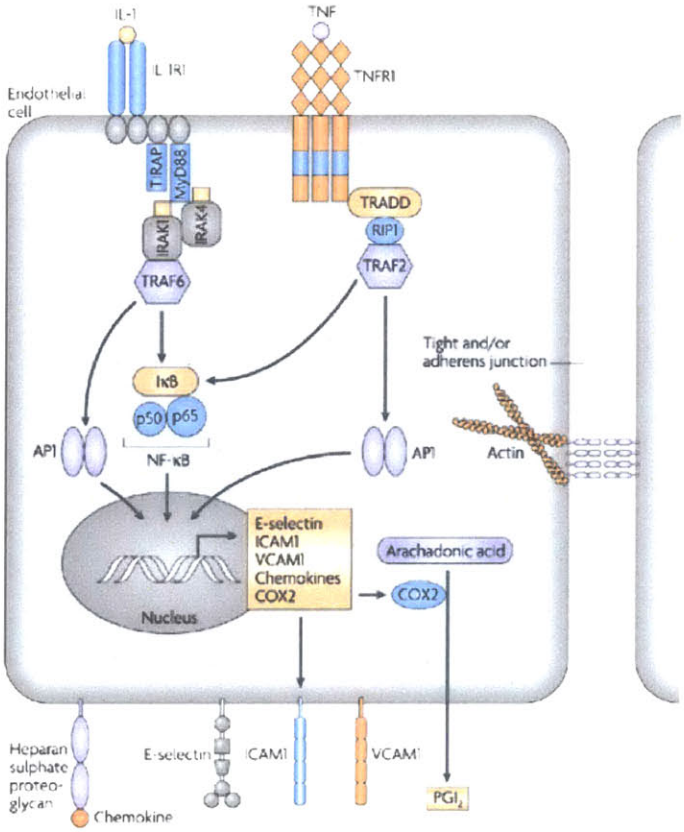

Figure 27: Signal transduction pathways activated in endothelial cells upon TNF-α/TNFR-1 binding. Multiple cellular functions are modulated including, apoptosis, cell surface adhesion molecule expression (e.g. ICAM1), tight junction and adherens junction reorganization, cytoskeletal changes and NF-κβ signaling [figure from (186)]

TNF-α targeted therapy

TNF-α is involved in a variety of human diseases, such as autoimmune, cancer, cardiovascular, diabetes, neurologic and pulmonary diseases (180). A number of TNF-α targeted therapeutics have been approved by the FDA for autoimmune diseases (rheumatodis arthritis and psoriasis) and others are in ongoing clinical trials (180). These therapeutics are mainly TNF-α antagonists, including monoclonal antibodies and receptor derivatives. Adverse effects from these therapeutics include increased risk of infection, blood disorders, lymphomas and solid tumors.

5.2. Biochemical stimulation methods

TNF-α stimulation in intravasation assay

3D matrices seeded only with MDA231MenaINV breast carcinoma cells were injected into devices prepared using the methods described in chapter 4. Forty-eight hours after seeding a single endothelial cell suspension in the endothelial channel to ensure the formation of a confluent monolayer, and different doses of TNF-α were added only to the endothelial channel. Endothelial permeability was measured 48hours after TNF-α stimulation and devices were fixed, stained and imaged to identify tumor cells that had intravasated. We also performed tracking of tumor cell migration in the intravasation experiments in order to investigate the effect of TNF-α on tumor cell migration. Endothelial monolayers had been stimulated for at least 40 hours before live cell imaging to monitor cell migration using the methods described in chapter 3.

5.3. Biochemical regulation of endothelial permeability and intravasation

Modulation of endothelial barrier function with TNF-α in the presence of tumor cells

We were interested to investigate whether perturbation of endothelial permeability with biochemical factors in the absence of macrophages, could also result in enhanced intravasation rates. We designed experiments under the same experimental conditions as those described in the control experiments (chapter 4). Stimulation with 2ng/ml TNF-α resulted in higher permeability values (2.27×10^{-5} cm/s) compared to control (1.8×10^{-5} cm/s), resulting in a 1.26-fold statistically significant ($p=0.0363$) increase (Figure 28B).

Tumor cell intravasation under biochemically perturbed endothelial barrier function

We found that a significantly ($p=0.034$) higher percentage of MDA231MenaINV tumor cells (7.25%) intravasated after 2ng/ml TNF-α stimulation compared to the control conditions (0.45%). We also compared the tumor cell migration speed of tumor cells in the vicinity of the endothelium and found that it did not significantly ($p=0.39$) change after TNF-α stimulation. More specifically, the breast carcinoma cells migrated at 13.23 μm/hr under control conditions compared to 14.82 μm/hr under TNF-α conditions.

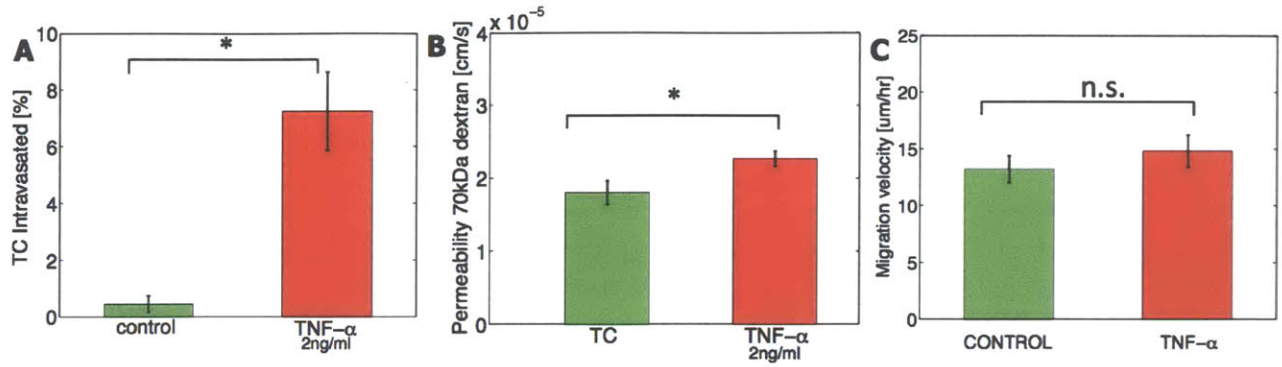

Figure 28: (A) TNF-α stimulation increases carcinoma cell intravasation in the absence of macrophages. Average values for n=3 devices per condition. (B) Absolute endothelial permeability to 70kDa dextran in the intravasation experiments. Average values for n=6 regions per condition. (C) Quantification of breast carcinoma mean migration speed. Average values for n=10 trajectories per condition. Error bars represent standard error of the mean.

5.4. Discussion of underlying mechanism and comparison with macrophage-induced intravasation

To further test the hypothesis that endothelial barrier impairment is associated with higher tumor cell intravasation efficiency, we stimulated the endothelial barrier with TNF-α and measured the number of tumor cells that had intravasated. We showed that exposing endothelial monolayers to TNF-α can also increase endothelial permeability in the presence of tumor cells, consistent with our results of the TNF-α dose response on the endothelial monoculture in chapter 2. Under these conditions, tumor cell intravasation was increased, whereas we did not observe a significant increase in tumor cell motility. The measured increase in intravasation rate upon endothelial barrier perturbation with TNF-α provides further support to our findings of macrophage-induced endothelial barrier impairment to assist tumor cell intravasation in chapter 4. Taken together these results suggest that the endothelium poses a barrier to tumor cell intravasation and that factors in the tumor microenvironment that can impair endothelial barrier function can facilitate intravasation.

Effects of TNF-α on endothelial cells

Our measurement of TNF-α effects on endothelial permeability in the intravasation studies (Figure 28) are in agreement with the endothelial monoculture dose response (Figure 12) and experiments using human fibrosarcoma cells under invasive growth conditions (Figure 17). It is important to note that a more sensitive measurement can be obtained by monitoring the temporal profile of transendothelial transport in the same device after addition of TNF-α, compared to average measurements from multiple devices. We also discussed this issue in chapter 2 and have suggested that it might be explained by variations in endothelial seeding in different devices.

Apart from the upregulation of the inflammation related signal transduction pathways in endothelial cells through TNF-α stimulation, an important additional point that should be further investigated is the potential effects of endothelial permeability increases on establishing altered exogenous (e.g. EGF) and endogenous (e.g. tumor cell CSF-1 autocrine) gradients. Under TNF-α stimulation conditions, the effective EGF concentration inside the 3D matrix can be different

than the control experiments. In order to get an order of magnitude estimate for these concentrations we may consider that EGF has the same diffusive permeability as the 10kDa dextran and calculate the effective concentration on the basal endothelial surface under assumptions of negligible EGF binding to the matrix and to the endothelial surface. The first assumption requires further study since Yang et al showed that EGF can bind to collagen type I (194), whereas the latter assumption is warranted due to the low expression of EGF receptors by endothelial cells (121).

TNF-α effects on tumor cells

Previous studies have shown that the TNF-α effects on tumor cell migration depend on cell type, TNF-α concentration and duration of treatment. Hou et al (195) showed that a very high concentration (100ng/ml) is required to increase migration of chondrosarcoma cells, whereas Montensano et al showed that dose as low as 1ng/ml is sufficient to induce enhanced 3D invasion after 48hours (184). Studies of epithelial cells in 3D collagen gels have demonstrated increased expression of MMP-9 and α2β1 after stimulation with 10ng/ml TNF-α (184). We have shown that under stimulation with 2ng/ml of TNF-α, tumor cell migration speed is not significantly affected in the first 12 hours. However, there might be activation of other inflammation related signal transduction pathways (e.g. expression of surface adhesion molecules) which may also regulate the ability of tumor cells to intravasate, in addition to the endothelial barrier impairment. Future studies are required to investigate the expression of these pathways (e.g. integrins, MMPs) in tumor cells when in contact with the endothelial barrier.

TNF-α effects on transendothelial migration and intravasation

Our results of TNF-α induced enhancement of tumor cell intravasation and tumor-endothelial cell interactions are in agreement with a transwell study by Okada et al (138). In this study, HUVEC monolayers and the fibrosarcoma HT1080 cell line were used to demonstrate that stimulation of HUVEC cells with 1ng/ml TNF-α resulted in a 2-fold increase in the number of HT1080 cells that invaded the HUVEC seeded filters in a E-selectin dependent mechanism. Interestingly, the role of TNF-α has also been shown in transmigration of other cell types apart from tumor cells. Teo et al used a live-cell imaging based transmigration assay, where mesenchymal stem cells (MSC) were seeded on top of endothelial monolayers on glass coverslips and demonstrated that TNF-α enhanced bone marrow-derived MSC transmigration (187). Stimulation of endothelial barriers with high doses of TNF-α (100ng/ml) has also been shown to be critical for transendothelial migration of dendritic cells across lymphatic endothelial monolayers and was also associated with impaired barrier function (175) with increases comparable to our results.

An important direction for future work is to investigate the molecular mechanism of enhanced tumor cell intravasation in TNF-α treated endothelial monolayers. In particular, the effects on both endothelial and tumor cells should be investigated, as well as effects on their juxtracrine or paracrine interactions. For example, it would be necessary to investigate in the microfluidic device, how TNF-α alters endothelial cell-cell junctions and whether the endothelial cell secreted basement membrane integrity is affected. Both mechanisms are possible since previous *in vitro*

studies have demonstrated that TNF-α alters both endothelial basement membrane integrity (191) and VE-cadherin junctions (189).

Relationship between endothelial barrier function and transendothelial migration

The association between transendothelial transport of cells and biomacromolecules (cellular and diffusive permeability) is not surprising and could also be explained by common molecular players regulating these transendothelial transport routes. For example, myosin light chain kinase has been reported to be involved in both endothelial permeability changes in response to TNF-α (172) and also in tumor cell transendothelial migration via endothelial cytoskeleton contraction (43). Similarly, cell surface adhesion molecules which have been implicated in transendothelial migration (e.g. ICAM-1 (64) expressed on endothelial cells and linked with reverse transendothelial migration) have also been reported to regulate endothelial barrier function (196)

The association between vascular permeability and tumor cell transendothelial migration has also been demonstrated in the context of extravasation. Weis et al showed that in an experimental metastasis model, tail vein injection of tumor cells overexpressing VEGF resulted in enhanced extravasation efficiency (129). Stoletov et al, also showed that tumor cells overexpressing VEGF were more potent in sending invasive protrusions into the blood vessels of a transparent zebrafish (52), and relevant findings have been shown in the clinic where higher number of circulating tumor cells were found in colorectal tumors with higher blood vessel density (51). Apart from the role of cytokines in linking tumor cell transendothelial migration and permeability, Shen et al showed that breast cancer cell adhesion on the endothelial monolayer activated endothelial MMP-2 expression, which promoted transendothelial migration and decreased transendothelial resistance (197). The authors showed that these effects could be reduced by inhibiting TIMP-2 / MMP-14. In the future it would be interesting to perform MMP inhibition studies in the microfluidic device presented here and investigate the potential role of MMPs in intravasation. Finally, extracellular matrix proteins in the tumor microenvironment have also been shown to regulate both endothelial permeability and transendothelial migration. Sahni et al showed that fibrinogen enhanced transendothelial migration of metastatic tumor cells and interacted with VE-Cadherin to increase endothelial permeability (174).

Mechanism of tumor cell intravasation

An interesting analysis that could be performed using the unique capabilities of our assay is to characterize the time required for tumor cells to intravasate and relate this to the presence of macrophages. Furthermore, the sequence of events occurring during intravasation should also be characterized, as well as, whether macrophages need to be in contact with the tumor cells at the location of intravasation. Careful analysis of these movies may also lead to interesting observations, such as those in chapter 3 of hotspots of tumor cells crossing onto the endothelial channel, that could be explained by macrophages or tumor cells inducing remodeling of VE-Cadherin at spots where "leader" tumor cells have interacted with the endothelium that could be probed by the "follower" tumor cells as they are trying to migrate onto the channel (124).

Detailed observation of live cell movies of tumor cell intravasation demonstrated that tumor cells were heterogeneous in their ability to intravasate. This could be explained either by a

heterogeneous tumor cell population or by local changes to the microenvironment (e.g. local remodeling of the endothelial barrier (e.g. via macrophages?). Although, studies from the Quigley group have provided evidence for a heterogeneous tumor cell population (e.g. VEGF expression) (57), newer studies from the same group (16), as well as work by the Condeelis group (13), critically implicate factors in the tumor microenvironment to explain the measured differences in intravasation. Comparative analysis of serially injected prostate carcinoma cells in the chicken embryo assay, demonstrated that cancer cells that had been grown continuously in the embryo assay for seven or more passages, exhibited significantly higher intravasation rates compared to the parental cells (57). An important point to be considered is that this heterogeneity may also be relevant for human tumors in patients, which are continuously evolving during tumor progression and cancer metastasis. On the other hand, if we assume that local microenvironmental remodeling is responsible for this observed heterogeneous response, it would be interesting to investigate effective ways (including TNF-α with combination of other cytokines or endothelial-macrophage adhesion) to target the macrophage's ability to facilitate intravasation. Furthermore, a very interesting and open question that can be addressed with our assay is whether specific tumor-endothelial adhesion is required on the endothelial basal surface for tumor cell intravasation and what heterotypic cell adhesion molecules are involved.

Our findings of increased intravasation under conditions of increased permeability show a correlative relationship and additional investigations are required to identify a possible causal relationship. One of the challenges is how to uncouple the potential effects of macrophage-secreted and exogenously applied (TNF-α and cAMP) factors on tumor cell invasiveness from the effects on tumor cell intravasation, in order to accurately demonstrate that the increased permeability values are predominantly responsible for the increased intravasation rates. Finally, although we have demonstrated that macrophage-secreted TNF-α critically regulates tumor cell intravasation, additional blocking antibody studies should be performed to identify more possible targets that reduce intravasation (e.g. tumor-endothelial cell adhesion).

Chapter 6: Conclusions and Future work

6.1 Conclusions and thesis contributions

Tumor cell entry into the blood vessels is a rate-limiting step in cancer metastasis and ultimately accounts for 90% of cancer-related deaths. A major barrier for the development of effective targeted therapies against cancer metastasis is the lack of complete knowledge of the underlying mechanisms. Although, imaging tumor cell motility *in vivo* has significantly advanced recently, our limited understanding of cancer cell intravasation is in part because of the lack of physiologically relevant *in vitro* models and the challenges associated with dissecting tumor-endothelial interactions *in vivo*. In this thesis, we have designed and validated a microfluidic-based 3D assay to monitor tumor-endothelial-macrophage interactions in the context of intravasation. We employed our novel assay and approach to address a critical question in cancer research and determine whether tumor cell intravasation requires endothelial barrier impairment.

Compared to other *in vitro* models of tumor-endothelial cell interactions, the assay presented in this thesis has the advantages of a well-characterized endothelial barrier with a hollow lumen on a 3D matrix and the inclusion of a third cell type. Furthermore, it allows for direct observation of cellular shape and endothelial junction integrity, combined with real-time, spatially resolved measurement of the endothelial barrier function. The utility of our assay is supported by the demonstration of size-selective endothelial barriers with comparable permeability values to other *in vitro* systems. Dose response studies to the inflammatory cytokine TNF-α showed a graded endothelial permeability response, and our method was able to differentially measure endothelial permeability for various endothelial cell lines. Using a human metastatic fibrosarcoma cell line we also demonstrated the ability to image and quantify tumor cell intravasation in a 3D matrix across a hollow vascular lumen.

Transport of oxygen, nutrients, biomolecules and cells across different organs is regulated by the vascular endothelium operating as a selective and dynamic barrier. Tumor blood vessels are both structurally and functionally abnormal, however it has been largely unknown whether endothelial barrier dysfunction plays a role in tumor cell intravasation. We employed our model to address this question and have showed, that an intact endothelial monolayer poses a barrier to tumor cell intravasation with less than 0.5% of tumor cells intravasating under control conditions. Using biochemical stimulation with TNF-α and dysfunctional endothelial barriers, we showed that higher values of endothelial permeability were associated with increased intravasation, ranging from a four-fold to a ten-fold increase compared to the control conditions. These results may be explained by common molecular mechanisms (e.g. mediated via endothelial cell-cell junctions) regulating transport of both biomolecules and cells across the endothelial barrier. Not surprisingly, the association between permeability and transendothelial migration has also been shown in the context of cancer cell extravasation (129) as well as for other cell types including dendritic (175) and white blood cells (198).

The ability to visualize tumor cells in the process of intravasation is critical for gaining insights into the underlying mechanisms of tumor-endothelial-macrophage interactions. We performed real-time imaging of tumor cell invasion at single cell resolution and also high-resolution

endpoint imaging to assess endothelial monolayer integrity. By tracking the trajectories of tumor cells as they migrate towards and across the endothelial barrier we provide new data on the largely unexplored time-scales of tumor-endothelial interactions under a well-controlled microenvironment. Careful observation of the time-lapse videos led to a number of interesting qualitative observations: (i) tumor cells formed dynamic invasive protrusions to probe the 3D environment and the endothelial barrier, (ii) endothelial cells were not static but actively migrating within the endothelial monolayer, (iii) tumor cell shape changed significantly in the process of intravasation and (iv) tumor cells migrated preferentially towards regions of endothelial monolayer remodeling. Interestingly, this last observation of tumor-endothelial interaction "hotspots", suggests possible tumor-tumor cell cooperation during tumor cell invasion and active bidirectional tumor-endothelial signaling. Consistent with the intravasation results, we found that endothelial barrier impairment also regulated the number and dynamics of tumor-endothelial interactions.

Macrophage infiltration in breast tumors has been associated with poor prognosis, however the role of macrophages on vessel remodeling and their contribution to tumor cell dissemination remains largely unknown. Using our microfluidic-based approach we found that the presence of macrophages resulted in increased intravasation and also led to an impaired endothelial barrier function via secretion of soluble TNF-α. In these experiments, macrophages were localized to both the apical and basal endothelial surfaces, suggesting that both paracrine and juxtracrine interactions were possible in our experiments. To demonstrate the robustness of the observed phenotype, we performed intravasation experiments with different endothelial and tumor cell lines and found similar results. Characterization of macrophage polarization status in a M1 or M2 state was performed via measurement of secreted cytokines and immunostaining. Macrophages formed a heterogeneous and mixed M1/M2 population under control monoculture conditions, which could be driven to an M1 or M2 state through biochemical stimulation with LPS or IL-4 respectively. However, we did not observe any significant changes in M1 and M2 marker expression between macrophage monoculture and conditions of macrophage-tumor-endothelial coculture. To investigate the specificity of macrophage-induced endothelial barrier impairment, we cocultured epithelial and cancer cells and measured endothelial permeability. Comparison of endothelial permeability values revealed that macrophages were the most potent in impairing endothelial barrier function. To further investigate this mechanism, we stimulated the endothelial barriers with cAMP to decrease permeability. Although, we found that there was a significant reduction in permeability, intravasation rates were only mildly reduced under these conditions.

Using our assay we investigated whether tumor cell intravasation can be regulated both by tumor cell-intrinsic and -extrinsic factors. We showed that factors in the microenvironment such as inflammatory cytokines and macrophages enhanced tumor cell intravasation for different breast carcinoma cell lines. Furthermore, in experiments with breast cancer cell lines of the same genetic background, we found that the cells expressing the MenaINV actin binding protein were more effective in crossing the endothelial barrier. Other investigators have also shown tumor cell intravasation regulation by investigating the role of other immune cells (16), as well as EMT-related signal transduction pathways (47). In agreement with these results, we found that human fibrosarcoma tumor cells of mesenchymal origin exhibited higher intravasation rates compared to breast carcinoma cells of epithelial origin. Intravasation rate was also dependent on the

phenotype of the endothelial cells, where breast carcinoma cells intravasated more readily across macrovascular endothelial cells that expressed lower levels of basement membrane glycoproteins.

Our findings on the interplay between endothelial barrier function and tumor cell intravasation are graphically shown below (Figure 29). Under conditions of intact endothelial monolayer, the endothelial barrier poses a barrier to tumor cell intravasation. The presence of macrophages in the vicinity of the tumor and endothelial cells results in endothelial barrier impairment via macrophage-secreted e TNF-α. Under these conditions of endothelial hyperpermeability, tumor cells intravasated more efficiently. In order to confirm this interplay between endothelial permeability and tumor cell intravasation, we performed multiple experiments to perturb endothelial barrier function using cytokine stimulation, different endothelial cell lines and neutralization antibody experiments.

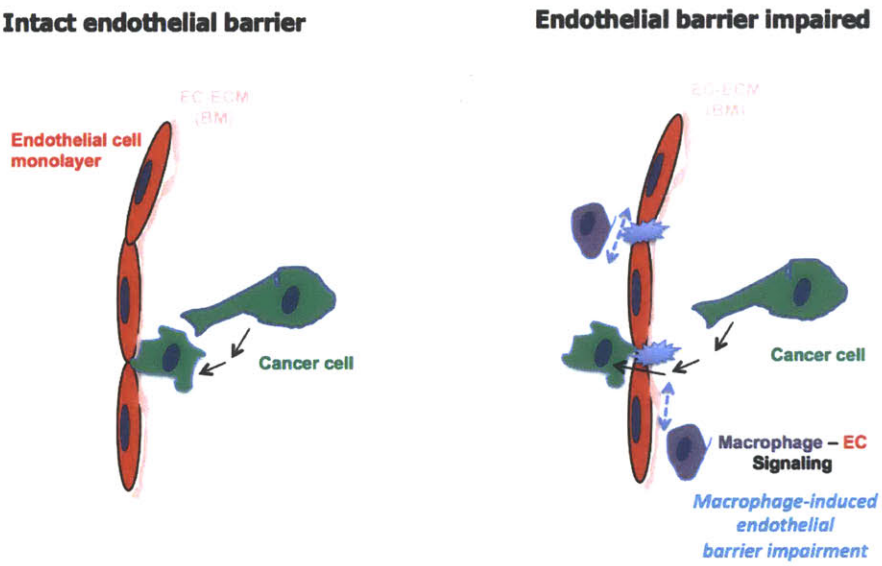

Figure 29: Proposed mechanism of endothelial permeability - tumor cell intravasation association and macrophage-facilitated intravasation

6.2 Implications

Our findings demonstrate that endothelial cell phenotypes and barrier function play a critical role in tumor cell intravasation. An important implication for *in vivo* and clinical studies is that tumor cell intravasation rates would be higher in leaky tumor vessels. This could be validated using the *in vivo* models described in chapter 2, where endothelial permeability would be measured in combination with tumor cell motility. Our results also raise an important implication for *in vitro* studies employing transwell systems, that endothelial monolayer growth and its functional characteristics should be thoroughly examined. Particularly, the presence of tumor cells and other cell types might lead to endothelial barrier impairment and remodeling, which could result in tumor cell migration across gaps in the endothelium and not through the endothelial cell-cell junctions. This is an important point, since although it is well established that tumor blood vessels are functionally and structurally abnormal (28, 50), it is unclear if tumor cells

transmigrate *in vivo* across a continuous endothelial layer or across inter-endothelial gap spaces. Hence, one may speculate that a possible mechanism by which macrophages facilitate tumor cell intravasation could be the induction of gaps between endothelial cell-cell junctions, through which tumor cells can invade. Our device and approach offers a great tool to address these questions and investigate tumor intravasation dynamics.

Along these lines, an important question that could be addressed with our assay is whether the occurance of cancer cell intravasation itself impairs endothelial barrier function. This has implications for cancer drug delivery and therapeutic targeting of cancer metastasis, arguing that normalization of tumor blood vessels can reduce intravasation rates but further work is required to investigate how vessel normalization will impact drug penetration and whether this limits the available drug concentration in tumors.

6.3 Future research directions

Technical innovation and analysis

Analysis of intravasation efficiency showed that tumor cell intravasation is a rare event with a probability of occurrence approximately around 5%. While low occurrence events can be analyzed with imaging methods, as demonstrated in this thesis, use of this assay for drug screening would require a large number of different conditions (e.g. drug combinations and different concentrations) rendering imaging-based analysis methods inadequate. This challenge can be overcome by methods that allow for collection of the tumor cells that have intravasated for subsequent off-chip analysis. In addition, collection of tumor cells would enable DNA and RNA analysis, which would be complementary to the high-resolution imaging analysis presented here. These methods require cell numbers in the order of a few thousand. Thus given the 5% occurrence of intravasation events, the total surface area of the endothelial monolayer would need to be increased by a factor of 500, in order to ensure that at least 1000 cells intravasate. An important challenge here is how to selectively isolate only the tumor cells that have intravasated. We propose that the collection of these cells could be performed via two different methods: a) selective labeling of only the intravasated cells through flushing the endothelial channel with a dye that would only minimally diffuse (e.g. large molecular weight) across the endothelial barrier and b) establishment of a high enough flow-rate that could dislodge the tumor cells from the apical endothelial surface after they have intravasated. The successful integration of cell isolation after intravasation will open new avenues to use the device, not only for drug discovery and screening, but also for biochemical analysis of small volume clinical specimen samples.

Another important device characteristic that could be improved is the minimization of the 3D matrix total area that is in contact with the PDMS posts and where intravasation events can occur. Device designs as those presented by Liu et al (123) which do not require in-plane posts could be implemented. However, these designs still include stiff two-dimensional supports, which could lead to heterogeneous stiffness sensing by the endothelial cells. To overcome this limitation, a thin ECM coating layer spanning the full channel perimeter (bottom coverslip-3D ECM-top PDMS surface) can be introduced, to ensure the presence of a basement membrane with uniform properties. This would provide a more physiologically relevant substrate and would improve differential adhesion on the collagen versus glass and PDMS surfaces. To address this

aim, preliminary experiments in the Kamm lab have shown that a thin layer of Matrigel can be incorporated into the microchannels after the 3D matrices have been injected into the gel region. Finally, to mimic more closely the *in vivo* conditions, fluid flow control should be incorporated into the endothelial channel. This may require design modifications (e.g. channel dimensions) to achieve physiologically relevant blood flow velocities and shear rates to be achieved. A point to be considered is that reduction of channel width from its current dimension of 500 μm, may lead to challenges with endothelial cell seeding.

Taken together the results of endothelial barrier impairment and tumor cell expression of actin binding regulatory protein suggest multiple processes (e.g. chemotaxis and endothelial junction integrity) can control that intravasation. Future work could include the analysis of these processes using a systems-level approach, where these processes are modeled as sequential or parallel steps. By designing experiments to modulate these processes independently, weighting coefficient could be calculated to identify the most critical processes. This approach could provide useful information for combined inhibition studies at the tumor, endothelial and cell-cell interaction levels to minimize the number of intravasating tumor cells.

Macrophage polarization and macrophage effects on tumor cell invasion

An exciting direction for future work is the investigation of the role of macrophage polarization during interactions with tumor cells and endothelial cells in the context of tumor cell migration, intravasation and endothelial permeability regulation. This is particularly important for a comprehensive understanding of the mechanism by which macrophages facilitate intravasation and the identification of M1/M2 related cytokines. In our TNF-α blocking experiments intravasation rate was not reduced down to the baseline levels, suggesting that there may be additional factors that regulate tumor cell intravasation. This result may also be explained by a heterogeneous macrophage population secreting both M1 and M2 associated cytokines and highlight the need for new blocking antibody experiments against both M1 and M2 related cytokines. To effectively inhibit intravasation, we propose designing blocking experiments against, e.g. VEGF and TNF-α, or coculture with macrophages deficient in producing M1/M2 cytokines. These results would also have implications for the role of macrophages in regulating endothelial barrier function in the context of other diseases [e.g. atherosclerosis (180)], where macrophages may as well be polarized to an M1 or M2 phenotype.

The focus of this thesis has been on the role of macrophages in regulating endothelial barrier function and intravasation. We established a correlative relationship between tumor cell intravasation and endothelial permeability, however additional work with engineered cell lines and blocking antibody experiments would be required to prove a causal relationship. An important point here is that although we showed that blocking TNF-α reduced intravasation effiency, we have not investigated whether this also regulated tumor cell invasion. Although, an EGF/CSF-1 paracrine loop has been shown (160) to critically modulate tumor cell invasion, there may also be additional macrophage secreted factors that could regulate critical tumor cell functions (e.g. MMP expression) for transendothelial migration. Future studies should investigate any macrophage-induced alterations in tumor cell invasiveness in our systems which could contribute to tumor cell intravasation, in order to establish a causal relationship between tumor cell intravasation and endothelial permeability. One possibility here, is to perform the

intravasation assay with tumor cells which would be insensitive (e.g. no TNF-α receptor) to the biochemical stimulation on the endothelial cells to perturb permeability.

Molecular mechanism of intravasation

The ability to form well-characterized endothelial monolayers with a hollow lumen in the presence of invading tumor cells enables us to study the transmigration mechanism when tumor cells encounter the basal surface of the endothelial monolayer. Although a number of studies have investigated the mechanisms of tumor and white blood cell adhesion on the endothelial apical surface (45), the molecular mechanism of tumor-endothelial interactions on the basal endothelial surface remains largely unknown. In particular, it is not clear whether tumor cells can specifically adhere on the basal surface where endothelial cells also form a basement membrane. Studies with macrophages and neutrophils that investigated basal-to-apical transendothelial migration have shown the involvement of the endothelial adhesion molecules JAM-C and ICAM-1. In addition to designing experiments to investigate the role of these endothelial adhesion molecules on tumor cell intravasation, it would be interesting to investigate the role of MMPs, which could be secreted by the tumor cells and/or the macrophages. Interestingly, it has also been shown that MMP secretion by endothelial cells can facilitate tumor cell extravasation (88).

An interesting question with important implications is whether tumor cell intravasation impairs endothelial barrier function, and whether this is reversible. It should be noted, that future studies are also required to examine whether the normal endothelial cells used in our study are representative of the endothelial phenotypes in the tumor microenvironment. Although, we showed that an endothelial barrier comprised of "dysfunctional" endothelial cells can be more easily transversed by tumor cells, future work should investigate the intravasation efficiency of patient derived human tumor cells and tumor-derived endothelial cells.

Tumor microenvironment and endothelial barrier regulation in other applications

An obvious direction for future work is the investigation of the role of additional microenvironmental factors, such as fluid flow (blood flow induced shear stress or interstitial flow) and other cell types such as neutrophils, platelets, pericytes and fibroblasts on intravasation. Platelets have been shown to be critically involved in extravasation by secreting TGF-β, which can result in enhancing tumor cell invasion (199), however their role in intravasation is currently unknown. Preliminary results of endothelial cell alignment under application of physiological levels of shear stress are briefly presented in Appendix A8.

The approach developed in this thesis may also find application in studying other physiological and pathophysiological phenomena where endothelial barrier function is important. For example, tumor cell extravasation can be studied with minor modifications of the experimental protocols. Tumor cells can be added in suspension in the endothelial channel after the endothelial barrier has formed. Also, the role of leukocyte transmigration and leukocyte-endothelial interactions in the context of other diseases (e.g. atherosclerosis and inflammation) where endothelial barrier function is important (30) can be studied with our assay. Finally, our assay design allows us to investigate and decouple the relative roles of juxtracrine and paracrine interactions. This is

particularly important because different molecular mechanism may be involved in paracrine/juxtracrine signaling and the microfluidic device can allow for studying both of these phenotypes, by seeding the cell type of interest in a microchannel distally located from the endothelial barrier.

Although the focus in this thesis has been on hematogenous metastasis, that is cancer invasion through the blood vessels, it would be interesting to develop new protocols for using the microfluidic assay to also study the mechanisms of blood-vessel independent metastasis, such as peritoneal metastasis of ovarian cancer.

References

1. Siegel R, *et al.* (2012) Cancer treatment and survivorship statistics, 2012. *CA Cancer J Clin* 62(4):220-241.
2. Sporn MB (1996) The war on cancer. *Lancet* 347(9012):1377-1381.
3. Hanahan D & Weinberg RA (2011) Hallmarks of cancer: the next generation. *Cell* 144(5):646-674.
4. DeVita VT, Jr. & Rosenberg SA (2012) Two hundred years of cancer research. *N Engl J Med* 366(23):2207-2214.
5. Turner NC & Reis-Filho JS (2012) Genetic heterogeneity and cancer drug resistance. *Lancet Oncol* 13(4):e178-185.
6. Spano D, Heck C, De Antonellis P, Christofori G, & Zollo M (2012) Molecular networks that regulate cancer metastasis. *Semin Cancer Biol* 22(3):234-249.
7. Society AC (2012) Cancer Facts & Figures.
8. Bastid J (2012) EMT in carcinoma progression and dissemination: facts, unanswered questions, and clinical considerations. *Cancer Metastasis Rev* 31(1-2):277-283.
9. Valastyan S & Weinberg RA (2011) Tumor metastasis: molecular insights and evolving paradigms. *Cell* 147(2):275-292.
10. Weinberg RA (2006) *The Biology of Cancer* (Garland Science, New York).
11. Gupta GP & Massague J (2006) Cancer metastasis: building a framework. *Cell* 127(4):679-695.
12. Robinson BD, *et al.* (2009) Tumor microenvironment of metastasis in human breast carcinoma: a potential prognostic marker linked to hematogenous dissemination. *Clin Cancer Res* 15(7):2433-2441.
13. Wyckoff JB, *et al.* (2007) Direct visualization of macrophage-assisted tumor cell intravasation in mammary tumors. *Cancer Res* 67(6):2649-2656.
14. Roussos ET, Condeelis JS, & Patsialou A (2011) Chemotaxis in cancer. *Nat Rev Cancer* 11(8):573-587.
15. Calvo F & Sahai E (2011) Cell communication networks in cancer invasion. *Curr Opin Cell Biol.*
16. Bekes EM, *et al.* (2011) Tumor-recruited neutrophils and neutrophil TIMP-free MMP-9 regulate coordinately the levels of tumor angiogenesis and efficiency of malignant cell intravasation. *Am J Pathol* 179(3):1455-1470.
17. Polacheck WJ, Zervantonakis IK, & Kamm RD (2012) Tumor cell migration in complex microenvironments. *Cell Mol Life Sci.*
18. Scallan J, Huxley VH, & Korthuis RJ (2010).
19. Jaffe EA, Hoyer LW, & Nachman RL (1973) Synthesis of antihemophilic factor antigen by cultured human endothelial cells. *J Clin Invest* 52(11):2757-2764.
20. Gimbrone MA, Jr., Cotran RS, & Folkman J (1973) Endothelial regeneration: studies with human endothelial cells in culture. *Ser Haematol* 6(4):453-455.
21. Dudley AC (2012) Tumor endothelial cells. *Cold Spring Harb Perspect Med* 2(3):a006536.
22. Franses JW, Baker AB, Chitalia VC, & Edelman ER (2011) Stromal endothelial cells directly influence cancer progression. *Sci Transl Med* 3(66):66ra65.
23. Aird WC (2012) Endothelial cell heterogeneity. *Cold Spring Harb Perspect Med* 2(1):a006429.

24. Folkman J (1971) Tumor angiogenesis: therapeutic implications. *N Engl J Med* 285(21):1182-1186.
25. Nagy JA, *et al.* (2006) Permeability properties of tumor surrogate blood vessels induced by VEGF-A. *Laboratory Investigation* 86(8):767-780.
26. Nagy JA & Dvorak HF (2012) Heterogeneity of the tumor vasculature: the need for new tumor blood vessel type-specific targets. *Clin Exp Metastasis*.
27. Benjamin LE, Golijanin D, Itin A, Pode D, & Keshet E (1999) Selective ablation of immature blood vessels in established human tumors follows vascular endothelial growth factor withdrawal. *J Clin Invest* 103(2):159-165.
28. Hashizume H, *et al.* (2000) Openings between defective endothelial cells explain tumor vessel leakiness. *Am J Pathol* 156(4):1363-1380.
29. Baluk P, Morikawa S, Haskell A, Mancuso M, & McDonald DM (2003) Abnormalities of basement membrane on blood vessels and endothelial sprouts in tumors. *Am J Pathol* 163(5):1801-1815.
30. Goel S, *et al.* (2011) Normalization of the vasculature for treatment of cancer and other diseases. *Physiol Rev* 91(3):1071-1121.
31. Joyce JA & Pollard JW (2009) Microenvironmental regulation of metastasis. *Nat Rev Cancer* 9(4):239-252.
32. Nguyen DX, Bos PD, & Massague J (2009) Metastasis: from dissemination to organ-specific colonization. *Nat Rev Cancer* 9(4):274-284.
33. Rakha EA, *et al.* (2012) The prognostic significance of lymphovascular invasion in invasive breast carcinoma. *Cancer* 118(15):3670-3680.
34. Fidler IJ & Hart IR (1982) Biological diversity in metastatic neoplasms: origins and implications. *Science* 217(4564):998-1003.
35. Eyles J, *et al.* (2010) Tumor cells disseminate early, but immunosurveillance limits metastatic outgrowth, in a mouse model of melanoma. *J Clin Invest* 120(6):2030-2039.
36. Lu J, *et al.* (2010) Isolation of circulating epithelial and tumor progenitor cells with an invasive phenotype from breast cancer patients. *Int J Cancer* 126(3):669-683.
37. Tammela T & Alitalo K (2010) Lymphangiogenesis: Molecular mechanisms and future promise. *Cell* 140(4):460-476.
38. Sleeman JP, Cady B, & Pantel K (2012) The connectivity of lymphogenous and hematogenous tumor cell dissemination: biological insights and clinical implications. *Clin Exp Metastasis*.
39. Kerjaschki D, *et al.* (2011) Lipoxygenase mediates invasion of intrametastatic lymphatic vessels and propagates lymph node metastasis of human mammary carcinoma xenografts in mouse. *J Clin Invest* 121(5):2000-2012.
40. Bockhorn M, Jain RK, & Munn LL (2007) Active versus passive mechanisms in metastasis: do cancer cells crawl into vessels, or are they pushed? *Lancet Oncol* 8(5):444-448.
41. Giampieri S, *et al.* (2009) Localized and reversible TGFbeta signalling switches breast cancer cells from cohesive to single cell motility. *Nat Cell Biol* 11(11):1287-1296.
42. Woodfin A, *et al.* (2011) The junctional adhesion molecule JAM-C regulates polarized transendothelial migration of neutrophils in vivo. *Nat Immunol* 12(8):761-769.
43. Khuon S, *et al.* (2010) Myosin light chain kinase mediates transcellular intravasation of breast cancer cells through the underlying endothelial cells: a three-dimensional FRET study. *J Cell Sci* 123(Pt 3):431-440.

44. Muller WA (2011) Mechanisms of leukocyte transendothelial migration. *Annu Rev Pathol* 6:323-344.
45. Strell C & Entschladen F (2008) Extravasation of leukocytes in comparison to tumor cells. *Cell Commun Signal* 6:10.
46. Roussos ET, *et al.* (2011) Mena invasive (MenaINV) promotes multicellular streaming motility and transendothelial migration in a mouse model of breast cancer. *J Cell Sci* 124(Pt 13):2120-2131.
47. Yang J, *et al.* (2004) Twist, a master regulator of morphogenesis, plays an essential role in tumor metastasis. *Cell* 117(7):927-939.
48. Mantovani A & Sica A (2010) Macrophages, innate immunity and cancer: balance, tolerance, and diversity. *Curr Opin Immunol* 22(2):231-237.
49. Hagendoorn J, *et al.* (2006) Onset of abnormal blood and lymphatic vessel function and interstitial hypertension in early stages of carcinogenesis. *Cancer Res* 66(7):3360-3364.
50. Nagy JA, *et al.* (2006) Permeability properties of tumor surrogate blood vessels induced by VEGF-A. *Lab Invest* 86(8):767-780.
51. Tien YW, *et al.* (2001) Tumor angiogenesis and its possible role in intravasation of colorectal epithelial cells. *Clin Cancer Res* 7(6):1627-1632.
52. Stoletov K, Montel V, Lester RD, Gonias SL, & Klemke R (2007) High-resolution imaging of the dynamic tumor cell vascular interface in transparent zebrafish. *Proc Natl Acad Sci U S A* 104(44):17406-17411.
53. Zijlstra A, Lewis J, Degryse B, Stuhlmann H, & Quigley JP (2008) The inhibition of tumor cell intravasation and subsequent metastasis via regulation of in vivo tumor cell motility by the tetraspanin CD151. *Cancer Cell* 13(3):221-234.
54. Kim J, Yu W, Kovalski K, & Ossowski L (1998) Requirement for specific proteases in cancer cell intravasation as revealed by a novel semiquantitative PCR-based assay. *Cell* 94(3):353-362.
55. Deryugina EI, *et al.* (2005) Unexpected effect of matrix metalloproteinase down-regulation on vascular intravasation and metastasis of human fibrosarcoma cells selected in vivo for high rates of dissemination. *Cancer Res* 65(23):10959-10969.
56. Conn EM, *et al.* (2008) Cell surface proteomics identifies molecules functionally linked to tumor cell intravasation. *J Biol Chem* 283(39):26518-26527.
57. Conn EM, *et al.* (2009) Comparative analysis of metastasis variants derived from human prostate carcinoma cells: roles in intravasation of VEGF-mediated angiogenesis and uPA-mediated invasion. *Am J Pathol* 175(4):1638-1652.
58. Ma L, Teruya-Feldstein J, & Weinberg RA (2007) Tumour invasion and metastasis initiated by microRNA-10b in breast cancer. *Nature* 449(7163):682-688.
59. Gligorijevic B, *et al.* (2012) N-WASP-mediated invadopodium formation is involved in intravasation and lung metastasis of mammary tumors. *J Cell Sci* 125(Pt 3):724-734.
60. Le Devedec SE, *et al.* (2009) An improved model to study tumor cell autonomous metastasis programs using MTLn3 cells and the Rag2(-/-) gammac (-/-) mouse. *Clin Exp Metastasis* 26(7):673-684.
61. Mathias JR, *et al.* (2006) Resolution of inflammation by retrograde chemotaxis of neutrophils in transgenic zebrafish. *J Leukoc Biol* 80(6):1281-1288.
62. Starnes TW & Huttenlocher A (2012) Neutrophil reverse migration becomes transparent with zebrafish. *Adv Hematol* 2012:398640.

63. Buckley CD, *et al.* (2006) Identification of a phenotypically and functionally distinct population of long-lived neutrophils in a model of reverse endothelial migration. *J Leukoc Biol* 79(2):303-311.
64. Randolph GJ & Furie MB (1996) Mononuclear phagocytes egress from an in vitro model of the vascular wall by migrating across endothelium in the basal to apical direction: role of intercellular adhesion molecule 1 and the CD11/CD18 integrins. *J Exp Med* 183(2):451-462.
65. Bates SE, Amiri-Kordestani L, & Giaccone G (2012) Drug development: portals of discovery. *Clin Cancer Res* 18(1):23-32.
66. Sharma SV, Haber DA, & Settleman J (2010) Cell line-based platforms to evaluate the therapeutic efficacy of candidate anticancer agents. *Nat Rev Cancer* 10(4):241-253.
67. Li J, *et al.* (2012) A review on various targeted anticancer therapies. *Target Oncol* 7(1):69-85.
68. Jayson GC, Hicklin DJ, & Ellis LM (2012) Antiangiogenic therapy--evolving view based on clinical trial results. *Nat Rev Clin Oncol* 9(5):297-303.
69. Yang JC, *et al.* (2003) A randomized trial of bevacizumab, an anti-vascular endothelial growth factor antibody, for metastatic renal cancer. *N Engl J Med* 349(5):427-434.
70. DeNardo DG, *et al.* (2011) Leukocyte complexity predicts breast cancer survival and functionally regulates response to chemotherapy. *Cancer Discov* 1(1):54-67.
71. Cooke VG, *et al.* (2012) Pericyte depletion results in hypoxia-associated epithelial-to-mesenchymal transition and metastasis mediated by met signaling pathway. *Cancer Cell* 21(1):66-81.
72. Chen Q & Massague J (2012) Molecular Pathways: VCAM-1 as a Potential Therapeutic Target in Metastasis. *Clin Cancer Res.*
73. Podar K, *et al.* (2011) The selective adhesion molecule inhibitor Natalizumab decreases multiple myeloma cell growth in the bone marrow microenvironment: therapeutic implications. *Br J Haematol* 155(4):438-448.
74. Zhang XH, *et al.* (2009) Latent bone metastasis in breast cancer tied to Src-dependent survival signals. *Cancer Cell* 16(1):67-78.
75. Valastyan S, Chang A, Benaich N, Reinhardt F, & Weinberg RA (2011) Activation of miR-31 function in already-established metastases elicits metastatic regression. *Genes Dev* 25(6):646-659.
76. Kim S, *et al.* (2011) High-throughput single-molecule optofluidic analysis. *Nat Methods* 8(3):242-245.
77. Rohde CB, Zeng F, Gonzalez-Rubio R, Angel M, & Yanik MF (2007) Microfluidic system for on-chip high-throughput whole-animal sorting and screening at subcellular resolution. *P Natl Acad Sci USA* 104(35):13891-13895.
78. Duffy DC, McDonald JC, Schueller OJ, & Whitesides GM (1998) Rapid Prototyping of Microfluidic Systems in Poly(dimethylsiloxane). *Anal Chem* 70(23):4974-4984.
79. Berthier E, Young EW, & Beebe D (2012) Engineers are from PDMS-land, Biologists are from Polystyrenia. *Lab Chip* 12(7):1224-1237.
80. Chung S, *et al.* (2009) Cell migration into scaffolds under co-culture conditions in a microfluidic platform. *Lab Chip* 9(2):269-275.
81. Huang CP, *et al.* (2009) Engineering microscale cellular niches for three-dimensional multicellular co-cultures. *Lab Chip* 9(12):1740-1748.

82. Song JW, *et al.* (2009) Microfluidic endothelium for studying the intravascular adhesion of metastatic breast cancer cells. *PLoS One* 4(6):e5756.
83. Li YH & Zhu C (1999) A modified Boyden chamber assay for tumor cell transendothelial migration in vitro. *Clin Exp Metastasis* 17(5):423-429.
84. Regehr KJ, *et al.* (2009) Biological implications of polydimethylsiloxane-based microfluidic cell culture. *Lab Chip* 9(15):2132-2139.
85. Sitohy B, Nagy JA, & Dvorak HF (2012) Anti-VEGF/VEGFR therapy for cancer: reassessing the target. *Cancer Res* 72(8):1909-1914.
86. Stine MJ, *et al.* (2011) Integration of genotypic and phenotypic screening reveals molecular mediators of melanoma-stromal interaction. *Cancer Res* 71(7):2433-2444.
87. Vargo-Gogola T & Rosen JM (2007) Modelling breast cancer: one size does not fit all. *Nat Rev Cancer* 7(9):659-672.
88. Kargozaran H, *et al.* (2007) A role for endothelial-derived matrix metalloproteinase-2 in breast cancer cell transmigration across the endothelial-basement membrane barrier. *Clin Exp Metastasis* 24(7):495-502.
89. Voura EB, Sandig M, & Siu CH (1998) Cell-cell interactions during transendothelial migration of tumor cells. *Microsc Res Tech* 43(3):265-275.
90. Mierke CT (2011) Cancer cells regulate biomechanical properties of human microvascular endothelial cells. *J Biol Chem* 286(46):40025-40037.
91. Ingthorsson S, *et al.* (2010) Endothelial cells stimulate growth of normal and cancerous breast epithelial cells in 3D culture. *BMC Res Notes* 3:184.
92. Baker BM & Chen CS (2012) Deconstructing the third dimension - how 3D culture microenvironments alter cellular cues. *J Cell Sci* 125(Pt 13):3015-3024.
93. Hutmacher DW (2010) Biomaterials offer cancer research the third dimension. *Nat Mater* 9(2):90-93.
94. Debnath J & Brugge JS (2005) Modelling glandular epithelial cancers in three-dimensional cultures. *Nat Rev Cancer* 5(9):675-688.
95. Lee GY, Kenny PA, Lee EH, & Bissell MJ (2007) Three-dimensional culture models of normal and malignant breast epithelial cells. *Nat Methods* 4(4):359-365.
96. Weaver VM, *et al.* (2002) beta4 integrin-dependent formation of polarized three-dimensional architecture confers resistance to apoptosis in normal and malignant mammary epithelium. *Cancer Cell* 2(3):205-216.
97. Kenny PA, *et al.* (2007) The morphologies of breast cancer cell lines in three-dimensional assays correlate with their profiles of gene expression. *Mol Oncol* 1(1):84-96.
98. Fischbach C, *et al.* (2009) Cancer cell angiogenic capability is regulated by 3D culture and integrin engagement. *Proc Natl Acad Sci U S A* 106(2):399-404.
99. Young EW & Simmons CA (2010) Macro- and microscale fluid flow systems for endothelial cell biology. *Lab Chip* 10(2):143-160.
100. Price GM & Tien J (2011) Methods for forming human microvascular tubes in vitro and measuring their macromolecular permeability. *Methods Mol Biol* 671:281-293.
101. Wong KH, Truslow JG, & Tien J (2010) The role of cyclic AMP in normalizing the function of engineered human blood microvessels in microfluidic collagen gels. *Biomaterials* 31(17):4706-4714.
102. Chung S, Sudo R, Vickerman V, Zervantonakis IK, & Kamm RD (2010) Microfluidic platforms for studies of angiogenesis, cell migration, and cell-cell interactions. Sixth

International Bio-Fluid Mechanics Symposium and Workshop March 28-30, 2008 Pasadena, California. *Ann Biomed Eng* 38(3):1164-1177.
103. Kaji H, Yokoi T, Kawashima T, & Nishizawa M (2010) Directing the flow of medium in controlled cocultures of HeLa cells and human umbilical vein endothelial cells with a microfluidic device. *Lab Chip* 10(18):2374-2379.
104. Zheng C, *et al.* (2012) Quantitative study of the dynamic tumor-endothelial cell interactions through an integrated microfluidic coculture system. *Anal Chem* 84(4):2088-2093.
105. Shin MK, Kim SK, & Jung H (2011) Integration of intra- and extravasation in one cell-based microfluidic chip for the study of cancer metastasis. *Lab Chip* 11(22):3880-3887.
106. Brown E, Munn LL, Fukumura D, & Jain RK (2010) In vivo imaging of tumors. *Cold Spring Harb Protoc* 2010(7):pdb prot5452.
107. Zervantonakis IK, Kothapalli CR, Chung S, Sudo R, & Kamm RD (2011) Microfluidic devices for studying heterotypic cell-cell interactions and tissue specimen cultures under controlled microenvironments. *Biomicrofluidics* 5(1):13406.
108. Curry FE, Huxley VH, & Adamson RH (1983) Permeability of single capillaries to intermediate-sized colored solutes. *Am J Physiol* 245(3):H495-505.
109. Albelda SM, *et al.* (1988) Permeability characteristics of cultured endothelial cell monolayers. *J Appl Physiol* 64(1):308-322.
110. Young EW, Watson MW, Srigunapalan S, Wheeler AR, & Simmons CA (2010) Technique for real-time measurements of endothelial permeability in a microfluidic membrane chip using laser-induced fluorescence detection. *Anal Chem* 82(3):808-816.
111. Douville NJ, *et al.* (2010) Fabrication of two-layered channel system with embedded electrodes to measure resistance across epithelial and endothelial barriers. *Anal Chem* 82(6):2505-2511.
112. Michel CC & Curry FE (1999) Microvascular permeability. *Physiol Rev* 79(3):703-761.
113. Dreher MR, *et al.* (2006) Tumor vascular permeability, accumulation, and penetration of macromolecular drug carriers. *J Natl Cancer Inst* 98(5):335-344.
114. Yuan SY & Rigor RR (2010) Regulation of Endothelial Barrier Function. *Integrated Systems Physiology: From molecule to disease*, (Morgan & Claypool Life Sciences, San Rafael), 2011/06/03 Ed.
115. Farahat WA, *et al.* (2012) Ensemble analysis of angiogenic growth in three-dimensional microfluidic cell cultures. *PLoS One* 7(5):e37333.
116. Gribbon P & Hardingham TE (1998) Macromolecular diffusion of biological polymers measured by confocal fluorescence recovery after photobleaching. *Biophys J* 75(2):1032-1039.
117. Stylianopoulos T, Diop-Frimpong B, Munn LL, & Jain RK (2010) Diffusion anisotropy in collagen gels and tumors: the effect of fiber network orientation. *Biophys J* 99(10):3119-3128.
118. Chrobak KM, Potter DR, & Tien J (2006) Formation of perfused, functional microvascular tubes in vitro. *Microvasc Res* 71(3):185-196.
119. Burke-Gaffney A & Keenan AK (1993) Modulation of human endothelial cell permeability by combinations of the cytokines interleukin-1 alpha/beta, tumor necrosis factor-alpha and interferon-gamma. *Immunopharmacology* 25(1):1-9.

120. Mark KS & Miller DW (1999) Increased permeability of primary cultured brain microvessel endothelial cell monolayers following TNF-alpha exposure. *Life Sci* 64(21):1941-1953.
121. Garg P, *et al.* (2011) Thrombospondin-1 opens the paracellular pathway in pulmonary microvascular endothelia through EGFR/ErbB2 activation. *Am J Physiol Lung Cell Mol Physiol* 301(1):L79-90.
122. Nooteboom A, Hendriks T, Otteholler I, & van der Linden CJ (2000) Permeability characteristics of human endothelial monolayers seeded on different extracellular matrix proteins. *Mediators Inflamm* 9(5):235-241.
123. Liu T, Lin B, & Qin J (2010) Carcinoma-associated fibroblasts promoted tumor spheroid invasion on a microfluidic 3D co-culture device. *Lab Chip* 10(13):1671-1677.
124. Haidari M, *et al.* (2012) Integrin alpha2-beta1 Mediates Tyrosine Phosphorylation of Vascular Endothelial Cadherin Induced by Invasive Breast Cancer Cells. *J Biol Chem.*
125. Peng HH & Dong C (2009) Systemic Analysis of Tumor Cell-Induced Endothelial Calcium Signaling and Junction Disassembly. *Cell Mol Bioeng* 2(3):375-385.
126. Heyder C, *et al.* (2002) Realtime visualization of tumor cell/endothelial cell interactions during transmigration across the endothelial barrier. *J Cancer Res Clin Oncol* 128(10):533-538.
127. Hu L, Ferrara N, & Jaffe RB (2006) Paracrine VEGF/VE-cadherin action on ovarian cancer permeability. *Exp Biol Med (Maywood)* 231(10):1646-1652.
128. Utoguchi N, *et al.* (1995) Tumor-conditioned medium increases macromolecular permeability of endothelial cell monolayer. *Cancer Lett* 89(1):7-14.
129. Weis S, Cui J, Barnes L, & Cheresh D (2004) Endothelial barrier disruption by VEGF-mediated Src activity potentiates tumor cell extravasation and metastasis. *J Cell Biol* 167(2):223-229.
130. Kenig S, Alonso MB, Mueller MM, & Lah TT (2010) Glioblastoma and endothelial cells cross-talk, mediated by SDF-1, enhances tumour invasion and endothelial proliferation by increasing expression of cathepsins B, S, and MMP-9. *Cancer Lett* 289(1):53-61.
131. Mierke CT, *et al.* (2008) Breakdown of the endothelial barrier function in tumor cell transmigration. *Biophys J* 94(7):2832-2846.
132. Issa A, Le TX, Shoushtari AN, Shields JD, & Swartz MA (2009) Vascular endothelial growth factor-C and C-C chemokine receptor 7 in tumor cell-lymphatic cross-talk promote invasive phenotype. *Cancer Res* 69(1):349-357.
133. Liang M, Zhang P, & Fu J (2007) Up-regulation of LOX-1 expression by TNF-alpha promotes trans-endothelial migration of MDA-MB-231 breast cancer cells. *Cancer Lett* 258(1):31-37.
134. Voura EB, Chen N, & Siu CH (2000) Platelet-endothelial cell adhesion molecule-1 (CD31) redistributes from the endothelial junction and is not required for the transendothelial migration of melanoma cells. *Clin Exp Metastasis* 18(6):527-532.
135. Voura EB, Ramjeesingh RA, Montgomery AM, & Siu CH (2001) Involvement of integrin alpha(v)beta(3) and cell adhesion molecule L1 in transendothelial migration of melanoma cells. *Mol Biol Cell* 12(9):2699-2710.
136. Peyri N, *et al.* (2009) Breast tumor cells transendothelial migration induces endothelial cell anoikis through extracellular matrix degradation. *Anticancer Res* 29(6):2347-2355.
137. Dubois F, *et al.* (2006) Digital holographic microscopy for the three-dimensional dynamic analysis of in vitro cancer cell migration. *J Biomed Opt* 11(5):054032.

138. Okada T, Okuno H, & Mitsui Y (1994) A novel in vitro assay system for transendothelial tumor cell invasion: significance of E-selectin and alpha 3 integrin in the transendothelial invasion by HT1080 fibrosarcoma cells. *Clin Exp Metastasis* 12(4):305-314.
139. Sica A, Allavena P, & Mantovani A (2008) Cancer related inflammation: the macrophage connection. *Cancer Lett* 267(2):204-215.
140. Qian BZ & Pollard JW (2010) Macrophage diversity enhances tumor progression and metastasis. *Cell* 141(1):39-51.
141. Hagemann T, *et al.* (2004) Enhanced invasiveness of breast cancer cell lines upon co-cultivation with macrophages is due to TNF-alpha dependent up-regulation of matrix metalloproteases. *Carcinogenesis* 25(8):1543-1549.
142. Wang Q, *et al.* (2010) Fra-1 protooncogene regulates IL-6 expression in macrophages and promotes the generation of M2d macrophages. *Cell Res* 20(6):701-712.
143. Zhang B, *et al.* (2009) Alternatively activated RAW264.7 macrophages enhance tumor lymphangiogenesis in mouse lung adenocarcinoma. *J Cell Biochem* 107(1):134-143.
144. Qian BZ & Pollard JW (2012) New tricks for metastasis-associated macrophages. *Breast Cancer Res* 14(4):316.
145. Wolburg H, *et al.* (1994) Modulation of tight junction structure in blood-brain barrier endothelial cells. Effects of tissue culture, second messengers and cocultured astrocytes. *J Cell Sci* 107 (Pt 5):1347-1357.
146. Zenker D, Begley D, Bratzke H, Rubsamen-Waigmann H, & von Briesen H (2003) Human blood-derived macrophages enhance barrier function of cultured primary bovine and human brain capillary endothelial cells. *J Physiol* 551(Pt 3):1023-1032.
147. Wakamoto S, *et al.* (2008) Endothelial permeability is increased by the supernatant of peripheral blood mononuclear cells stimulated with HLA Class II antibody. *Transfusion* 48(10):2060-2068.
148. Farley KS, Wang LF, Law C, & Mehta S (2008) Alveolar macrophage inducible nitric oxide synthase-dependent pulmonary microvascular endothelial cell septic barrier dysfunction. *Microvasc Res* 76(3):208-216.
149. Zhao YD, Ohkawara H, Vogel SM, Malik AB, & Zhao YY (2010) Bone marrow-derived progenitor cells prevent thrombin-induced increase in lung vascular permeability. *Am J Physiol Lung Cell Mol Physiol* 298(1):L36-44.
150. Gainor JP, Morton CA, Roberts JT, Vincent PA, & Minnear FL (2001) Platelet-conditioned medium increases endothelial electrical resistance independently of cAMP/PKA and cGMP/PKG. *Am J Physiol Heart Circ Physiol* 281(5):H1992-2001.
151. Curry FE, Clark JF, & Adamson RH (2012) Erythrocyte-derived sphingosine-1-phosphate stabilizes basal hydraulic conductivity and solute permeability in rat microvessels. *Am J Physiol Heart Circ Physiol* 303(7):H825-834.
152. McGuire PG, Rangasamy S, Maestas J, & Das A (2011) Pericyte-derived sphingosine 1-phosphate induces the expression of adhesion proteins and modulates the retinal endothelial cell barrier. *Arterioscler Thromb Vasc Biol* 31(12):e107-115.
153. Warboys CM, Overby DR, & Weinberg PD (2012) Dendritic Cells Lower the Permeability of Endothelial Monolayers. *Cellular and Molecular Bioengineering* 5(2):184-193.
154. Zervantonakis IK, *et al.* (2012) Three-dimensional microfluidic model for tumor cell intravasation and endothelial barrier function. *Proc Natl Acad Sci U S A.*

155. Daniel PB, Walker WH, & Habener JF (1998) Cyclic AMP signaling and gene regulation. *Annu Rev Nutr* 18:353-383.
156. Montminy M (1997) Transcriptional regulation by cyclic AMP. *Annu Rev Biochem* 66:807-822.
157. Sayner SL (2011) Emerging themes of cAMP regulation of the pulmonary endothelial barrier. *Am J Physiol Lung Cell Mol Physiol* 300(5):L667-678.
158. Beese M, Wyss K, Haubitz M, & Kirsch T (2010) Effect of cAMP derivates on assembly and maintenance of tight junctions in human umbilical vein endothelial cells. *BMC Cell Biol* 11:68.
159. Burgess A, *et al.* (2010) Loss of human Greatwall results in G2 arrest and multiple mitotic defects due to deregulation of the cyclin B-Cdc2/PP2A balance. *Proc Natl Acad Sci U S A* 107(28):12564-12569.
160. Goswami S, *et al.* (2005) Macrophages promote the invasion of breast carcinoma cells via a colony-stimulating factor-1/epidermal growth factor paracrine loop. *Cancer Res* 65(12):5278-5283.
161. Ding Y, *et al.* (2010) NFAT1 mediates placental growth factor-induced myelomonocytic cell recruitment via the induction of TNF-alpha. *J Immunol* 184(5):2593-2601.
162. Ma J, *et al.* (2010) The M1 form of tumor-associated macrophages in non-small cell lung cancer is positively associated with survival time. *BMC Cancer* 10:112.
163. Caras I, *et al.* (2011) Influence of tumor cell culture supernatants on macrophage functional polarization: in vitro models of macrophage-tumor environment interaction. *Tumori* 97(5):647-654.
164. Yamashita H, Ueda K, & Kioka N (2011) WAVE2 forms a complex with PKA and is involved in PKA enhancement of membrane protrusions. *J Biol Chem* 286(5):3907-3914.
165. Lee TH, Avraham HK, Jiang S, & Avraham S (2003) Vascular endothelial growth factor modulates the transendothelial migration of MDA-MB-231 breast cancer cells through regulation of brain microvascular endothelial cell permeability. *J Biol Chem* 278(7):5277-5284.
166. Bouis D, Hospers GA, Meijer C, Molema G, & Mulder NH (2001) Endothelium in vitro: a review of human vascular endothelial cell lines for blood vessel-related research. *Angiogenesis* 4(2):91-102.
167. Pober JS & Cotran RS (1990) Cytokines and endothelial cell biology. *Physiol Rev* 70(2):427-451.
168. Pappenheimer JR, Renkin EM, & Borrero LM (1951) Filtration, diffusion and molecular sieving through peripheral capillary membranes; a contribution to the pore theory of capillary permeability. *Am J Physiol* 167(1):13-46.
169. Komarova Y & Malik AB (2010) Regulation of endothelial permeability via paracellular and transcellular transport pathways. *Annu Rev Physiol* 72:463-493.
170. Dejana E, Orsenigo F, & Lampugnani MG (2008) The role of adherens junctions and VE-cadherin in the control of vascular permeability. *J Cell Sci* 121(Pt 13):2115-2122.
171. DeMaio L, Antonetti DA, Scaduto RC, Jr., Gardner TW, & Tarbell JM (2004) VEGF increases paracellular transport without altering the solvent-drag reflection coefficient. *Microvasc Res* 68(3):295-302.
172. McKenzie JA & Ridley AJ (2007) Roles of Rho/ROCK and MLCK in TNF-alpha-induced changes in endothelial morphology and permeability. *J Cell Physiol* 213(1):221-228.

173. Puhlmann M, *et al.* (2005) Interleukin-1beta induced vascular permeability is dependent on induction of endothelial tissue factor (TF) activity. *J Transl Med* 3:37.
174. Sahni A, Arevalo MT, Sahni SK, & Simpson-Haidaris PJ (2009) The VE-cadherin binding domain of fibrinogen induces endothelial barrier permeability and enhances transendothelial migration of malignant breast epithelial cells. *Int J Cancer* 125(3):577-584.
175. Miteva DO, *et al.* (2010) Transmural flow modulates cell and fluid transport functions of lymphatic endothelium. *Circ Res* 106(5):920-931.
176. Warboys CM, Eric Berson R, Mann GE, Pearson JD, & Weinberg PD (2010) Acute and chronic exposure to shear stress have opposite effects on endothelial permeability to macromolecules. *Am J Physiol Heart Circ Physiol* 298(6):H1850-1856.
177. Huynh J, *et al.* (2011) Age-related intimal stiffening enhances endothelial permeability and leukocyte transmigration. *Sci Transl Med* 3(112):112ra122.
178. Aggarwal BB (2003) Signalling pathways of the TNF superfamily: a double-edged sword. *Nat Rev Immunol* 3(9):745-756.
179. Aggarwal BB, *et al.* (1985) Human tumor necrosis factor. Production, purification, and characterization. *J Biol Chem* 260(4):2345-2354.
180. Aggarwal BB, Gupta SC, & Kim JH (2012) Historical perspectives on tumor necrosis factor and its superfamily: 25 years later, a golden journey. *Blood* 119(3):651-665.
181. Carswell EA, *et al.* (1975) An endotoxin-induced serum factor that causes necrosis of tumors. *Proc Natl Acad Sci U S A* 72(9):3666-3670.
182. Lejeune FJ, Ruegg C, & Lienard D (1998) Clinical applications of TNF-alpha in cancer. *Curr Opin Immunol* 10(5):573-580.
183. Balkwill F (2009) Tumour necrosis factor and cancer. *Nat Rev Cancer* 9(5):361-371.
184. Montesano R, Soulie P, Eble JA, & Carrozzino F (2005) Tumour necrosis factor alpha confers an invasive, transformed phenotype on mammary epithelial cells. *J Cell Sci* 118(Pt 15):3487-3500.
185. Wu Y & Zhou BP (2010) TNF-alpha/NF-kappaB/Snail pathway in cancer cell migration and invasion. *Br J Cancer* 102(4):639-644.
186. Pober JS & Sessa WC (2007) Evolving functions of endothelial cells in inflammation. *Nat Rev Immunol* 7(10):803-815.
187. Teo GS, *et al.* (2012) Mesenchymal Stem Cells Transmigrate Between and Directly Through TNF-alpha-activated Endothelial Cells. *Stem Cells.*
188. Haraldsen G, Kvale D, Lien B, Farstad IN, & Brandtzaeg P (1996) Cytokine-regulated expression of E-selectin, intercellular adhesion molecule-1 (ICAM-1), and vascular cell adhesion molecule-1 (VCAM-1) in human microvascular endothelial cells. *J Immunol* 156(7):2558-2565.
189. Wojciak-Stothard B, Entwistle A, Garg R, & Ridley AJ (1998) Regulation of TNF-alpha-induced reorganization of the actin cytoskeleton and cell-cell junctions by Rho, Rac, and Cdc42 in human endothelial cells. *J Cell Physiol* 176(1):150-165.
190. Lopez-Ramirez MA, *et al.* (2012) Role of caspases in cytokine-induced barrier breakdown in human brain endothelial cells. *J Immunol* 189(6):3130-3139.
191. Ramasamy S, Lipke DW, McClain CJ, & Hennig B (1995) Tumor necrosis factor reduces proteoglycan synthesis in cultured endothelial cells. *J Cell Physiol* 162(1):119-126.

192. Koss M, *et al.* (2006) Ezrin/radixin/moesin proteins are phosphorylated by TNF-alpha and modulate permeability increases in human pulmonary microvascular endothelial cells. *J Immunol* 176(2):1218-1227.
193. Guo X, *et al.* (2009) ERM protein moesin is phosphorylated by advanced glycation end products and modulates endothelial permeability. *Am J Physiol Heart Circ Physiol* 297(1):H238-246.
194. Yang Y, *et al.* (2009) Collagen-binding human epidermal growth factor promotes cellularization of collagen scaffolds. *Tissue Eng Part A* 15(11):3589-3596.
195. Hou CH, Yang RS, Hou SM, & Tang CH (2011) TNF-alpha increases alphavbeta3 integrin expression and migration in human chondrosarcoma cells. *J Cell Physiol* 226(3):792-799.
196. Clark PR, Manes TD, Pober JS, & Kluger MS (2007) Increased ICAM-1 expression causes endothelial cell leakiness, cytoskeletal reorganization and junctional alterations. *J Invest Dermatol* 127(4):762-774.
197. Shen Q, Lee ES, Pitts RL, Wu MH, & Yuan SY (2010) Tissue inhibitor of metalloproteinase-2 regulates matrix metalloproteinase-2-mediated endothelial barrier dysfunction and breast cancer cell transmigration through lung microvascular endothelial cells. *Mol Cancer Res* 8(7):939-951.
198. Sumagin R, Kuebel JM, & Sarelius IH (2011) Leukocyte rolling and adhesion both contribute to regulation of microvascular permeability to albumin via ligation of ICAM-1. *Am J Physiol Cell Physiol* 301(4):C804-813.
199. Labelle M, Begum S, & Hynes RO (2011) Direct signaling between platelets and cancer cells induces an epithelial-mesenchymal-like transition and promotes metastasis. *Cancer Cell* 20(5):576-590.
200. Muthuswamy SK, Li D, Lelievre S, Bissell MJ, & Brugge JS (2001) ErbB2, but not ErbB1, reinitiates proliferation and induces luminal repopulation in epithelial acini. *Nat Cell Biol* 3(9):785-792.

APPENDIX

SUPPLEMENTARY FIGURES

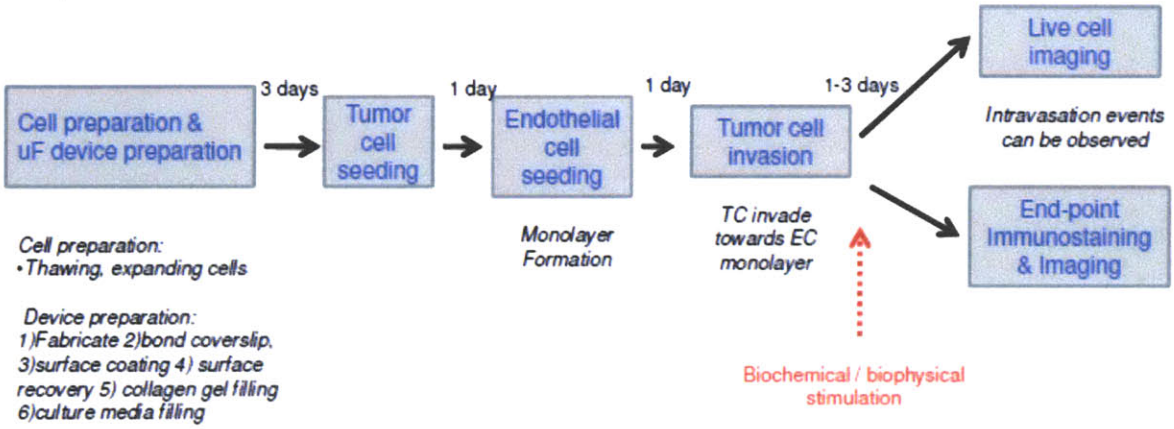

Figure S1: Protocol timeline and overview. Time-scales depend on tumor cell invasive potential and 3D ECM concentration (e.g. 1-3mg/ml)

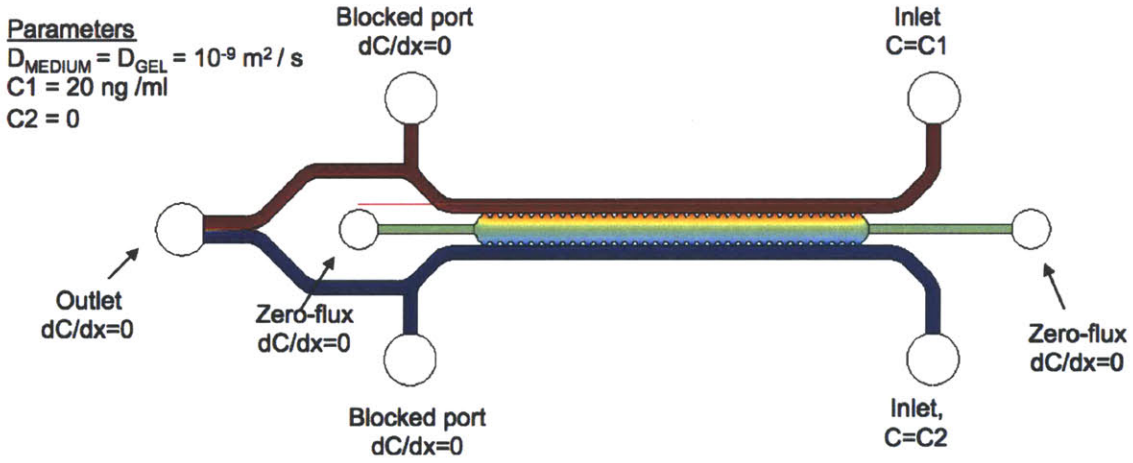

Figure S2: Boundary conditions and parameters for the computational model

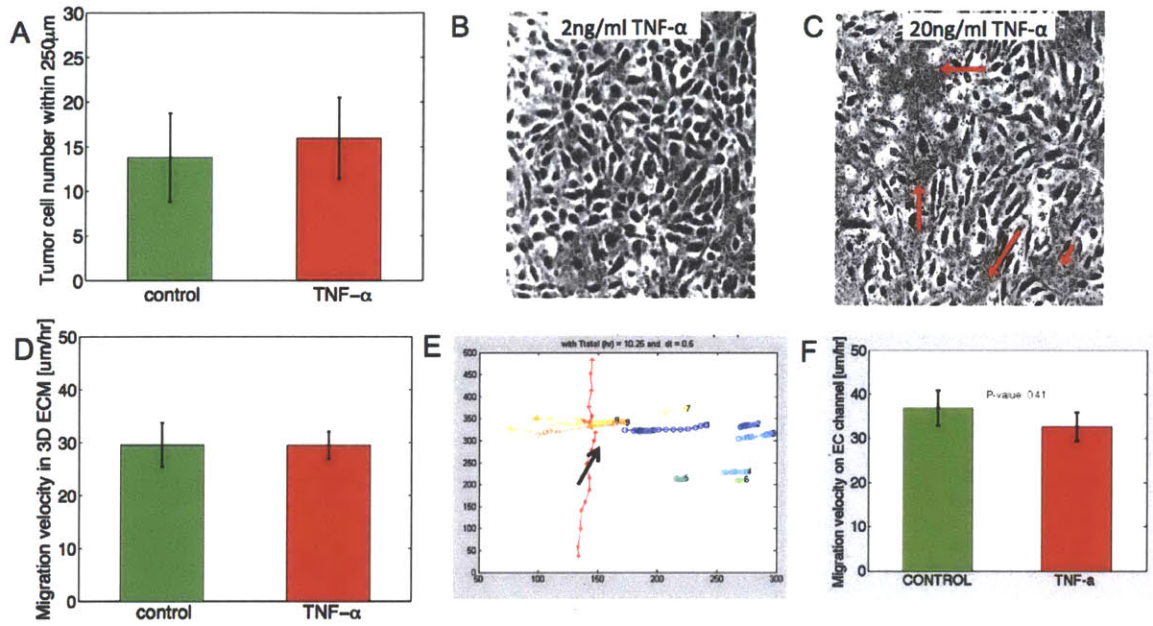

Figure S3: (A) Number of tumor cells within 250μm from endothelial monolayer in the TC-EC interaction experiments. Average values for n=3 devices per condition. (B-C) Titration experiments on endothelial monolayers formed on collagen gels to ensure monolayer confluence. (D) Migration velocity in the TC-EC interaction experiments for HT1080 cells. (E) Migration trajectories of HT1080 cells in the process of migration beyond the endothelial barrier (red line). Black arrow points to a "hotspot" of tumor-endothelial interactions (F) Migration speed of HT1080 on the endothelial channel. Average values for at least n=10 trajectories per condition. Error bars represent standard error of the mean.

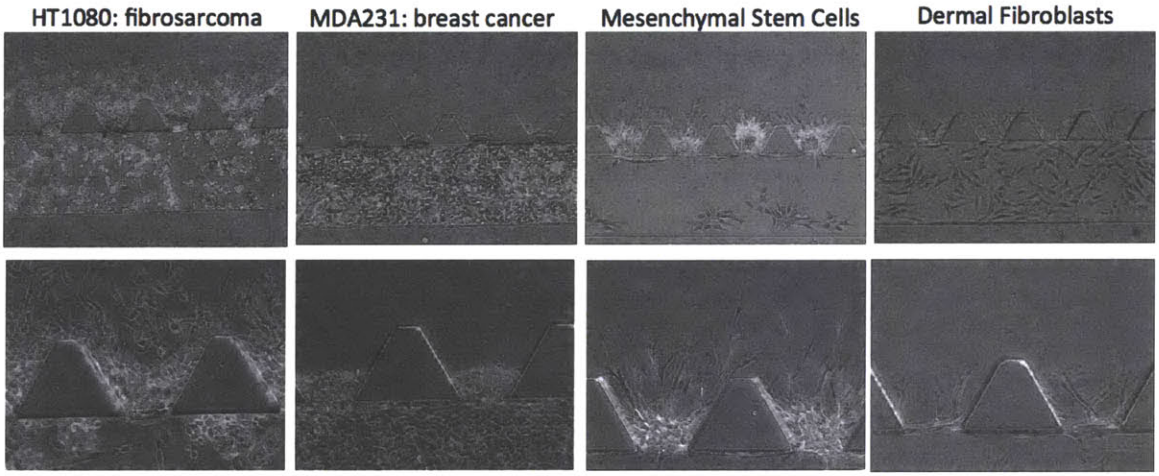

Figure S4: Different cell types invading in the 3D ECM in the presence of endothelial cells. Low magnification phase contrast (top row) and high magnification images (bottom row).

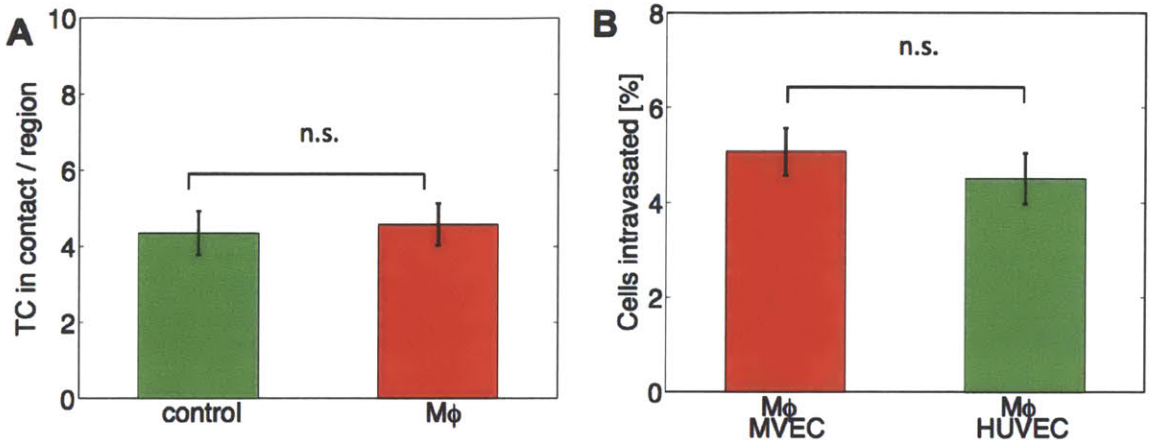

Figure S5: (A) Number of tumor cells in contact with the endothelial monolayer in the absence (control) and presence (Mφ) of macrophages. (B) Intravasation efficiency for MDA231MenaINV cells for microvascular and macrovascular primary endothelial cells in the presence of macrophages. Average values for n=3 devices per condition. Error bars represent standard error of the mean.

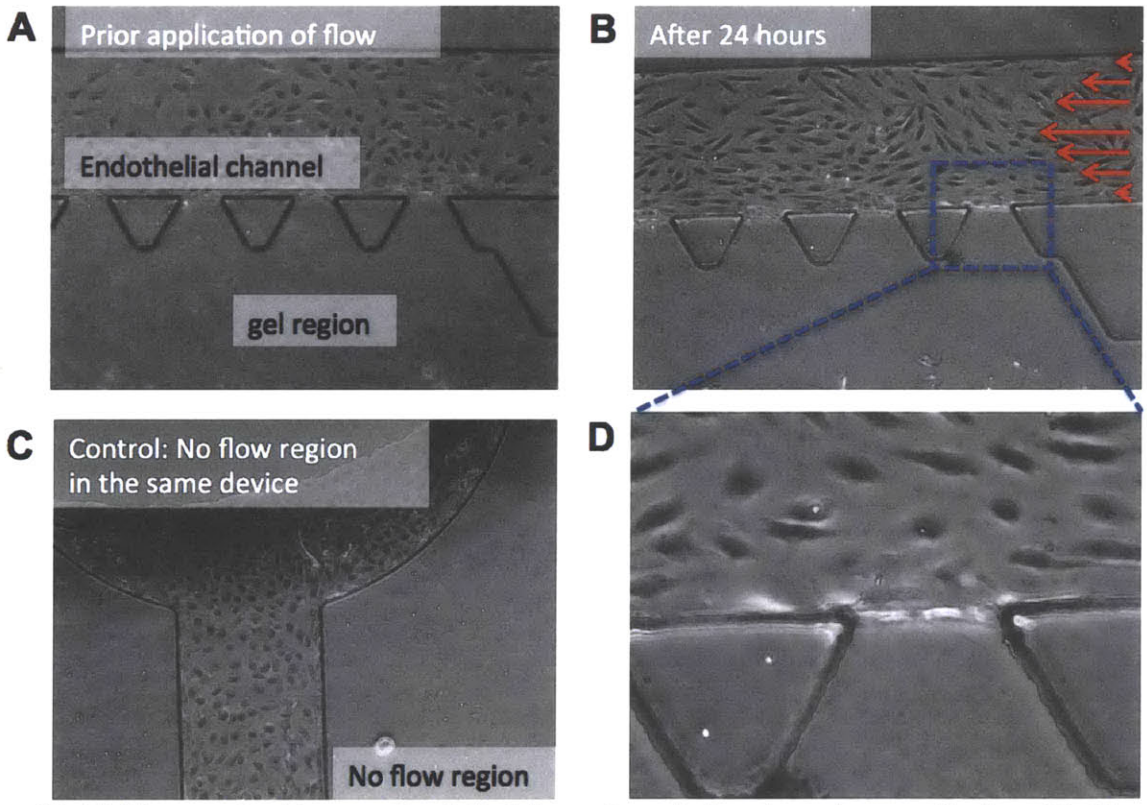

Figure S6: (A) Phase contrast images of endothelial monolayer before shear stress application. (B) Alignment of endothelial cells in response to a shear stress of 0.3Pa after 24hours. (C) Endothelial cells do not align in a region of the device where static conditions were established. (D) High magnification phase contrast image showing endothelial cell alignment in the dashed window shown in (B).

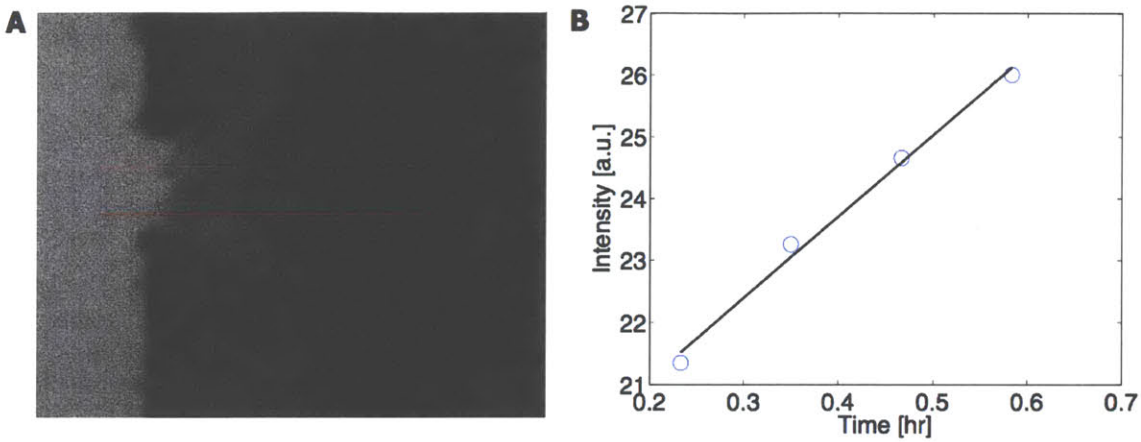

Figure S7: (A) Fluorescent intensity distribution of 70kDa and outline of the measurement window (red lines) (B) Evolution of average fluorescent intensity in the measurement window versus time (blue circles) and estimation of the slope (dI/dt)

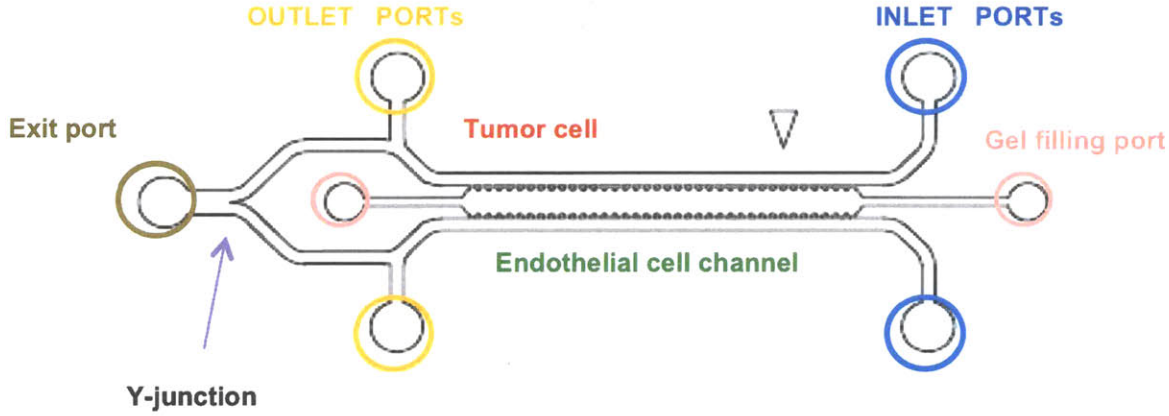

Figure S8: Device schematic with definitions for intravasation assay protocol

A1. Alternative analysis method of intensity profiles for endothelial permeability

We employed the method developed by Curry et al to quantify the diffusive permeability and compared the results to our method assuming steady state.

The diffusive permeability is given by the following equation:

$$P_D = w\left(\frac{dI}{dt}/\Delta I\right)$$

where w is the channel width, dI/dt the change in fluorescent intensity in the measurement window with time, and ΔI the difference in fluorescent intensity at t=0.

Using the above equation we estimated a P_D value of 1.92×10^{-5} cm^2/s, compared to a 70% higher coefficient of 3.42×10^{-5} cm^2/s for our method described in chapter 2. See Supplementary Figure 7 for a plot of dI/dt and the measurement window used to estimate these values.

A2. Device fabrication protocol

Materials

1. PDMS Body liquid (10 parts)
2. PDMS curing agent (1 part)

Procedure

PDMS Mixture Preparation

1. Pour 10parts of PDMS body liquid in a plastic cup while measuring its weight
2. Pour 1 part of PDMS curing agent while measuring its weight
3. Stir the mixture well
4. Remove the bubbles using the vacuum chamber
    a. Turn on vacuum and close the valve to sustain it
    (Make sure to cover the chamber with tissue)
    b. Let degassing for 20minutes
    c. Watch out for overflow

PDMS Pouring

5. Pour the PDMS onto the wafers
6. Degas the poured wafers into the vacuum chamber and poke remaining bubbles

PDMS Baking

7. Bake the poured wafers for 24 hours in 80C
8. Detach by cutting with razor

PDMS-Device punching

9. Punch holes and cut out separate devices
10. Clean devices with tape to remove PDMS debris and dust particles
11. Autoclave: First a wet and then a dry cycle (each 20 / 10 minutes)
12. Dry in oven overnight @ 80C

A3. Cell culture protocols

MVEC (Lonza) and HUVEC (Chan lab, National University of Singapore) were grown in EGM-2MV medium to confluence. MDA231MenaINV-GFP, MDA231GFP (Gertler lab, MIT) and HT1080 (ATCC) cells were grown in DMEM (Invitrogen) supplemented with 10% FBS (Invitrogen), L-glutamine and Penicillin-Streptomyocin (Invitrogen) to 70% confluence. RAW264.7 (ATCC) cells were grown in the same base medium as the tumor cells, but with heat-inactivated serum to minimize activation prior to culture in the devices. For the endothelial permeability experiments with different cell types, the human mammary epithelial cell line MCF10A (Brugge Lab, Harvard Medical School) was grown as previously described (200) to 70% confluence. All cells were grown in a humidified incubator and used only up to passage six.

A4. 3D ECM – Collagen gel recipe

<Recipe: collagen type I / rat tail from BD biosciences>
* The collagen solution can be used immediately or held on ice for 2–3 hours.
* New recipe required for every new collagen batch (adjust collagen concentration)
* pH of the gel may not be accurate. For example, pH9.0 gel may be pH 8.5–9.5.
* If you need an accurate pH value of the gel, you should measure the pH for every gel

(1) 2 mg/ml collagen gel

Solution	pH 5.5	pH 7.4	pH 9.0	pH 11.0
10×PBS	20 µl	20 µl	20 µl	20 µl
0.5N NaOH	µl	7.8 µl	µl	µl
water	µl	65.5 µl	µl	µl
3.75 mg/ml collagen **(6/30/09 opened)**	µl	106.7 µl	µl	µl
Total	200 µl	200 µl	200 µl	200 µl

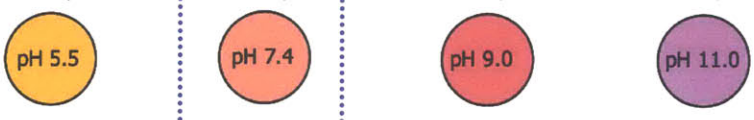

* pH 9.0 & 11.0 collagen gels are stiffer than pH 7.4 gel.

(2) 1 mg/ml collagen gel, pH 7.4

10×PBS	20 µl
0.5N NaOH	µl
water	µl
- mg/ml collagen (BD)	51.4 µl
Total	200 µl

(3) 2.5 mg/ml collagen gel, pH 7.4

10×PBS	20 µl
0.5N NaOH	µl
water	µl
- mg/ml collagen (BD)	128.5 µl
Total	200 µl

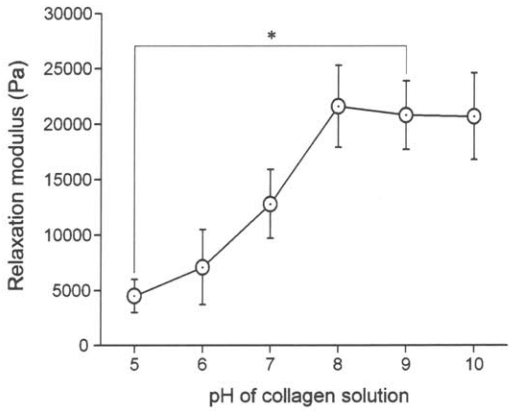

A5. Indirect Immunofluorescence staining

(Adapted from Acini Indirect Immunofluorescence staining from the Brugge Lab)

1) Fixation: Aspirate the medium from one side of each channel and immediately add 60ul of 3-4% paraformaldehyde at room temperature. Let it flow through and let it sit for 30min. Rinse twice in PBS and store in PBS at 4C.
2) Permeabilization: Permeabilize with PBS containing 0.5% Triton X-100 for 10 minutes at room temperature. Depending on the antibody utilized for immunostaining, the detergent concentration or duration of permeabilization may require modification.
3) Glycine Rinse: Rinse 3 times with 1x PBS/Glycine (130 mM NaCl; 7 mM Na_2HPO_4; 3.5 mM NaH_2PO_4; 100 mM glycine), 10-15 minutes per wash at room temperature.
4) Primary Block: Incubate with 1x IF Buffer (130 mM NaCl; 7 mM Na_2HPO_4; 3.5 mM NaH_2PO_4; 7.7 mM NaN_3; 0.1% BSA; 0.2% Triton X-100; 0.05% Tween-20) +10% goat serum for 45-60 minutes at room temperature.
5) Primary antibody: Add primary antibody in block solution. Let it flow through twice and add some more to all sides of the channels. Incubate overnight (15-18 hours) at 4°C. Although optimal antibody concentrations should be determined empirically on a case-by-case basis, a 1:200 to 1:300 dilution of the primary antibody is a good starting point.
6) Rinse 3 times (20 minutes each) with 1x IF Buffer at room temperature.
7) Secondary Antibody: Incubate with fluorescent conjugated secondary antibody in IF Buffer + 10% goat serum for 40-50 min at room temperature. We recommend Alexa™ conjugated, highly cross-absorbed secondary antibodies from Molecular Probes used at 1:200 dilution; in our experience, these secondary reagents exhibit low levels of background, and minimal cross-reactivity between species, making them useful for double immunostaining procedures.
8) Rinse 1 time (20 minutes) with IF Buffer at room temperature with gentle rocking.
9) Rinse 2-3 times with PBS (10 minutes).
10) In order to counterstain nuclei and/or actin filaments, incubate with PBS containing 0.5 ng /ml 4',6-diamidino-2-phenylindole (DAPI, Sigma) and/or phalloidin-conjugated-to-fluorophore for 15 minutes at room temperature.
11) Rinse 3 times with PBS for 5 minutes at room temperature.
12) Keep in dark and store at 4°C.

Notes:

1. *When adding the solutions in the device make sure to create interstitial flow by controlling the media levels in the central vs. side channels. This way the staining solution will flow through the gel and will stain all cells inside the gel*

BUFFER RECIPES:

10X PBS/Glycine:
38.0 g NaCl
9.38 g Na_2HPO_4
2.07 g NaH_2PO_4
37.5 g Glycine

10X IF Wash:
38.0 g NaCl
9.38 g Na_2HPO_4
2.07 g NaH_2PO_4
2.5 g NaN_3
5.0 g BSA
10.0 ml Triton-X 100
2.05 ml Tween-20

Bring both solutions up to a total volume of 500 ml, pH 7.4. Dilute to 1X solutions before use.

A6. Intravasation assay protocols

Overview:
The intravasation assay can be performed in two different ways:

a) **Assay 1, Single Cell**: By seeding the tumor cells and additional supporting cell types (e.g. macrophages) into the gel prior to endothelial cell monolayer formation
b) **Assay 2, Invasive Growth**: First fill the collagen gel without embedded cells, and then after 2-24hours seed the tumor cells onto the channel opposite to the endothelial cell channel, and allow 2-5 days for the tumor cells to invade (invasive growth) and reach the endothelial cell channel, before forming the endothelial monolayer

See Supplementary Figure 1 for an overview of the assay timeline and Supplementary Figure 8 for definitions of inlet, gel filling and outlet ports.

Cell preparation:
1 T25 flask of 80% EC (600,000 cells) required for 5 HTD devices
1 T25 flask of 80% TC (1,000,000 cells) required for 5 HTD devices (invasive growth)
1 T75 flask of 80% TC (5,000,000 cells) required for 5 HTD devices (single cell invasion)
1 T25 flask of 80% Macrophages (1,000,000 cells) required for 5 HTD devices

Device preparation:
Devices are prepared in the same way for the two assays. See Appendix A1 for the basic PDMS device fabrication. Plasma etching (2min vacuum/1min plasma), immediately after (within 2-5min) and then bind coverslip and coat with 120ul of 1mg/ml PDL solution (coating can be performed also with matrigel, collagen type I solution and fibronectin, laminin), then place in a humidified petri-dish (avoid evaporation) and incubate at 37C overnight. Next morning, wash twice with cell culture water (inject solution from gel filling port [Fig. 2 pink circle] to avoid bubbles forming in the channel). Make sure that during washing the water has completely flowed through all channels, aspirate carefully from gel filling port all water and place in 80C oven for drying out for 48hours, after which the channel/PDMS surfaces are very hydrophobic and the devices are ready for gel filling.

ASSAY 1: Single cell assay

The assay design 1 allows for shorter assay duration, since the tumor cells will be embedded inside the 3D matrix and some of them will be closely located to the endothelial monolayer (within 50-200um). Endothelial cells should be ready for seeding 1 day after the tumor cells are seeded in the gel.

Collagen gel preparation for ASSAY1: Single Cell Invasion Assay
Prepare 1.75-3mg/ml collagen type I gel (polymerization pH~9 / see Appendix A3). Mix 5-20µl (calculate required cell suspension density [typically 10-50million cells/ml growth medium]) of tumor cell suspension with 200-500ul (1:10 – 1:100 ratio) collagen gel solution, to get the desired concentration of tumor cells (typically 0.1 – 1million cells/ml gel). The pH and final collagen gel concentration will determine tumor cell invasive potential. Very low collagen

gel/matrigel concentration may lead to cell-mediated gel contraction forming a curved tumor/cell interface. Fill collagen gel (take 25ul/device with a 200ul pipette tip) from one side of the gel filling port (Supplementary Figure S8: pink circle), until halfway through the gel region, and then switch over to the other gel filling port and complete filling. In order to avoid having the cells settle down on the coverslip, flip the device by 180degress every 10minutes to achieve a 3D cell distribution. If a matrigel mixture (typically dilute 1:3 of stock matrigel) is used, then the devices should be flipped after 3minutes of filling, because matrigel polymerizes quicker than collagen. Allow 60min for the collagen gel to polymerize and make sure to place the devices in a humidified chamber to avoid the collagen drying out.

Culture medium filling

Fill complete endothelial cell growth medium in both channels, 1 hour after collagen gel filling. Place 60ul in each inlet port (blue circles in Fig.2), cut a 1mL pipette tip with scissors so the tip fits tightly to the outlet port (yellow circles in Fig.2) and apply suction 2-3times (set the pipette to 200ul) until the medium fills the channel. Then add 60ul to each outlet port to fill up the ports, and finally place a 60ul droplet on the exit port (fig.2 brown circle) to trap an air bubble at the Y-junction between the two channels, in order to be able to address them independently for the endothelial cell seeding. This air bubble would need to be removed if shear stress experiments are to be performed, since the Y-junction serves as a pressure-equalizing interface. An alternative protocol is to fill the Y-junction with collagen gel during the collagen gel-filling step of the protocol. This is achieved by filling the collagen gel from the exit port: cut a 200ul pipette tip, so it fits tightly to the exit port and fill 20ul of gel until it reaches the second gel filling port level, but don't fill all the way towards the outlet port, because the endothelial/tumor channels will be blocked. The channels can also be filled with other medium, however seeding endothelial cells in complete growth medium results in good quality monolayer formation.

Endothelial cell seeding

Time point to seed the endothelial cells should be decided based on when the tumor cells are close to the endothelial cell channel (usually 12 – 72 hours after tumor cell seeding in the gel). Prepare a 2 million cells/ml solution and add 60ul to the outlet port of the channel opposite of the tumor cell channel (endothelial cells can also be seeded in both channels, but make sure to seed one channel at a time to ensure that the endothelial cells stick to the collagen gel and form a nice monolayer on the gel). Cut a 200ul pipette tip, so that it fits tightly on the inlet port and aspirate 60ul of the cell solution through the channel. This way the cell suspension will have evenly filled the channel in order to ensure uniform monolayer formation along the device length. Add another 30ul/port to induce a slow interstitial flow that will push the endothelial cells towards the collagen gel wall. An alternative method for cell seeding is, to flip the device 90deg for 30min in a humidified chamber to get the endothelial cells to adhere to the collagen gel wall through gravity. Endothelial cells form a good monolayer, covering the endothelial channel completely, usually after 24hours, depending on seeding density, endothelial channel coating solutions (e.g. matrigel and collagen type I coating work better than PDL, but the gel contracts more easily)

Changing culture medium and application of biochemical conditions

Medium should be refreshed every 24 hours, and devices should be kept in a humidified incubator and petri-dish. To change medium, gently aspirate 60ul manually with a pipette from each port (or adequate volume to remove all medium from top PDMS surface, but keep the

bottom of the port filled with medium), then add a 60ul droplet at the inlet port, wait for 2 minutes until it flows through the channel towards the outlet port, replenishing the old medium with fresh. Aspirate 60ul from the outlet port and replace it with 60ul of fresh medium. If unsure whether channel medium has been completely replenished repeat one more time. The biochemical conditions are applied in the same way as changing the medium.

Setting up the device for live cell imaging
Binding 2nd PDMS layer to ensure enough culture medium is present and to avoid evaporation.

Fixation
By using the same protocol as culture medium change, add 4% PFA solution for 30minutes to all ports and make sure it has flowed completely inside the channels. Then wash three times with PBS for 30minutes intervals to make sure no residual PFA is left in the device channels/gel.

Common problems encountered:

1. Cell debris: Tumor or endothelial cell seeding density is too high

2. Cells are not viable right after seeding: PDL washing might not be performed properly, residual PDL (at high concentration) can affect cell viability

3. Embedded cells in the gel settle to the glass coverslip: Flip the devices upside down to redistribute cells across z-height every 10 minutes for collagen gel, or after 3 minutes for the matrigel.

4. Particles are seen in collagen gel. Particles can form inside the gel if the PDL washing is not performed properly. Try filling the same collagen gel solution in PDL-untreated devices and look for particles.

5. Cells are not viable after a few days: Medium drying out from ports can affect cell viability. The devices should be kept in a humidified environment with the inlet/outlet ports being continuously covered with at least 60ul of culture medium.

6. Collagen gel seems to be non-uniform: Make sure to keep the collagen gel on ice while mixing and filling devices. Also, devices should be allowed to cool down after removing from the 80C oven and prior to gel filling.

ASSAY 2: Invasive growth assay

Here, the protocol is very similar to assay 1, and the major difference is the introduction of the tumor cells in the channel. This allows for running the assay for longer times and having a pure collagen/matrigel ECM between the tumor/endothelial cell interface.

Collagen gel preparation for ASSAY2: Invasive Growth
Prepare 1.75-3mg/ml collagen type I gel (polymerization pH~9 - see Appendix A3) for invasive growth assay. The pH and collagen gel concentration will determine the time duration for the

tumor cells to cross the 1.3mm wide gel region and interact with the endothelial cells. Fill collagen gel from one side of the gel filling port, until halfway through the gel region, and then switch over to the other gel filling port and complete filling. Fill also the Y-junction with gel to make the two channels independent. Allow 60min for the collagen gel to polymerize and make sure to place the devices in a humidified chamber to avoid the collagen drying out.

Tumor cell seeding for ASSAY2: Invasive Growth

Tumor cells should be ready for seeding 1 day after filling the collagen gel. Prepare a 2-3million cells/ml cell solution and add 60ul to the outlet of one of the channels. Make sure that the cells are flowing through the channel and sticking to the gel interface. Allow the cells to settle down to the bottom channel surface and adhere to the channel, before adding 60ul culture medium droplets to all ports.

Endothelial cell seeding protocol and biochemical condition application are identical to assay 1

A7. Shear stress experiments

Methods

To create a more physiologically relevant microenvironment, we developed protocols to apply fluid flow in the microfluidic channels. Briefly, upstream reservoirs (~30mL) were connected to the inlet ports (see previous image) and the outlet and gel filling ports were blocked using a 2nd layer PDMS block. A syringe pump was connected to the outlet port and constant flow-rates of 3-20 μl/min were established.

Technical Challenges

One of the technical challenges with the application of shear stress on the endothelial monolayers in the microfluidic device is the development of protocols that ensure monolayer stability. We found that a critical step in the assembly of the external tubing to the upstream reservoirs and syringe pump is the connection of the tube connectors, which sometimes resulted in endothelial monolayer distortion. Another challenge was the frequent observation of 3D matrix contraction in the experiment where shear stress was applied, especially under conditions where fluid flow was driven only through one of the two microchannels. This could be due to the establishment of a differential pressure drop across the 3D matrix.

Results and discussion

Preliminary experiments with control endothelial monolayers (in the absence of tumor cells or macrophages) showed that we could observe endothelial cell alignment in response to a shear stress of 0.3 Pa, corresponding to a flow-rate of approximately 20ul/min (Supplementary Figure 6B, D). Endothelial cells were randomly oriented in regions inside the device were no flow was established (next to the blocked outlet ports, see Supplementary Figure 6C).

Previous studies on the effects of shear stress on endothelial permeability have shown that long term exposure to shear stress decreased endothelial permeability, whereas, permeability was increased during the first few hours of shear stress application (176). This is an important point that should be taken into consideration in experiments that will investigate the effect of shear stress on endothelial permeability.

A8. Permeability quantification MATLAB code

```
% Script to estimate Diffusive permeability
% Ioannis Zervantonakis ;

% Formula for steady state data:
% Pd=D * dC/dx / dC|driving difference in concentration

clear all;

% Selecting dextran size
dextag=10;
if dextag==10;
   D=9e-11;
elseif dextag==70;
   ratioD=(10/70)^(1/3);
   D=ratioD*(9e-11);
end

manoraut=input('Give 0 for manual input of evaluation parameters or 1 to go with previously stored: ');

if manoraut==0

% Scaling of pixels to microns;

dywconf=input('Give # of pixs corresponding to 100um (e.g. 126pix for HTDS22-D1): ');
dx=(100/dywconf)*(1e-6); %spacing in m;
dypix=input(['100um = ',num2str(dywconf),'Give # of pix across y (~1/5 of 100um): ']); % number of pix for
averaging
dypix=round(dypix);
if mod(dypix,2)==0 % create an even number
dypix=dypix;
else
dypix=dypix+1;
end

% Define whether image needs flipping
% if monor=1 image needs flipping to get EC channel on the left
monor=input('Give 0 for not flipping image of 1 for flipping image 180: ');

% Define parameters for slope estimation
dxfitdo=input('Give # of pixs for fitting downstream slope (e.g. 100): ' );
dxfitup=input('Give # of pixs for fitting upstream constant conc (e.g. 30): ');
% dxfitup, dxfitdo are very critical parameters for the slope accuracy

Zslicetot=input('Give the number of total zlices of dataset: ');

% Decide manual input of timepoints or automatic
cteval=input('Give 0 for automaticall evenly spaced time points or 1 for manual list: ');
if cteval~=0
   Tevalvm=input('Give the timesteps for manual evaluation: ');
   Tevalv=Tevalvm;
   T=length(Tevalvm);
   dt=input('Give the timestep between the timepoints (sec): ');
   T0=input('Give the starting timepoint of evaluation: ');
   Ntt=T;
```

```
   Dttt=floor((T)/Ntt); % round the timestep for e
else
   T=input('Give the number of timepoints of dataset: ');
   dt=input('Give the timestep between the timepoints (sec): ');
   T0=input('Give the starting timepoint of evaluation: ');
   Ntt=input('Give the number of timepoints (uniformely distributed) that you want to evaluate the dataset: ');
   Dttt=floor((T)/Ntt); % round the timestep for e
%   Defining vector for timepoints that will beevaluated
   Tevalv=zeros(Ntt,1);
   Tstart0=T0;
   for j=1:Ntt
   Tevalv(j,1)=T0+(j-1)*Dttt;
   end
end

Numf=T*Zslicetot; % Total number of slices

save(['evalpar.mat'],'dextag','D','dywconf','dypix','monor','dxfitdo','dxfitup','T','Zslicetot','Ntt','T0','Dttt','dt','dx','Teval
v','-mat');
else
load('evalpar.mat'); % Load the parameters from previous input
end

% temporary define colorSet
ColorSet=varycolor(Ntt); % needs to have many colors so that more than 15 z-slices can fit

% Compute the time axis in hours

Tevalvhr = zeros(Ntt,1);
Tevalvhr(1,1)=0;
for jtmp=2:Ntt
   Tevalvhr(jtmp,1)=(Tevalv(jtmp,1)-Tevalv(jtmp-1,1))*(dt/(3600))+ Tevalvhr(jtmp-1,1);
end

% Defining the images to be loaded
filelist = dir('*.tif');
fname = filelist(1).name;
% Default time for plotting everything
Tdef=1;

% first need to read the first Zslicetots and select region for averaging
totalfirst=[];
   for fidxt=1:Zslicetot                    %for T time points
   firstTimages=zeros(512,512,'double');
   tmpfirst = imread(fname,fidxt); % reading the zIDX .tif
   if monor~=0
   tmpfirst=imrotate(tmpfirst,180); % only if
   end
   tmpfirst= double(tmpfirst);
   firstTimages = [firstTimages + tmpfirst];    %overlay of images
   disp([fname ' loaded']);
   totalfirst=[totalfirst; firstTimages];
   end

tfdt=reshape(totalfirst',[512 512 Zslicetot]);
tfdt=imrotate(tfdt,90);
```

```
% loop for plotting all z-slices\

figure,
ispx=5;% Here need to be careful. so that total z-slices are less than 5x4
ispy=4;

for i=1:Zslicetot
% if i<0.5*Zslicetot
subplot(ispx,ispy,i), imagesc(tfdt(:,:,i))
set(gca,'YColor',[1 1 1],'XColor',[1 1 1],'XTick',[],'YTick',[])
%colormap(gray)
title(['Z-index', num2str(i)])
end

[zrange1]=input('Give range of z-slice indices Z1: ');
[zrange2]=input('Give range of z-slice indices Z2: ');

title(['Z-range selected: ', num2str(zrange1), ' - ', num2str(zrange2)])

fnamefig1 = fname(1:end-4);
fname1='Raw-Data';
fnamefinal1=strcat(fnamefig1,fname1);
print ('-dpng',fnamefinal1);
close;

dzeff=1+zrange2-zrange1;
Zidxevs=zrange1; % Set the index for the first evaluation of intensity profile equal to the first range before finding
slice with maximum intensity

% initialize the structure where the images will be saved
total =[];

% after we have defined the z-range for images to be read, compute the
% indices for reading images, and loop for reading images

% Loop to read the images
% total number of images to be read
Nttotal=Ntt*Zslicetot;

for j=1:Ntt
   Tevaltmp=Tevalv(j,1);

   Numfd1v=zrange1+(Tevaltmp-1)*Zslicetot;
   Numfdev=zrange2+(Tevaltmp-1)*Zslicetot;

% Loop for reading  images
   for ifz=Numfd1v:Numfdev                    %for T time points
   images = zeros(512,512,'double');
   tmp = imread(fname,ifz); % reading the zIDX .tif
   if monor~=0
   tmp=imrotate(tmp,180); % only if
   end
   tmp= double(tmp);
   images = [images + tmp];    %overlay of images
   disp([fname '  loaded']);
```

```
   total=[total; images];
   end
end

t4dt=zeros(512,512,dzeff,Ntt);
t4dt=reshape(total',[512 512 dzeff Ntt]);
t4d=t4dt;
%Rotating images 90deg
for j=1:dzeff
   for i=1:Ntt
      t4d(:,:,j,i)=imrotate(t4dt(:,:,j,i),90);
   end
end
t=t4d;
sizeimg=size(t4d(:,:,1,1));
hori=sizeimg(2);
verti=sizeimg(1);
%
% Averaging z-slices for better accuracy of slope and estimates
%
tproj=zeros(512,512,Ntt);

for jtidx=1:Ntt
tmpsum=0;
for j=1:dzeff
   tmpsum=t(:,:,j,jtidx)+tmpsum;
end
tproj(:,:,jtidx)=tmpsum/(1+zrange2-zrange1); %this is the image of the averaged/projected intensity
end
%
% Loop for plotting average concentration
%
figure,
title(['Dataset', fname])
subplot(3,1,1), imagesc(tproj(:,:,Tdef));
   title(['Choose 1 point on y-level defining area for averaging and x coordinate for defining A0, and 2nd point do
define A=const']);

   %choose first 2 points for interface spline
   [xindxa1,yindxa1]=ginput(2);
   xindxa1=round(xindxa1); yindxa1=round(yindxa1);

   % xindxa1 is the x-coordinate where the Area starts changing.

hold on,
plot([1 verti], [yindxa1(1,1) yindxa1(1,1)],'-r')
 hold on,
 plot([1 verti], [yindxa1(2,1) yindxa1(2,1)],'og')

title(['Dataset', fname])

% loop for averaging
ytmp=yindxa1(1,1);
yindxa1(1,1)=ytmp-0.5*dypix; %The averaging parameters are given as input
yindxa1(2,1)=ytmp+0.5*dypix;
```

```
for i=1:dzeff
dts(:,i)=single(t(yindxa1(2,1),:,i,Tdef));
end

dtsproj=single(tproj(yindxa1(2,1),:,Tdef));
dtsprojs=dtsproj;

% Y-Averaging for projected sli
for i=(yindxa1(1,1)+1):yindxa1(2,1)
dtsprojs=dtsprojs+single(tproj(i,:,Tdef));
end

dtsprojav=dtsprojs/(1+yindxa1(2,1)-yindxa1(1,1));
dtavp=dtsprojav;

for j=1:dzeff
for i=(yindxa1(1,1)+1):yindxa1(2,1)
hold on
dts(:,j)=dts(:,j)+ single(t(i,:,j,Tdef))';
end
dtav(:,j)=dts(:,j)/(1+yindxa1(2,1)-yindxa1(1,1));
dtavnt(:,j)=(dtav(:,j)-min(dtav(:,1)))/(max(dtav(:,1))-min(dtav(:,1))); %
pixavg=yindxa1(2,1)-yindxa1(1,1);
xaxmin=0;
xaxmax=600;
yaxmin=0;
yaxmax=2;
subplot(3,1,2),
plot(dtav(:,j),'Color',ColorSet(j,:)), %Plot verage concentrations
xlabel ('Distance across the scaffold [pix]');
ylabel (' Average fluorescence [-]');
title(['Average concentration ', num2str(pixavg) ' pixels' ]);
 axis([xaxmin xaxmax yaxmin yaxmax]);
end
atmp = [];

for itmp = 1:dzeff,
atmp = [atmp; {[num2str(itmp) ' ']}];
end

legend([atmp]);
axis ([-100 612 0 1.2*max(max(dtav))]);
subplot(3,1,3)
for jj=1:dzeff
   dtavdif(:,jj)=diff(dtavnt(:,jj));
   wdwsize=6;
   fdtavdif=filter( (1/wdwsize)*ones(1,wdwsize), 1, dtavdif);
   fdtavdifn(:,jj)=fdtavdif(:,jj)./max(dtavnt(:,1));
   plot(fdtavdifn(:,jj),'Color',ColorSet(jj,:)), %Plot verage concentrations
xlabel ('Distance across the scaffold [pix]');
ylabel ('Filtered  normalized/subtract difference to min intensity [-]');
   hold on,
 title(['Normalized DC/C with filter windowsize ', num2str(wdwsize) ' pixels' ]);
end
atmp = [];
for itmp = 1:dzeff,
```

```
atmp = [atmp; {[num2str(itmp) ' ']}];
end
legend([atmp]);
Teval=Tdef;
close;
%
% Quantification of PD
%
% Loop for getting slope of concentration profiles

figure,
title(['Dataset', fname])

dtavss=dtav(:,dzeff);

subplot(3,1,1), %imagesc(t{1,1});
plot(dtav(:,dzeff));
axis ([0 512 0.98*min(dtavss) 1.02*max(dtavss)]);
   title(['Choose 1 points for fitting conc. - Timepoint and z-slice ', num2str(Teval), ' - ' , num2str(zrange2)]);

   %choose first 2 points fitting the upstream intensity and the
   %downstream non-linear profile
   [xindxas1,yindxas1]=ginput(2);
   xindxas1=round(xindxas1); yindxas1=round(yindxas1);
hold on,
plot([xindxas1(1,1) xindxas1(1,1)],[yindxas1(1,1) yindxas1(1,1)],'*k')
hold on,
plot([xindxas1(2,1) xindxas1(2,1)],[yindxas1(2,1) yindxas1(2,1)],'ok')
title(['Dataset', fname])

xs1=(xindxas1(1,1)-dxfitup:xindxas1(1,1)+dxfitup);
xs2=(xindxas1(2,1)-dxfitdo:xindxas1(2,1)+dxfitdo);
xrec=1:512;
ids1=zeros(length(xs1),dzeff);
ids2=zeros(length(xs2),dzeff);
ids1rz=zeros(512,dzeff);
ids2rz=zeros(512,dzeff);
smdtav=zeros(511,dzeff);
dtavdiff=zeros(511,dzeff);
fitnorm=zeros(1,dzeff);
stdevdat=zeros(1,dzeff);
meandat=zeros(1,dzeff);
ndat=zeros(1,dzeff);
upsavg=zeros(1,dzeff);
xINFL=zeros(1,dzeff);
vertl_INFL=zeros(2,dzeff);
ids1rfix=zeros(512,dzeff);
dCdif=zeros(1,dzeff);
dCslope2=zeros(1,dzeff);
rsgood=zeros(1,dzeff);
dcmax=zeros(1,dzeff);
dcmaxidx=zeros(1,dzeff);
DCfit=zeros(1,dzeff);
Pdn_fit=zeros(1,dzeff);

for it=1:dzeff % T here is the number of slices
```

```
   tmpdif= diff(dtav(:,it));
   dtavdiff(:,it)=tmpdif;
   wdwsize1=3;
   wdwsize2=20;
   wdwsize3=30;
   smdtav(:,it)=smooth(tmpdif,wdwsize3);
ids1(:,it)=dtav((xindxas1(1,1)-dxfitup:xindxas1(1,1)+dxfitup),it);
upsavg(1,it)=mean(ids1(:,it));
% define the upstream intensity for a larger yregion
xs1=(xindxas1(1,1)-dxfitup:xindxas1(1,1)+dxfitup);
xs2=(xindxas1(2,1)-dxfitdo:xindxas1(2,1)+dxfitdo);
ids2(:,it)=dtav((xindxas1(2,1)-dxfitdo:xindxas1(2,1)+dxfitdo),it);
[coef1]=polyfit(xs1',ids1(:,it),1);
[coef2]=polyfit(xs2',ids2(:,it),1);
[coef2,Sfit2]=polyfit(xs2',ids2(:,it),1);
fitnorm(1,it)=Sfit2.normr;
stdevdat(1,it)=std(ids2(:,it));
meandat(1,it)=mean(ids2(:,it));
ndat(1,it)=length(ids2(:,it));
rsgood(1,it)=1-((fitnorm(1,it).^2)./((ndat(1,it)-1).*(stdevdat(1,it).^2)));
ids1rz(:,it)=coef1(1,2)*ones(512,1)+coef1(1,1)*(xrec');
tmpups=upsavg(1,it);
ids1rfix(:,it)=tmpups*ones(512,1);
ids2rz(:,it)=coef2(1,2)*ones(512,1)+coef2(1,1)*(xrec');%-xs2(1,1));
dCslope2(1,it)=coef2(1,1);

% Finding the maximum of the gradient
ttmp=smdtav( (wdwsize3*0.5:(512-wdwsize3*0.5)), it);
[t1tmp,t2tmp]=max(abs(ttmp));
dcmax(1,it)=t1tmp;
dcmaxidx(1,it)=t2tmp;
xINFL(1,it)=dcmaxidx(1,it)+wdwsize3*0.5;
vertl_INFL(:,it)=[0.1*dtav(xINFL(1,it),it) 10*dtav(xINFL(1,it),it)];
DCfit(1,it)= (upsavg(1,it))- (coef2(1,2)+coef2(1,1)*xINFL(1,it));
Pdn_fit(1,it)=abs(dCslope2(1,it))./DCfit(1,it);
end

% Estimating the slope and DCfit for the maximum upstream intensity =>
% Brightest z-slice
[maxupv maxupi]=max(upsavg);
Pd_fit_maxUP=(D/dx)*abs(dCslope2(1,maxupi))./DCfit(1,maxupi);
%
% Calculation of diffusive permeability
%
Pd_fit=Pdn_fit*D/dx;
%
Zplot=dzeff; % Z- slice index to evaluate

subplot(3,1,2), plot(xrec, dtav(:,Zplot),'-k'); hold on; plot(xrec, ids2rz(:,Zplot),'-r'); hold on;
hold on, plot(xrec,ids1rfix(:,Zplot),'-b')
plot([xindxas1(1,1) xindxas1(1,1)],[yindxas1(1,1) yindxas1(1,1)],'*m')
hold on,
plot([xindxas1(2,1) xindxas1(2,1)],[yindxas1(2,1) yindxas1(2,1)],'om')
hold on,
plot([xINFL(:,Zplot) xINFL(:,Zplot)],vertl_INFL,'m')
axis ([0 512 0.98*min(dtav(:,Zplot)) 1.02*max(dtav(:,Zplot))]);
```

```
xlabel ('Distance across the scaffold [pix]');
ylabel ('Normalized/subtract difference to min intensity [-]');
title( ['Slope downstream: ', num2str((dCslope2(:,Zplot)),2), ' Conc difference fit: ', num2str(DCfit(:,Zplot),2), '
Fitted Pd [cm/s] : ', num2str((Pd_fit(:,Zplot)*1e2),2) ])
subplot(3,1,3), imagesc(tproj(:,:,Tdef));
hold on,
plot([xINFL(:,Zplot) xINFL(:,Zplot)], [1 verti],'-m')
hold on,
plot([1 verti], [yindxa1(1,1) yindxa1(1,1)],'.-k')
hold on,
plot([1 verti], [yindxa1(2,1) yindxa1(2,1)],'.-k')
title( {['Z-slice: ', num2str(Zplot), ' Linear fit goodness : ', num2str(rsgood(:,Zplot),2)];[ ' # of pixels range for y-
avg: ' num2str(dypix), ' & for slope: ' , num2str(dxfitdo), ' and for filtering window for inflection point : ',
num2str(wdwsize3) ] });
legend('Identified monolayer','region for avergaging','region for avergaging')
dyavg=yindxa1(2,1)-yindxa1(1,1);
close;
```